Cape Peninsula
University of Technology

SIMULATION AND OPTIMISATION OF A HIGH TEMPERATURE POLYMER ELECTROLYTE MEMBRANE FUEL CELL STACK FOR COMBINED HEAT AND POWER

by

MYALELO VUYISA NOMNQA

Thesis submitted in fulfilment of the requirements for the degree

Master of Technology: Chemical Engineering

in the

Faculty of Engineering

at the

Cape Peninsula University of Technology

Supervisor: Prof. DIO IKHU-OMOREGBE
Mr. A RABIU

Cape Town
November 2011

DECLARATION

I, **Myalelo Vuyisa Nomnqa**, declare that the contents of this dissertation/thesis represent my own unaided work, and that the dissertation/thesis has not previously been submitted for academic examination towards any qualification. Furthermore, it represents my own opinions and not necessarily those of the Cape Peninsula University of Technology.

Signed Date

ABSTRACT

High temperature polymer electrolyte membrane fuel cells (PEMFC) operating between 120-180 ^{o}C are currently of much research attention. The acid doped polybenzimidazole (PBI) membranes electrolyte are known for their tolerance to relatively high levels of carbon monoxide impurity in the feed. Most fuel cell modelling are theoretical in nature and are solved in commercial CFD platforms such as Fluent. The models require a lot of time to solve and are not simple enough to be used in complex systems such as CHP systems. This study therefore, focussed on developing a simple but yet accurate model of a high temperature PEMFC for a CHP system.

A zero dimensional model for a single cell was developed and implemented in Engineering Equations Solver (EES) environment to express the cell voltage as a function of current density among others. Experimental results obtained from literature were used to validate and improve on the model. The validated models were employed for the simulation of the stack performance to investigate the effects of temperature, pressure, anode stoichiometry and the level of CO impurity in the synthesis gas, on the cell potential and overall performance. Good agreement was obtained from the simulation results and experimental data. The results showed that increasing temperature (up to 180^{o}C) and acid doping level have positive effects on the cell performance. The results also show that the cell can operate with a reformate gas containing up to 2% CO without significant loss of cell voltage at elevated temperatures.

The single cell model was extended to a 1 kW_e high temperature PEMFC stack and micro-CHP system. The stacks model was validated with experimental data obtained from a test station. The model was used to investigate the performance of PEMFC and CHP system by using uncertainty propagation. The highest combined cogeneration system efficiency of 87.3% is obtained with the corresponding electrical and thermal efficiencies are 41.3% and 46 % respectively. The proposed fuel processing subsystem provides an adequate rate of CH_4 conversion and acceptable CO-level, making it appropriate for integration with an HT PEMFC stack. In the steam methane reformer 97% of CH_4 conversion is achieved and the water gas shift reactors achieve about 98% removal of CO.

ACKNOWLEDGEMENTS

I wish to thank:

- My supervisors, Daniel Ikhu-Omoregbe and Ademola Rabiu for their guidance, encouragement and support
- Piotr Bujło for his help with the experiments to validate the model
- My parents, friends and family for their love and patience
- Finally I would like to thank Hydrogen South Africa for their financial assistance during the period of my post-graduate studies.

Table of Contents

LIST OF FIGURES

LIST OF TABLES

NOMENCLATURE

a	Catalyst specific area	(cm^2/mg)
C	Concentration	(mol/m^3)
cp	Specific heat capacity	(kJ/kg K)
$\mathbf{D}$	Diffusivity of reactants in phosphoric acid	(m^2/s)
E	Activation energy	(kJ/mol)
$\mathbf{F}$	Faradays constant	(C/mol)
$\dot{h}$	Partial enthalpy	(kJ/kg)
H	Henry's constant	(mol / m^3 Pa)
HV	Heating value	(kJ/kg)
I	Current	(A)
$\mathbf{j}$	Current density	(A/cm^2)
k	Conductivity	(S/m)
K_i	Adsorption constants of species	(bar^{-1})
K_{eq_i}	Equilibrium constants	
K_{Hs}	Standard catalyst activity	$mol_{CO2}/(s\ atm^{0.5}\ m^3)$
L	Catalyst loading	(mg/cm^2)
$\dot{m}$	Mass flowrate	(g/s)
MM	Molar mass	(kg/kmol)
m_{PA}	Mass of phosphoric acid per unit area	(mg/cm^2)
n	Number of moles of electrons	
N	Molar flux	(mol /s)
N_{stack}	number of cells in a stack	
$\mathbf{P}$	Pressure	(bar)
P_{elec}	Electrical power	(W)
Q	Heat produced	(W)
r	Reaction rates	(mol/kg h)
$\mathbf{R}$	Universal gas constant	(J/mol K)
$\mathbf{S_{Pt}}$	The specific surface area of Pt per unit area	
$\mathbf{T}$	Temperature	(^oC)
$\mathbf{V}$	Voltage	(V)
w_{PA}	Mass fraction of phosphoric acid	

$\mathbf{x_{PA}}$	Mole fraction of phosphoric acid
$\boldsymbol{y}$	Mass fraction of the component

Symbols

$\boldsymbol{\alpha}$	Transfer coefficient	
$\boldsymbol{\delta}$	Average thickness of the thin film layer	(m)
$\boldsymbol{\rho}$	Density of phosphoric acid	(g/cm^3)
$\boldsymbol{\varepsilon_{PA}}$	Volume fraction of free unbound phosphoric acid	
$\boldsymbol{\theta_{CO}}$	Surface coverance of the reaction site by CO	
$\boldsymbol{\varepsilon}$	Heat exchanger effectiveness	
$\boldsymbol{\gamma}$	Pressure coefficient or the reaction order	
$\boldsymbol{\tau}$	The tortuosity	

Subscripts

$\boldsymbol{stack}$	Fuel cell stack
$\boldsymbol{PA}$	Phosphoric acid
$\boldsymbol{elec}$	Electrical
$\boldsymbol{CO}$	Carbon monoxide
$\boldsymbol{a}$	anode
$\boldsymbol{c}$	cathode
$\boldsymbol{mix}$	mixer
$\boldsymbol{i}$	Species (H_2, O_2, CH_4 etc)
$\boldsymbol{eq}$	equilibrium
$\boldsymbol{\alpha}$	Transfer coefficient
$\boldsymbol{cogen}$	Cogeneration/CHP

CHAPTER ONE
INTRODUCTION

1.1 Background

There are various signs today, which indicate that continued use of fossil fuels and our lifestyle with respect to energy utilization and production needs to change. Excessive burning of fossil fuels over the last century has not gone by without noticeable problems. These problems are related to the rapid increase in the demand of energy caused by increase of the world's population. Firstly, there is a significant decrease of the fossil reserves which in turn results into rise in their price. Secondly, the use of fossil fuels is causing serious environmental impact, changing our global climate and causing extreme weather phenomena to be more frequent and severe. The global energy consumption was about five mega tonne of equivalent oil (Mtoe) in 2009 with 80% of this energy coming from fossil fuels. Burning of fossil fuels has resulted in an increase in the amount of anthropogenic green house gases (GHG's) in the atmosphere. These gases include carbon dioxide (CO_2), methane (CH_4), nitrous oxide (N_2O) and halocarbons. This increase resulted from the emission process of the gases being more than the removal process. Of these GHG's atmospheric concentration increase, CO_2 concentration has been the major increasing from pre-industrial value of about 280 ppm to 387 ppm in 2009 (Mathiesen *et al*., 2011).

For stationary energy applications there have been "newer" technologies that have been introduced so as to combat the problems that come with burning of fossil fuels and also to decrease dependence on fossil fuels as a primary energy source. These include solar, wind and tidal power and nuclear. The other approach is use of efficient technologies to generate electricity such as combined heat and power system. As the focus on energy sustainability and environmental protection has increased over the years and the unquestionable reality of volatility of oil prices, governments around the world have been considering development of hydrogen economy, which is based on hydrogen as an energy carrier (Hinnells, 2008). This is a strategic move towards the development of sustainable energy systems, which will reduce the greenhouse gas (GHG) and ensure security of energy supply.

The concept of hydrogen economy can be explained as a long term effort to change the current energy system that is based on fossil fuel burning, to one which uses the energy of hydrogen in high efficiency conversion technology such as fuel cells. Hydrogen is the most abundant element

known, although it is not an energy source itself, it is an energy carrier that is bounded up in many compounds such as water, natural gas, oil, coal and many others (Blanchette Jr, 2008). Today hydrogen is produced from steam reforming of natural gas and petroleum. This process emit significant amounts of carbon dioxide into the atmosphere, however, when combined with carbon capture and sequestration technologies designed to reduce CO_2 emissions, it can produce an ample fuel that can help to guide global climate change (Marbán and Valdés-Solís, 2007). Hydrogen can also be produced by lesser carbon dioxide emitting process such as electrolysis and renewable (wind, solar and geothermal).

The conversion of primary fossil fuels, such as coal and gas to electricity is a relatively inefficient process. Most of the energy used in the conversion process is released to the environment as waste heat; this is easily recognisable on power station cooling towers. For instance, in UK, power stations reject more energy as waste heat than is consumed by the entire domestic sector (Institution of Engineering and Technology, 2007). This huge loss motivated the development of combined heat and power (CHP) system, also known as co-generation, to recover and make use of this heat, and significantly raising the overall efficiency of the conversion process. Most of the heat wasted in electricity generation is carbon based, so if CHP systems could be more widely used there is potential significant energy, environmental and economic benefits that could be realised.

Combined heat and power systems based on fuel cells offer high efficiency, low emission, and decentralized power and heat supply for buildings and industries. Such system also offers reliability and availability; a significant long term reduction in the cost of energy and an overall increase in system efficiency because of the effective use of heat at the point of use (Hongbo and Weijun, 2010). There is considerable interest in installing CHP systems in domestic properties; called micro-CHP (Hongbo and Weijun, 2010). These systems could serve a single house-hold producing between 0.5 kW_e and 10 kW_e. Globally, pre-commercial projects have been initiated for the implementation of micro-CHP systems on the larger scale. According to Hongbo and Weijun (2010) five countries; Japan, Germany, UK, the Netherlands, and USA are most active in the research and development of micro CHP systems. With Japan having deployed more than 10,000 cumulative units by the end of 2010, providing home power and heating (Fuel Cell Today**,** 2011).

Platinum and its sister metals – palladium and rhodium collectively known as platinum group metals (PGM) are at the forefront of clean energy conversion. About 90% of cars that are produced nowadays are fitted with catalytic converters containing PGM and have resulted in

reduced green-house gases emissions. The PGM, particularly platinum, are also at the centre of fuel cell technology as most fuel cells utilise the metals as electrocatalysts. As projections have shown that there is no effective, efficient and cheaper alternative to PGM catalysis in fuel cells, this presented an opportunity for South Africa because of its reserves of the PGM which is about three quarters of global reserves (Mehlomakulu, 2010).

Towards this end, in 2007 the South African Department of Science and Technology (DST) launched the Hydrogen and Fuel Cell Strategic Plan that would see South Africa move towards developing a knowledge based instead of a resource based economy. This would see the country playing a role in the fuel cell market by producing and exporting key fuel cell components and systems instead of the status-quo of exporting the crude platinum metal, and in the process significantly increasing its human capital development.

1.2 Combined Heat and Power System

Combined heat and power (CHP) or co-generation can be simply defined as the simultaneous generation of electrical and thermal energy in a decentralized manner. This simultaneous production increases the utilization of the fuel energy which would have been otherwise released to the atmosphere as waste heat in conventional power generation plants. There is also a reduction in power lost through transmission to the end user in centralised power generation. The increase in fuel utilisation is achieved by capturing the “waste heat” released by the combustion or catalytic conversion of the fuel to produce hot water in domestic CHPs or steam industrial CHPs.

The main components of CHP systems are an electrical/energy generator, a supplementary thermal recovery system, heat exchangers and control instruments. The types of commercially available and widely researched CHP generation systems are classified based on their prime mover and source of energy (Hinnells, 2008). These are:

- ***Internal combustion engine based CHP systems*** - These systems use the same engines used in vehicles. Depending on the type of engine, the systems use either natural gas or diesel as a primary fuel. The overall efficiency of CHP systems based on internal combustion engines is in a range of 85 to 95% with the electrical efficiency ranging from 28 to 39%.

- ***Micro gas turbine based CHP systems*** – This is similar to the conventional turbine used in centralised power generation in coal fired plant but is at much more smaller scale. The electrical efficiency of micro-turbine systems is about 30% and the overall efficiency of these systems have been reported to be 80% and above.

- ***Fuel cell based CHP systems*** – The distinct advantages that fuel cell based system have over other technologies are low emissions, low noise level, and they are more receptive to changes in thermal demand (Staffell, 2009). Because of the immature technology the fuel cell systems have high capital cost (Staffell, 2009). They can offer about 85 to 90% overall efficiency and an electrical efficiency in the range of 30 – 60%.

- ***Stirling engine based CHP systems*** – these systems are similar to internal combustion engines systems except that the fuel is not combusted internally. The electrical efficiency of these systems is at 40% and the overall efficiency of the CHP system is reported to range from 65 to 85%.

1.3 Motivation for the study

For combined heat and power systems based on fuel cells to be commercially viable much effort is needed to understand the system and the parameters that have influence on its performance. Fuel cell systems have many parameters, which can have a range of possible values that may influence the performance of the systems. It would be quite costly and time consuming to experimentally investigate each parameter independently or all the possible combinations. Because of this, alternative ways like modelling have been sought.

Modelling provides alternatives to physical testing and hence speeds up the screening of design alternatives and eventually eases the task of integrating engineering design process. In fuel cell systems there are multiple complex phenomena occurring and various interacting components which need to be considered when designing and in optimization. Modelling can be an important research tool to study this. In order to optimize the overall design (with respect to cost and efficiency) and operation (in terms of lifetime or durability), it is necessary to develop laboratory scale prototype CHP-systems and accurate modelling tools. *HySA* Systems, a competence centre for hydrogen and fuel cell technology established at the University of the Western Cape, will be developing prototypes to test and validate various CHP-system configurations. This modelling study is closely aligned with this hardware development.

1.4 Objectives of the study

The focuses of this research is to developing a model for high temperature polymer electrolyte membrane fuel cell for combined heat and power systems and thus integrate it with other models for the other components of a CHP system. The purpose of the study is to develop a model that will describe steady state operation of the fuel cell stack. The specific objectives are to:

- Develop a model that describes thermodynamic and electrochemical behaviour of the PEMFC stack.
- Validate the model using data from a single cell operated with pure hydrogen.
- Simulate the validated models to investigate effects of different fuel cell parameters and variables on single, stack and CHP system performance.

1.5 Approach

- **Model development** – Equations that describe thermodynamic and electrochemical phenomena of the PEM fuel cell were gathered from literature.
- **Computation** and Simulation – A code to solve the system equations were generated and implemented using EES. The intention was to compute cell polarization curves at different operating points for validation purposes.
- **Validation** – Validation of a model is important because a model must be validated to some degree to be a useful and credible. The model was validated using data from Sousa *et al*., (2010)
- **Parametric Studies** – When the model validation was completed, it was used to investigate different parameters for a single cell. In this study the effects the following have on the overall cell performance were investigated: catalyst loading, amount of CO in fuel, current density, temperature and acid doping level. The model was further used to study the engertic outputs of a 1 kW stack and 1 kW CHP system with fuel processor.

1.6 Statement of Purpose

Most of the HT-PEM fuel cell models are mathematically complex and require heavy programming of commercial modelling software for simulations. The purpose of this work is to

develop a model that is simple and yet accurate without having to use complex mathematical model. The model developed must be simple enough to be incorporated into to a CHP system model.

1.7 Thesis Outline

- Chapter 1 gives the background of the research project, an overview of micro-CHP systems. The objectives of the dissertation are outlined and the primary methodology used is presented.
- Chapter 2 provides background information regarding the governing principles of fuel cells, a concise description of the six well established fuel cell technologies together with a comparative analysis of the types of PEMFC technology leading to the particular choice of PEMFC used in this work, the HT PEM fuel cell. A review of selected work done on fuel cell modelling that will be used as basis of the modelling work presented in this project is also given.
- Chapter 3 shows the development of the model, model validation and simulation results for a single cell
- In chapter 4 an energy model for a multiple cell stack is developed and a parametric analysis of the stack is presented.
- Chapter 5 the multiple cell stack model is incorporated with a fuel processor model forming a CHP system. A multiple parameter sensitivity analysis of the CHP system is also presented in this chapter
- Chapter 5 summarizes the work done; concluded on the research and outlines recommendations for future work.

CHAPTER TWO
LITERATURE REVIEW

2.1 Fuel Cells Systems

A fuel cell is an electrochemical reactor that converts chemical energy of a fuel directly into direct current (DC) electricity by oxidizing a fuel. Fuel cells are similar to batteries in that they both produce DC through an electrochemical process without direct combustion of a fuel. However, whereas a battery delivers power from a finite amount of stored energy, fuel cells can operate indefinitely provided that a fuel source is continuously supplied. At the heart of the fuel cell is an electrolyte sandwiched between two porous electrodes; a positive electrode (anode) and a negative electrode (cathode). The combination of the three layers is called the membrane electrode assembly (MEA). The electrodes are made porous so as to allow both the fuel and the oxidant to reach the catalyst layer. The catalyst layer is a thin interface between the electrodes and the membrane where electrochemical reactions occur.

The MEA is then sandwiched between collector plates for single cell configuration or between bipolar plates for multi-cell configurations. Fig. 2.1 depicts the operating principle of a fuel cell and the different layers of the MEA.The reaction occurring in a fuel cell is an exothermic reaction which means heat is liberated during the reaction. The heat produced is what makes fuel cells attractive for combined heat and power production. The electrochemical reactions occurring in the fuel cell depend on the type of fuel cell but the overall reaction is the opposite of electrolysis

$$H_2 + \tfrac{1}{2} O_2 \leftrightarrow H_2O \tag{2.1}$$

This equation occurs in two separate half reactions that take place simultaneously at the anode and cathode. A hydrogen rich fuel is fed continuously to the anode where the hydrogen is oxidised into protons and electrons in a catalytic reaction. In hydrogen-air fuel cells, the protons diffuse through the electrolyte towards the cathode and the electrons travel through the external circuit where they produce electricity and complete the circuit by travelling to the cathode, where they take part in the cathode reaction. The anode-halve reaction is called the Hydrogen Oxidation Reaction (HOR) and is expressed as:

$$H_2 \rightarrow 2H^+ + 2e^- \tag{2.2}$$

At the cathode oxygen is supplied and it gets reduced by reacting with the protons and electrons from the anode to from water. The cathode halve reaction is called the Oxygen Reduction Reaction (ORR)

$$O_2 + 2H^+ + 2e^- \rightarrow H_2O \tag{2.3}$$

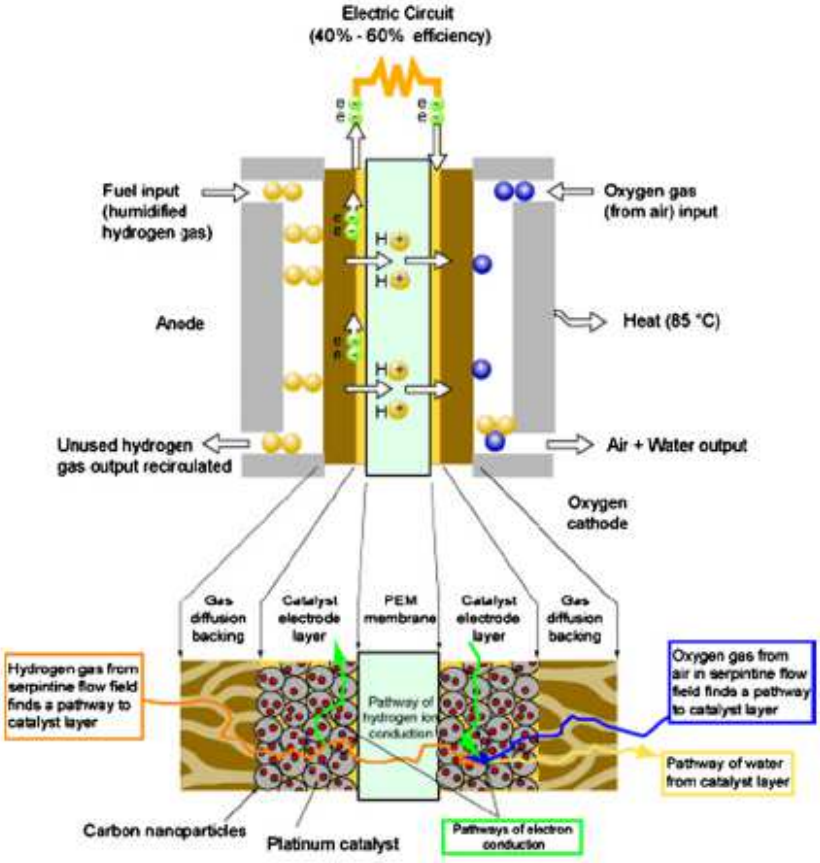

Figure 2.1: Operating principle of a fuel cell (Andújar and Segura, 2009)

2.2 Overview of fuel cell technologies

Fuel cells can be categorized in different ways; these include the type of electrolyte used, operating temperature and the type of fuel used (Li, 2006). However, fuel cells are named by the type of electrolyte used with the exception of direct methanol fuel cell. This is because the electrolyte determines almost every aspect of the fuel cell from operating principle, design and material of construction (Li, 2006). There are six well established fuel cell technologies and a comparative summary of these technologies is given in Table 2.1:

- **AFC:** Alkaline Fuel Cells
- **DMFC :** Direct Methanol Fuel Cells
- **PAFC:** Phosphoric Acid Fuel Cells

- **PEMFC:** Proton Exchange Membrane Fuel Cells
- **SOFC:** Solid Oxide Fuel Cells
- **MCFC :** Molten Carbide Fuel Cells

Table 2.1: A comparative summary of fuel cell technologies

Fuel Cell Type	PEMFC	DMFC	AFC	PAFC	MCFC	SOFC
Electrolyte	Polymer Ion	Polymer Ion	Potassium Hydroxide	Phosphoric Acid	Molten Carbonate salts	Yttrium stabilized Zirkondioxide
Temperature (°C)	Low : 30 - 80 High: 120-180	60 – 130	Low : 25 – 70 High : 150-200	150-200	650	600-1000
Fuels	H_2 / Reformate	CH_3OH	H_2	H_2 / Reformate	H_2/CO/ Reformate	H_2/CO_2/CH_4 Reformate
Catalyst	Platinum	Platinum	Platinum	Platinum	Nickel	-
Electrical efficiency (HHV)	40-50 %	35-40%	40-50 %	40-50 %	50-60 %	45-55 %
Power range (kW_e)	1 - 250	0.1-1	0.6 – 20	50-200	0.6-12	5 -1MW
Applications	-Portable -Stationary -Transport	-Portable	-Portable -Stationary -Transport	-Transport -Stationery	-Transport -Stationery	-Transport -Stationary

2.2.1 The Alkaline Fuel cell

Alkaline fuel cells are classified as low temperature fuel cells because of their relatively low operating temperature of 70 ^oC-130 ^oC. AFC was the first fuel cell technology that made the production of electricity from hydrogen to be feasible and was the first to be developed for practical applications (McLean *et al*., 2002, Verhaerta *et al*., 2009). Like most low temperature fuel cells one of the disadvantages of AFC is its intolerance of CO_2 (EG&G Technical Services, 2004:4-11). Consequently pure hydrogen (instead of hydrocarbon) and scrubbed or pure oxygen must be used as gas reactants in order to achieve longer lifetime operation (Crawley, 2006). Due to the required level of purity of reactant gases complex systems are required, this in turn increase the cost of the systems (EG&G Technical Services, 2004:4-11). In the early development stages AFC were used by NASA on space missions to produce electricity and water aboard a spacecraft. AFC nowadays are mainly used in niche transport applications such as forklifts, boats and submarines. They can achieve as high as 60 percent chemical to electrical conversion efficiency (Crawley, 2006).

2.2.2 The Direct Methanol Fuel Cell

Direct methanol fuel cells are a variant of PEMFC, the only difference being that for traditional PEMFCs hydrogen is used as a fuel instead of methanol. Direct methanol fuel cells are seen as the best approach for small portable fuel cell systems and there is a considerable research effort focusing on this area *(*Cowey *et al., 2004,* Kamarudina *et al.*, 2009, Krewer *et al*., 2004). They are used in niche applications such as mobile electronic devices (laptops and mobile phones) or chargers and in forklifts. This type of fuel cell is also classified as a low temperature fuel cell operating at temperature ranges of 60 ^{o}C to 130 ^{o}C with up to 40% efficiencies. The DMFC uses pure methanol as a fuel, which eliminates the need for fuel reforming and it is easy to refuel the cell (Kim *et al*., 2006, Schulze *et al.*, 2004). The other advantage of DMFC systems is the ease of handling of methanol as compared to the handling of hydrogen used in other fuel cell systems.

2.2.3 The Proton Exchange Membrane Fuel Fell

Of all types of fuel cells, proton exchange membrane fuel cells (PEMFC) are the most popular and most widely researched and developed. The fuel used in PEMFC can either be directly fed into the fuel cell, or sent to a reformer to produce pure hydrogen, which is then directly fed to the fuel cell. PEMFC systems are available from a few kilowatts up to 250 kilowatts. Excluding the DMFC, there are two main type of PEMFC: these are the low and high temperature PEM fuel cells. The low temperature operates between 30^{o}C and 80 ^{o}C and the high temperature PEM operates between 120 ^{o}C and 180 ^{o}C. The main difference in the components of the two types is the electrolyte used. The low temperature PEMFC uses a perfluorinated sulfonic acid membrane and the high temperature PEMFC uses acid doped polybenzimidazole (PBI) membranes as electrolyte (Crawley, 2006). PEM fuel cells were primarily used for automotive applications, but are now strong candidates to for small-scale distributed stationary power generation, and portable power applications (Andújar and Segura, 2009).

2.2.4 The Phosphoric Acid Fuel Cell

Phosphoric acid fuel cell (PAFC) were the first commercially available fuel cell systems and have since enjoy a wide spread installations around the globe, making them the mainstream commercial fuel cells available (Larminie and Dicks, 2003:16). They use concentrated

phosphoric acid (~100%) as the electrolyte. The poly-phosphoric acid is usually stabilized in a SiC-based matrix and the catalyst used on both the cathode and anode is platinum. Phosphoric acid fuel cells are used for distributed power generation in commercial buildings for cogeneration and as uninterrupted power supply systems. They have electrical efficiency of about 40% and up to 85% efficiency in cogeneration systems (Andújar and Segura, 2009). One of their major advantages is the tolerance of about 30% carbon dioxide, thus allowing the use of air directly from atmosphere. The major challenge caused by their use of corrosive acid electrolyte which give rise to safety and handling problems.

2.2.5 The Molten Carbonate Fuel Cell

Molten carbonate fuel cells (MCFC) use a molten salt electrolyte of lithium and potassium carbonates, which is retained in a ceramic matrix of $LiAlO_2$ and operate at about 650 ^oC. The high temperature means that a good reaction rate is achieved by using a comparatively inexpensive catalyst like nickel (Larminie and Dicks, 2003:16)**.** MCFC can utilize crude hydrocarbon fuels directly without external reforming; external reforming is not needed because the temperatures at which MCFC operate are above the temperature at which steam reforming occurs. The fuel is therefore reformed inside the fuel cell in a process known as internal reforming, which eliminates the need for expensive reformers (Larminie and Dicks, 2003:16). These fuel cells are used in large power generation plants in the range of megawatts capacity for electrical and cogeneration purposes. They offer electrical efficiency of up to 60% electrical and about 80% when used in cogeneration systems.

2.2.6 The Solid Oxide Fuel Cell

Solid Oxide fuel cells (SOFC) are completely made of solid materials and are simpler in design than other fuel cell technologies. They are classified as high temperature fuel cells operating at between 600 ^oC to 1000 ^oC. The high temperature operation means that there is no requirement of precious metal catalysis and allows for a variety of hydrocarbon fuels to be used. The two main configurations of SOFC are tubular and planar (flat). Planner designs are similar to other fuel cell designs, the reactants flow through channels in the cathode and anode. In tubular designs the inside of the tube is the cathode where air is supplied, and the other components are built around the tube (Andújar and Segura, 2009). SOFC are used in both large and small scale power generation plants for cogeneration. Similarly to MCFC they offer electrical efficiencies of up to 60 percent and over 80% when used in cogeneration systems.

2.3 PEM Fuel Cell Structure

In this section the structure of a single cell PEM fuel cell and its main components are described. A single cell consists of two bipolar/current collector plates and the membrane electrode assembly as shown in Figure 2.2. The MEA is made of five components: anode gas diffusion layer, anode catalyst layer, membrane, cathode catalyst layer and the cathode gas diffusion layer.

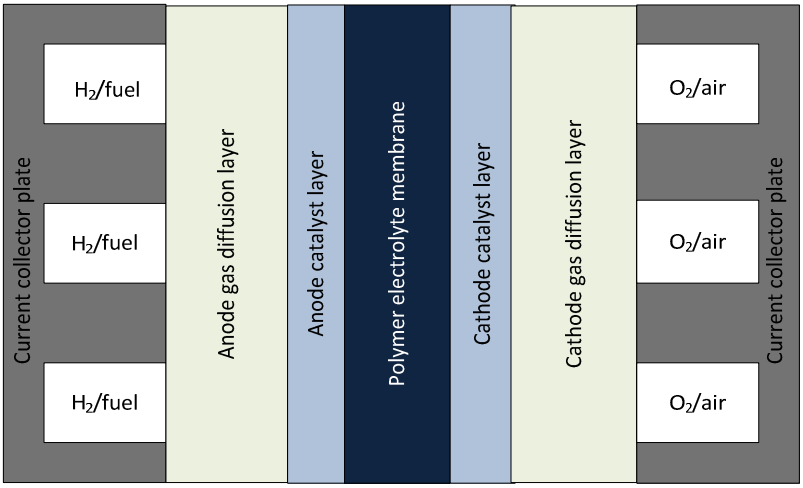

Figure 2.2: Two-Dimensional Cross section of a single PEM fuel cell

2.3.1 Gas Diffusion Layers

The gas diffusion layer (GDL) is a thin porous layer found between the catalyst layer and the current collector/bipolar plate. It is made of porous material such as carbon paper, woven paper or carbon cloth (see fig. 2.3). They are made porous in order to facilitate reactant species transport from flow channels to the catalyst layer and the reaction product from the catalyst layer back to the flow channels. The species are transported mainly by diffusion and to some extent by convection given that there is a pressure gradient between the GDL and the flow field channels (Songprakorp, 2008).

The gas diffusion layer also serves as media to transport electrons from carbon support of the catalyst layer to the current collector plate. The GDL must necessarily exhibit low resistivity to conduction of electrons hence it is made to be as thin as possible in range of 100-400 µm. They

also conduct heat produced in the catalyst layer to the current collector plate. As mentioned above, the reactant product needs to be removed from the electrodes, gas diffusion layers are made hydrophobic so as not to allow water to accumulate in the electrode. The hydrophobic nature is achieved by treating the GDL with hydrophobic materials such as Teflon (Barbir, 2005).

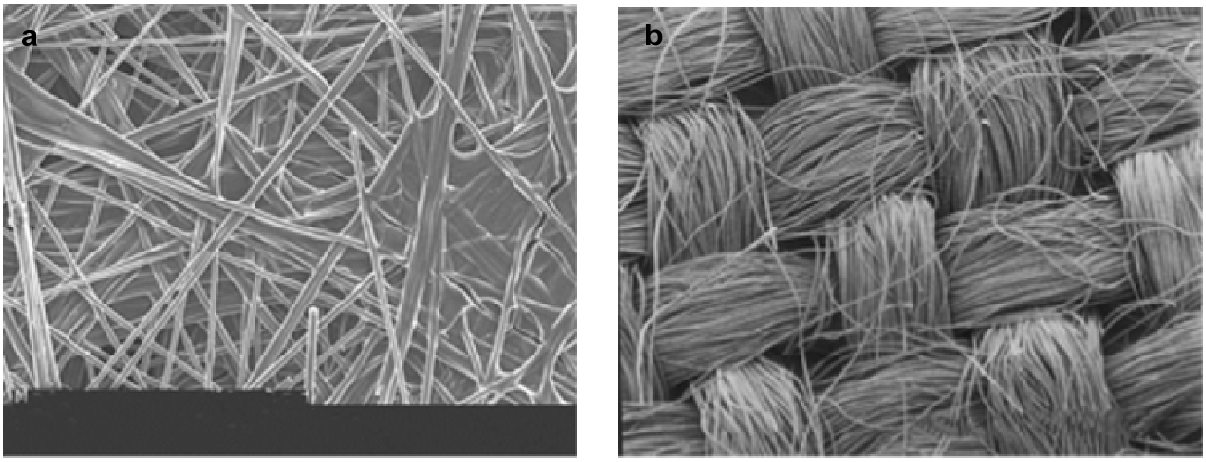

Figure 2.3: SEM Micrographs of two gas-diffusion-media substrates, (a) Carbon fiber paper, Spectracorp 2050A (b) Carbon cloth, Textron Avcarb 1071 HCB. (Adapted from Mathias et al., 2003)

The most important characteristics of gas diffusion layers are its thickness, porosity and electrical conductivity. Thinner GDL allows for better mass transport and have less resistance to electrical conductivity. Porosity also improves mass transport for reactants and products. A high porous GDL is preferable; however, there is a limit to porosity as this also decreases conductivity (Larminie and Dicks, 2003). A balance of porosity, thickness and conductivity should be reached in order to have good performance from the fuel cell.
In summary, the gas diffusion layer serves the following purposes:

- Provide reactant path-ways to the catalyst layer
- Conducts electrons to and from the current collector plates
- Gives structural rigidity to the catalyst layer
- Provides path-ways for products to the gas flow field channel

2.3.2 Membrane

The electrolyte is arguably the most important component of a fuel cell, because the characteristic of a fuel cell which include operating temperature and construction depend on the

type of electrolyte employed (Li, 2006). There are two types of electrolyte membranes used in PEM fuel cells and they are both function of the operating temperature of the fuel cell. The first type is made of perfluorocarbon-sulphonic acid monomers (PSA) used in PEM fuel cells operating below 90 ^{o}C. The chemical structure of these PSA groups of electrolytes comprises of the back bone, the side chains and the acidic end group (shown in figure 2.4(a)).The second group is made from acid doped polybenzimidazole (PBI) membrane and is used when the stack operating temperatures are between 120 – 180 ^{o}C and its chemical structure is shown in Figure 2.4(b). The primary objective of the electrolyte is to separate the anode electrode from the cathode electrode and to act as a salt bridge, conducting protons from the anode to the cathode. This means the electrolyte should exhibit good proton conductivity and should prevent reactant crossover from electrodes. Good proton conductivity is essential to reduce resistance to proton conduction, and limiting the voltage losses associated with this resistance. Electrolytes must be thin (ranging from 20 – 80 µm) and are made to be mechanically and chemically stable to be able to survive in the strong oxidation environments they are exposed to (Barbir, 2005).

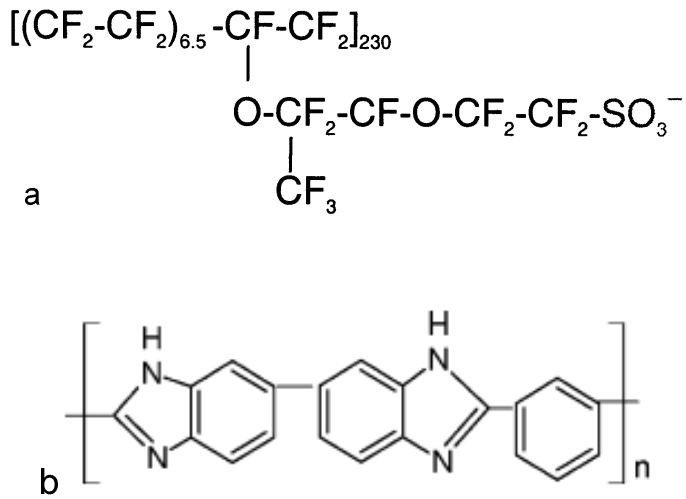

Figure 2. 4: (a) Molecular structure of NAFION 117 (Adapted from(Haubold *et al*., 2001)), (b) Poly 2,2-*m*-(phenylene)-5,5_-bibenzimidazole (Adapted from(Li *et al*., 2009))

2.3.3 Catalyst Layer

The catalyst layer of a PEM fuel cell is a micro porous structure of carbon particles impregnated with the electrolyte. Both the hydrogen oxidation (HOR) and oxygen reduction (ORR) reactions are catalytic reactions and hence the catalyst is there to promote these electrode half reactions. For these reaction to occur all three species (electrons, protons and gases) must have access to the catalyst surface. The protons travel through the monomer, so the catalyst should be in

contact with the monomer. The gases travel through voids; therefore the electrodes need to be porous and the electrons travel through electrically conductive solid so the catalyst must be electrically connected to the substrate.

The widely used catalyst for both the ORR and HOR is platinum. The platinum catalyst is finely dispersed on the carbon particles, which also serves as electric transport media as can be seen in figure 2.5(b). The catalyst layer is either applied to the membrane or onto the side of the GDL in contact with the electrolyte, either way; it must be attached to the electrolyte in order to access the reactants. In the latter case hot pressing is required to ensure good contact between the monomer in the catalyst layer and the membrane (Litster and McLean, 2004).

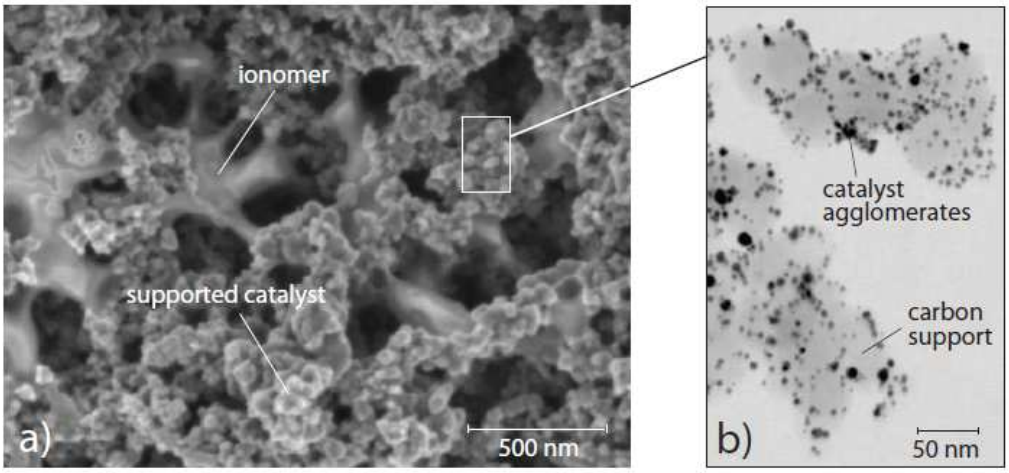

Figure 2. 5: Structure of a PEMFC catalytic layer; a) SEM-micrograph of the impregnated carbon structure, b) TEM-micrograph of the carbon support with dispersed catalyst agglomerates (adapted from Reum, 2008)

In the electrode the reactions are considered to proceed through all of the following elementary steps:

- Bulk flow and diffusion of reactant molecules through large electrode pores.
- Adsorption of molecules on reaction site viz. platinum or platinum alloy catalysts.
- Discharge of ionic species, proton to electrolyte.
- Surface reactions between adsorbed molecules, discharged ions or radicals.
- Desorption of products and transport into the electrolyte or pores.

2.3.4 Bipolar Plates

PEM fuel cells are normally constructed in multiple cells that are connected in series using bipolar plates/current collector plates. These components ensure that there is a net drain of electrons and heat from each cell in a stack. Their function includes:

- Distribution of reactant gases within the cell
- Separates individual cells in a stack
- Removal of products from the cells
- Conducts electrons to the external circuit
- Provides structural rigid to the cells in a stack

From the above functions it can be seen that the key properties of bipolar plates are good electrical conductivity, low gas permeability, mechanical and thermal stability. Furthermore, because they form 80% (mass) of a fuel cell (Murphy *et al*., 1998), they should be made thin and light for minimum stack volume and weight respectively (Larminie and Dicks, 2003:96). One other important feature is the layout or topology of the flow field structure, which ultimately direct the quality of the gas distribution into and across the cell area. The choice of bipolar plates is based on the requirements of flow field, materials and system requirements.

Materials: The types of materials from which bipolar plates are manufactured from are; metal plates, graphite and composite materials. Table 2.2 gives an overview of these types and their properties. Graphite plates are made from either natural or synthetic graphite. They have good chemical stability to survive in the acidic fuel cell environment. They also exhibit good electrical conductivities as well as low contact resistance to the GDL, since they are made from similar material. Their shortcomings are high cost, low mechanical strength, high gas permeability and the need for machining to form the flow fields (Hermann *et al*., 2005).

Alternatively thin metal plates can be used, which have an advantage of good mechanical stability, high electrical and thermal conductivity, and low gas permeability. The highly corrosive and acidic environment of fuel cells (pH 2 to 3 and temperature 60^{o}C - 180 ^{o}C) would lead to corrosion and dissolution of the metal plate, thus poisoning the reaction environment. To avoid this metallic plate are normally coated with protective coating layers.
To get the best of both the metallic and graphite plates, a composite material made from both have been used to produce bipolar plates. This concept combines the advantages of both graphite (corrosion resistance) and metallic plates (impermeability and structural rigidity), and results in a lightweight, durable, and easy-to-manufacture bipolar plate.

Table 2.2: Types, materials and properties of flow field plates for PEMFC (adapted from Reum, 2008)

TYPE	Metal	Graphite	Composite
MATERIAL	- noble metal coated Al, Ni, Ti - stainless steel	- flexible graphite - sintered carbon	- metal based (layered structure, polycarbonate) - carbon based (raisin w. carb. filler, fibre backing)
ADVANTAGE	- mechanical stable - low resistance	- low contact resist. - chemical stable	- low density - chemical stable
DISADVANTAGE	- expensive coatings - corrosive (uncoated)	- high permeability - unstable, brittle	- expensive and complex machining - low conductivity

2.4 Fuel cell performance

The performance of a fuel cell is measured using a graph that shows the current -voltage characteristics. The graph is called the polarisation curve and it relates the output (voltage) as a function of input (current density). Operational fuel cells are made of single cells connected in series in order to get higher voltages from the stack and because of this the polarisation curve is normalised so as to get comparable performance for stacks with different number of cells or voltage output. Typical characteristics of voltage and current density of a PEM fuel cell is shown in Figure 2.6.The initial drop of voltage in the performance curve of a fuel cell is due to sluggish electrode kinetics, particularly the oxygen reduction reaction in the cathode. The rapid drop in performance depends mostly upon the operating temperature of the stack. A visible change in the curve is noticeable for high temperature fuel cells like SOFC and MCFC, as there is no rapid fall in the performance curve (Larminie and Dicks 2003). The electrode kinetics gives rise to an operational fuel cell voltage loss known as activation polarization, which is dominant in the low current density region. The concept of activation polarization will be discussed in detail in chapter 3.

After the rapid fall of the cell voltage, the voltage drops further as more current is drawn from the fuel cell. The second part of voltage drop is linear with the current density and is mainly due to two resistances in the cell; the resistance of flow of electrons through the electrode and the

resistance of flow of ions/protons through the electrolyte/membrane. This linear drop in performance obeys ohms law of resistance and is referred to as the ohmic polarization. The ionic resistance is mainly influenced by the conductivity of the electrolyte and the electric resistance by the conductivity of the electrode; these will be discussed in details in chapter 3.

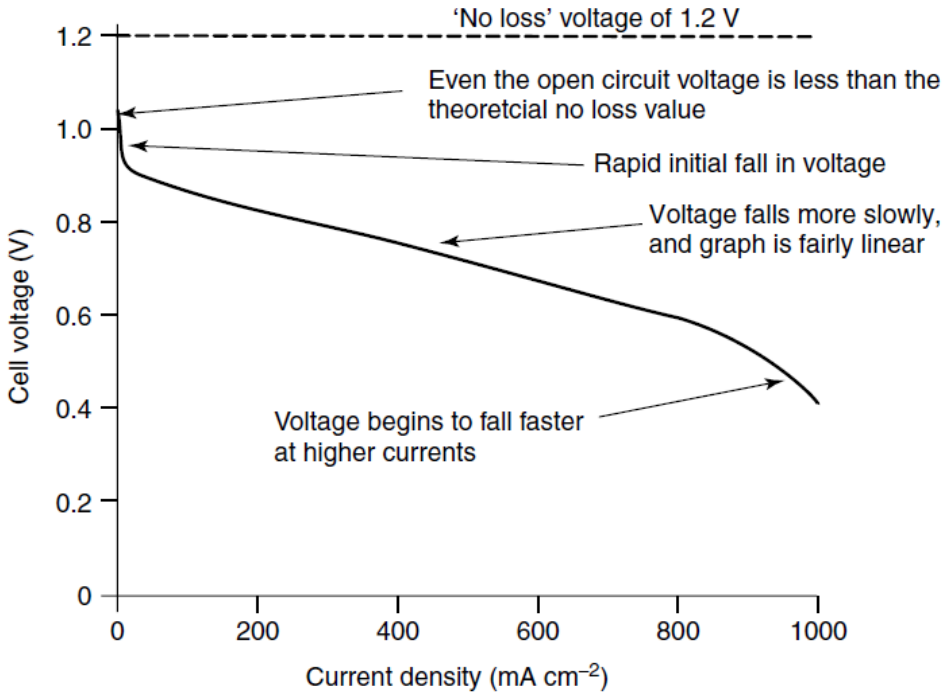

Figure 2. 6: Typical voltage losses in the PEM fuel cell (adapted from Larminie and Dicks 2003)

The last rapid voltage drop in the performance curve is due to reactant/mass transport limitations in the fuel cell. This arises when the reactants in the catalyst layers are consumed faster than they are supplied, thus causing a concentration gradient. The mass transport limitations can be caused by a number of phenomena occurring in the fuel cell electrode such as electrode flooding. This is referred to as concentration polarization and is prevalent in the high current density region of an operational fuel cell.

2.5 Low Temperature PEM Fuel Cell

Low temperature PEM fuel cells (LT PEMFC) are characterised mainly by their lower operating temperature and the polymer membrane used as electrolyte. There are different types of these polymer membranes that can be used in this type of fuel cell, but they are all characterised by one common property i.e. the need for liquid water in the membrane matrix for proper proton

conduction. The widely used membrane which has come to be the bench mark is a polymer electrolyte (Nafion®) produced by Du Pont. These polymer electrolytes exhibit good proton conductivity given that they are adequately humidified. When the electrolyte is dehydrated the conductivity of membrane decreases and this results in decreased performance of the fuel cell stack. Too much hydration also becomes a problem as the water droplets tend to accumulate in the gas flow channels thus decreasing reactant transport (Litster and McLean, 2004). It is therefore required to strike a balance in humidification for good performance. Although there are different methods of predicting and mitigating membrane dehydration and flooding, this still remains as an area of concern in this technology (Mérida *et al*., 2006). Figure 2.7 shows performance curves for different commercially available fuel cells.

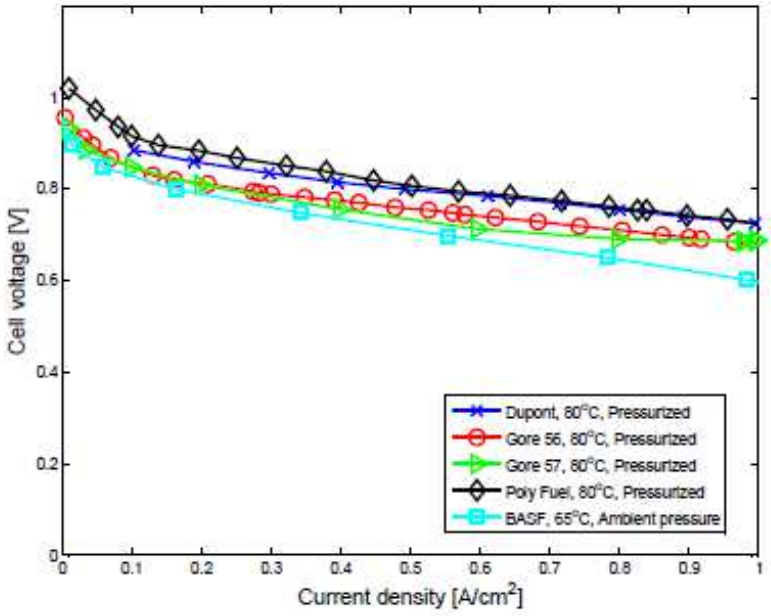

Figure 2. 7: Polarization curves for low temperature PEMFC (adapted from Andreasen, 2009)

Low temperature PEM fuel cells are intolerant to carbon monoxide traces in a fuel, requiring a percentage that is less than 100 ppm. The heat produced from the reactions generally needs to be removed so as not to degrade the fuel cell components. LT PEM fuel cells produces heat at about ± 90 ^{o}C, for this heat to be successfully removed, it requires complicated cooling systems as the temperature gradient between the fuel cell stack and the surrounding environment is small. The advantages and disadvantages of low temperature PEM fuel cells are listed below:

Advantages

- Fast start-up time
- Well known and established technology

- Higher operating voltage

Disadvantages

- Low operating temperatures leads to larger cooling areas resulting in complex cooling systems
- Requires high catalyst loading because at low temperatures the reaction kinetics are slower
- Complicated water management within the fuel cell stack due to the presence of liquid water
- Complicated fuel processor needed for reformate fuel operation (more system components to reduce carbon monoxide percentage)

2.6 High Temperature PEM Fuel Cell

The hydration requirement for LT-PEM fuel cell for better conductivity leads to a need for complex humidification systems. The low temperature operation also requires large cooling surface areas thus leading to complex cooling systems. Furthermore, the intolerant behaviour to carbon monoxide in the anode at low temperatures limits the use of reformate fuel. This is important as hydrogen is currently largely produced from fossil fuels through reforming. All the above short comings of LT-PEM fuel cell technology led to the development of alternative polymer electrolytes that does not depend on liquid water level for conductivity, thus allowing operation at temperatures above 120 ^{o}C called High Temperature PEM fuel cells (HT PEMFC). This does not only increase the operating temperature of the stack, but also the reaction kinetics gets accelerated at high temperature. The high temperature operation also results in a higher temperature gradient between the fuel cell stack and the ambient environment, thus leading to less surface area for cooling. Acid doped polybenzimidazole membranes are used as electrolytes in HT-PEM fuel cells. Figure 2.8 shows performance curves for different commercially available HT-PEM fuel cell stacks.

As about 40 – 50% of the energy produced by the fuel cell is heat, operating at elevated temperatures would result in a higher quality heat being produced. This is important for cogeneration as this heat would increase the overall efficiency of the fuel system. The higher operating temperature also results to increased diffusion of reactants in the GDL and catalyst layer, this can also results in better performance of the fuel cell stack (Zhang *et al*., 2006). The advantages and disadvantages of high temperature PEM fuel cells are listed below

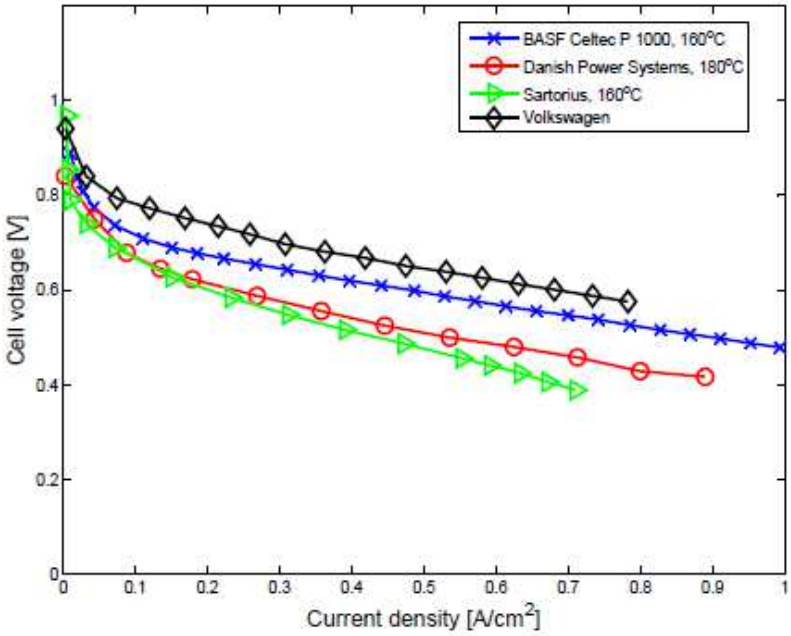

Figure 2. 8: Polarization curves for high temperature PEMFC (adapted from Andreasen, 2009)

Advantages

- Improved reaction kinetics
- Improved tolerance to catalyst contaminants
- Improved water management
- Improved species transport
- High quality heat produced
- CO tolerance reduces complexity of fuel processor system

Disadvantages

- Faster component degradation
- Longer start-up time

2.7 PEM Fuel Cell Technology of Choice

By looking at the performance curves of both the low temperature and high temperature PEMFC one might fancy choosing the former because of its higher voltage and power density. This would be correct if the desired application needed high power density (such as for mobile applications), however, for the required application (CHP system) this is over weighed by the advantages of high temperature operation. Operating at high temperatures (120-180 ^{o}C) would

mean tolerable amounts of CO in fuel, allowing reformate fuel use and thus reducing the fuel processing unit (see fig. 2.9). The preferential oxidation reactor (for CO cleaning) which is required in LT-PEM fuel cell would be phased out; this simplifies the system and reduces paratactic losses of energy that comes with additional components. Secondly, the high quality heat produced at high temperatures can be used for cogeneration thus increasing the overall system efficiency.

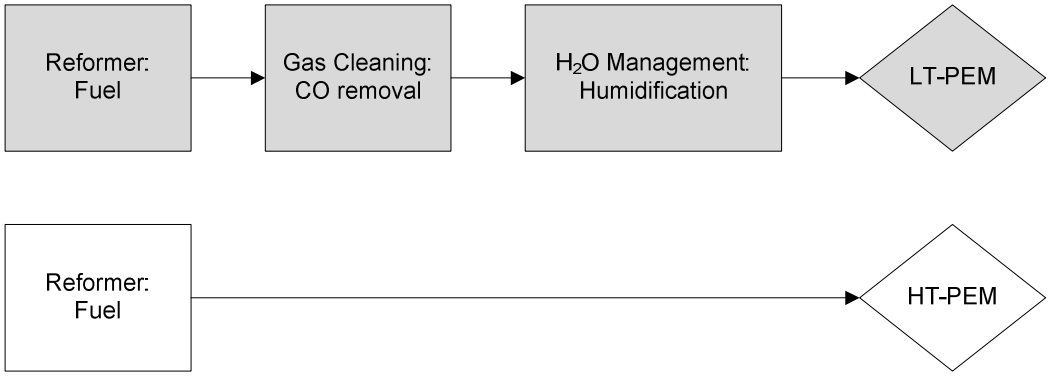

Figure 2. 9: Compares the simplicity of HT- PEM system to LT-PEM system

2.8 Modelling of PEM fuel cells

Models play an important role in fuel cell development because they facilitate a better understanding of parameters affecting the performance of fuel cells and fuel cell systems. The modelling approaches in literature are classified into three main categories: a) theoretical (sometimes referred to as 'mechanistic'), b) semi-empirical, and c) empirical. The level of complexity increases from the lowest for empirical models to the highest for theoretical models. A further classification is made for each approach, which indicates whether the model accounts for steady-state or dynamic phenomena, or both.

Steady-state models describe the performance of a fuel cell at a single operating point, i.e. at a single cell temperature and reactant pressure. These models are primarily used to make predictions that are validated with laboratory test results. On the other hand, dynamic models are used to predict performance of fuel cell when there is a change in operating parameters. These are particularly useful in analysis of start-up and shutdown portions of operating cycle of fuel cell and also optimization of response time to changes in load (Haraldsson and Wipke, 2004).

Theoretical cell models are constructed from partial differential and algebraic equations that are solved either numerically or analytically to determine the fuel cell polarization curve. These models make use of equations such as the Nernst-Planck equation for species transport, the Butler-Volmer equation describing electrochemical cell voltages and the Stefan-Maxwell equation governing gas phase transport. Empirical models are based entirely on experimental data; their predictive outputs match the experimental values almost exactly (Haraldsson and Wipke, 2004). These models are only valid for the specific fuel cell or stack for which the experimental data was obtained. Semi-empirical modelling combines theoretically derived differential and algebraic equations with empirically determined relationships. Empirical relationships are employed when the physical phenomena are difficult to model or the theory governing the phenomena is not well understood (Cheddie and Munroe, 2005).

Kim *et al* (1995) presented an empirical model to account for the cell overvoltage over the entire voltage range. Their analytical expression was able to fit the experimental polarization curves exactly. The main goal of their work was to investigate the departure of the previous model predictions from linearity of the polarization curve in the region of high current density (>500 mA/cm^2). They showed that change in potential varies linearly with the natural logarithm of current, and thus change in potential can be expressed as an exponential function of current density. Their results showed an exact fit of the predicted results with the experimental results at different temperature, pressure and oxygen composition in the cathode gas mixture. They included an exponential term to account for the polarization caused by mass transport limitations in the high density region. Models prior to the one developed by the authors predicted polarization curves for special case, for instance when the electrode reactions are either activation and ohmic or ohmic and mass transport controlled (Kim *et al*., 1995).

After these earlier models a lot of modelling work has been done in LT PEMFC, these models have been used by different researchers to investigate different phenomena occurring within the fuel cell, these include; water management which is one of the most challenging phenomena in these type of fuel cell, reactant gas transport, electrochemical performance, membrane degradation amongst others.

Fewer publications have been made in modelling of PBI based PEMFC as compared to the work published for Nafion® based PEMFC. Kosgaard *et al.* (2006) presented a semi empirical model to express the polarization of a fuel cell. In their work they assume the anode polarization is negligible for pure hydrogen operation and they derived linear regressions for diffusive

resistance, ohmic resistance, charge transfer and an exponential regression for exchange current density. The authors presented experimental results showing performance effects related to cathode stoichiometric ratio versus temperature and the synthesis gas influence on anode polarization. Their experimental results showed that CO surface coverage is highly dependent on temperature, this could however not be predicted by their model as it neglected the anode polarization (Korsgaard *et al*., 2006). The modelling results indicated that the total ohmic losses were three times what the resistance of the membrane itself would predict which they believed to be realistic. This model is zero dimensional and because of its simplicity it can be used for CHP systems (Korsgaard *et al*., 2006).

Peng and Lee (2006) presented a three dimensional model that include mass, momentum, energy, species and charge transport in the PEM fuel cell. The electron transport equations were solved in the catalyst layer, current collector plate instead of being assumed to be constant throughout the cell. This gives more accurate predictions of electrode polarization and current density (Peng and Lee, 2006). The authors presented results comparing the numerical solutions with experimental data, which did not cover the whole current density region (did not extend to the mass transport region). Additional results showed the effects of temperature on the average current density, oxygen molar concentration and local electrode polarization distribution. They found that these decreased along the channel and the decrease is influenced by the decrease of reactants along the channel.

The model presented by Cheddie and Munroe (2006) is a one dimensional through the thickness of the MEA model. The domain of interest was the MEA excluding the gas flow channels i.e. anode gas diffusion layer, membrane and cathode gas diffusion layer. The authors were interested on how the cell behaves when air and oxygen are supplied as oxidants. They presented results showing how their model compared with results from literature. The results of the polarisation curve did not extend to the mass transport region. They argue that the limiting current conditions do not result from mass transport limitations but rather when the activation and ohmic losses equalled the reversible cell potential. The authors also present results showing the performance increases with increased membrane conductivity. The performance was shown to increase significantly by increasing conductivity from 1.87 S/m to 9.6 S/m, however when the conductivity was increases from 9.6 S/m to 17 S/m there was no significant change in the performance of the cell.

Cheddie and Monroe (2007) extended their work on the previous model to make it a two dimensional, two phase model which was the first comprehensive model for PBI based PEMFC. The model included transport of mass, momentum, gas species, electrons and protons within the MEA. A no slip boundary condition was applied at the gas channels and a there were phase changes between gaseous and dissolved species at the diffusion layer/catalyst layer interface. The comparison of the model results and literature results were presented by the authors. Simulation results show how the cell performance varies with membrane doping level, catalyst activity, dissolved gases in the electrolyte and absorption of phosphoric acid ions onto the catalyst sites.

Scott *et al*. (2007) presented a steady state, isothermal and one dimensional model using transport and kinetic equations. The model accounted for one dimensional electrode potential and reactant partial pressure distributions. This enabled predictions of the effects of temperature, pressure and gas composition on fuel cells voltages and power densities. The model was validated with experimental data from a single MEA that was prepared in-house. The model was used to simulate effects of catalyst loading and platinum to carbon ratio on the cell performance. The model predictions agreed with the experimental results, however this model did not account for the effects of crossover of reactants to the kinetics and thus the cell potential. In their experiments the fuel source used was hydrogen and this could limit predictions of the model in that it does not account for CO poisoning in the anode and since fuel cell CHP systems use a reformate gas as the fuel source this model cannot be ideal for use in a CHP system.

Bergmann *et al*. (2010) presented a predictive time dependent model to account for carbon monoxide poisoning effects in a HT-PEM fuel cell. The model was used to evaluate gas flows in the gas channels and GDL and to evaluate the electrochemistry of CO adsorption/desorption and electro oxidation on the catalyst surface. The temperature distributions in the cell were also determined by the model. The results presented by the authors include performance curve at different operating temperatures and the effects of CO on the performance of the cell. An increase in cell performance with an increment in temperature was observed and this, the authors argue, is due to a presence of a thin acid film in the catalyst layer which is strongly dependent on the operating temperature of the fuel cell. The simulation of the CO poisoning effect did not compare well with the experimental data; the model predicted a higher performance than the experimental results. This, the authors explained, is a result of the model being able to predict occurrence of electro-oxidation of CO in the anode catalyst layer, which reverses the CO effect on the cell. Dynamics of CO effects on the fuel cell were simulated by

introducing a pulse in the anode electrode. Their simulated results agreed well with experimental results, showing a fast drop in the current density after the pulse was introduced and it had a recovery time of about 17 min, showing the reversible nature of CO poisoning.

The model presented by Jiao and Li (2010) is a three dimensional along the channel model to investigate the effects of temperature, doping level and relative humidity (RH) in the cell performance. The authors used a semi empirical approach to determine the proton conductivity of the phosphoric acid doped PBI membrane by using Arrhenius Law and well known published experimental data. When validating the model against the experimental data from Li *et al.* (2001), good agreement between the results was obtained. The authors presented results showing the performance effects related to the membrane acid doping level, reactant stoichiometry, pressure, RH and temperature. They find that increasing the doping level, temperature and pressure have significant improvement on the cell performance. However, they caution that the thermal sensitivity of the PBI membrane decreases with increase of both temperature and doping level, and thus the maximum allowable temperature and doping level should not be exceeded. Their results also showed that there is no need for extra humidification of gases, as this does not significantly improve the cell performance.

Sousa *et al*. (2010) presented a two-dimensional agglomerate model that was solved along the channel; it included all fuel cell elements from anode to cathode gas channel. The solution domain was divided into nine sub-domains. The results presented by the authors compared simulation and experimental results for the whole current density region. The models results were generally in good agreement with the experimental results. Other results presented included the comparison of effects of porous media when air and heliox (mixture of O_2 and helium) were used as oxidants. They also presented the effects on cell performance when a reformate fuel was used, H_3PO_4 loading and gas channel effects.

Most of the models presented above are theoretically complex models that require programming platforms like fluent and CFD. The model presented by Scott *et al*. 2007 was simple but was limited to expressing the conductivity as a function of temperature. In this work, this model was taken as basis and the conductivity of the membrane was modified to include the effects of acid doping level.

CHAPTER THREE
SINGLE CELL MODELLING

3 Introduction

The purpose of this chapter is to describe the model equations governing kinetic phenomena inside the membrane electrode assembly (MEA) of a HTPEM fuel cell. The approach adopted and developed in this chapter is a one dimensional, through the thickness model that focuses on kinetics excluding transport phenomena inside the MEA. This approach is chosen because of its simplicity for implementation on Engineering Equation Solver (EES) modelling platform. The model framework is based on the isothermal model developed by Scott and Mumlouk (2009). In the model the hydrogen oxidation and oxygen reduction reaction kinetics are expressed using Bulter-Volmer equations, which allows for analysing the cell performance for different electrochemical surface area and catalyst loadings. The approached used by Cheddie and Munroe (2007) of using species solubility in phosphoric acid for expressing the membrane conductivity activity is used. In the following sections, a model is developed to calculate the cell voltage. In doing so, expressions to determine the electrode overpotentials (activation and ohmic) are presented. The chapter is divided into three sections. The first sections describe the models used to analyze the cathode electrode and the anode electrode, second section describes models used to analyze the proton exchange membrane and the last sections describes models to calculate the thermodynamic equilibrium potential.

3.1 Assumptions

- Scott *et al.,* (2007) showed that the resistance to mass transfer in the GDL was small, and for this reason the mass transport limitations on the operational fuel cell are ignored in this model.
- Because the fuel cell operates at temperature above 120 ^{o}C, single phase flow is assumed. The gases are assumed have ideal gas behaviour.
- The basic nature of the model allows for isothermal operation assumption.
- The membrane is assumed to be impervious to gases and the voltage losses associated with reactant crossover is therefore ignored.
- A steady state operation is assumed.

3.2 Cathode electrode model

In this section a description of models of reaction kinetics, oxygen diffusion, electron and proton transport in the cathode catalyst layer and GDL is given.

3.2.1 Cathode reaction kinetics

On both side of the PBI membrane there are thin layers made of platinum supported on carbon known as the catalyst layer. This layer is very thin (about 10-50 µm) and is a mixture of platinum, carbon and electrolyte. When considering a macroscopic view of catalyst layer, the reactions occur at the agglomerates where there are free available reaction sites. The agglomerate is where the platinum and carbon particles are in contact with the electrolyte (Songprakorp, 2008). In the cathode catalyst layer oxygen reduction reaction occurs at the surface of the platinum particles. Electrons from the external circuit are conducted to the catalyst surface via carbon particles and the hydrogen protons from the anode are transported through the electrolyte to the catalyst reaction site. At the agglomerate film the three species react to form water and heat is released. The half reaction occurring at the cathode at temperatures above 100 ^{o}C can be written as follows:

$$^{1}/_{2}\ O_2 + 2H^+ + 2e^- \xrightarrow{Pt} 2H_2O\ (g) \tag{3.1}$$

For every chemical reaction there is an energy barrier that needs to be overcome before the reaction could proceed. In the electrochemical reactions occurring in a fuel cell this activation energy barrier is associated with the reaction rate. In order to lower this energy barrier a voltage is needed, this voltage that is sacrificed to overcome the activation energy barrier is known as activation polarization. The activation polarization is present in both anode and cathode catalyst layers and can be expressed as a reaction rate. The reaction rate of a fuel cell cannot be measured directly; it is measured using the exchange current density, which is a measure of reaction rate at equilibrium conditions (Das and Bansode, 2009). The cathode reaction rate or activation polarization is expressed as an exponential function of current density using a Bulter-Volmer equation:

$$j = j_{o,c}\ \left[\exp\left(\frac{-\alpha_{Rd,c}nF}{RT}V_c\right) - \exp\left(\frac{-\alpha_{Ox,c}nF}{RT}V_c\right)\right] \tag{3.2}$$

Where j represents the current density of an operational fuel cell, $j_{o,c}$ the cathode exchange current density at the studied conditions, α is the oxidation and reduction transfer coefficients (symmetry coefficient) and V_c is the cathode activation polarization. The exchange current density is a function of catalyst layer parameters such as amount of catalyst, available reaction sites and temperature. This dependency on these parameters is express by the following equation at any given temperature and pressure:

$$j_{o,c} = i_o^{ref} a_c L_c \left(\frac{C_{O_2}}{C_{O_2}^{ref}}\right)^{\gamma} \exp\left[-\frac{E_c}{RT}\left(1 - \frac{T}{T_{ref}}\right)\right] \quad (3.3)$$

Where: E_c is the activation energy of the oxygen reduction reaction in hot phosphoric acid, γ is the reaction order with respect to oxygen reduction in phosphoric acid. i_o^{ref} is the reference exchange current density measured at reference oxygen concentration on the catalyst surface $C_{O_2}^{ref}$ and reference temperature T_{ref}. a_c is the available catalyst specific area and L_c is the catalyst loading, with their product being a dimensionless parameter known as the roughness factor. By assuming symmetry ($\alpha_{Rd,c} = \alpha_{Ox,c}$) the Bulter-Volmer equation can be expressed as a hyperbolic sine function:

$$j = 2j_{o,c} \sinh\left[\frac{\alpha nF}{2RT} V_c\right] \quad (3.4)$$

By rearranging equation results in an expression for the cathode electrode polarization

$$V_c = \frac{RT}{\alpha nF} \sinh^{-1}\left[\frac{j}{j_{o,c}}\right] \quad (3.5)$$

Taking the natural logarithm results in a final expression for the electrode polarization

$$V_c = -\frac{RT}{\alpha nF} \ln\left[\frac{j}{j_{o,c}} + \sqrt{1 + \left(\frac{j}{j_{o,c}}\right)^2}\right] \quad (3.6)$$

3.2.2 Cathode gas transport

The cathode electrode is supplied with air/oxygen that is transported through the GDL to the catalyst. The oxygen in air dissolves in the PBI and diffuses through the phosphoric acid to the

catalyst reaction sites. The reactant supply to the electrode can be expressed using Faraday's Law:

$$N_{O_2} = \frac{I_{cell}}{nF} \tag{3.7}$$

Where N_{O_2} represents the oxygen molar flux, which corresponds to the amount of oxygen to be supplied in order to produce the required current, I_{cell} is the operating current. In the cathode agglomerate the catalyst is covered by the thin film of acid and the oxygen must diffuse through this layer to reach the catalyst surface. The average thickness of the thin film layer can be estimated using:

$$\delta_c = \frac{m_{PA}/\rho_{PA}}{S_c + S_{Pt}} \tag{3.8}$$

Where m_{PA} is the mass of phosphoric acid per unit area, S_c is the surface area of carbon, S_{Pt} is the roughness factor and ρ_{PA} is the density of phosphoric acid. The oxygen diffusivity depends on its solubility phosphoric acid. In order to determine the oxygen concentration on the platinum surface, its solubility and Henry's constant needs to be determined. There are a lot of studies done on the oxygen reduction reaction in phosphoric acid (Li *et at*., 2001) and these studies found the solubility and Henry's constant to be a strong function of temperature and the concentration of phosphoric acid. Klindinst *et al.* (1974) showed that the solubility and diffusivity of oxygen in hot phosphoric acid solutions were temperature dependent to about 96 wt% H_3PO_4. Using experimental data from MacDonald and Boyack (1969) and Sousa *et al.* (2010) generated an equation to couple the concentration of phosphoric acid with the water partial pressure

$$\mathrm{x_{PA}} = \frac{\ln(\mathrm{P_{H_2O}}) + \frac{2765.1}{\mathrm{T}} - 22.002}{\frac{-4121.9}{\mathrm{T}} + 2.5929} \tag{3.9}$$

Where x_{PA} is the mole fraction of phosphoric acid and P_{H_2O} is the water partial pressure. From Scott and Mumlouk (2007) the mole fraction can be converted to mass fraction as

$$w_{PA} = \frac{0.0544\, x_{PA}}{x_{PA}\,(0.0544 - 0.01) + 0.01} \tag{3.10}$$

Sousa *et al.* (2010) used the experimental data of (Klinedinst *et al*., 1974) to express the Henry's constant as a function of acid concentration and came up with the expression

$$H_{O_2} = \left[(-1.27E4\, w_{PA} + 1.23E4)\frac{1}{T} + (35.2\, w_{PA} - 46.6)\right] \quad (3.11)$$

The diffusivity of oxygen in phosphoric acid as a function of temperature and acid concentration can be expressed as (Cheddie and Munroe 2007):

$$10^9\, \mathrm{D}_{\mathrm{O_2}}^{\mathrm{PA}} = \left(\text{-}192.55\mathrm{w_{PA}}^2 + 323.55\mathrm{w_{PA}} \text{-} 125.61\right) + \frac{(62010\mathrm{w_{PA}}^2 \text{-} 105503\mathrm{w_{PA}} + 40929)}{\mathrm{T}} \quad (3.12)$$

The diffusion coefficient increases with increase in volume fraction of unbound phosphoric acid in the electrolyte. Therefore, an effective diffusion is used in order to account for the effects of unbound phosphoric acid. A Bruggman type relationship can be used to express the effective diffusivity:

$$D_{O_2}^{eff} = D_{O_2}^{PA}\, \varepsilon^{\tau} \quad (3.13)$$

Where ε represents is the volume fraction of unbound phosphoric acid in the electrolyte, τ is the tourtosity. Once the oxygen diffuse through the thin film it reaches the catalyst surface and its concentration on the surface can be expressed using a form of Fick's law of diffusion

$$\frac{N_{O_2}}{S_{Pt}} = \frac{-D_{O_2}^{PA}\left(C_{O_2}^{Pt} - C_{O_2}^{eq}\right)}{\delta_c} \quad (3.14)$$

$C_{O_2}^{eq}$ denotes the equilibrium oxygen concentration in the acid thin film. Klidinst *et al.* (1974) showed that the concentration of oxygen varied exponentially with the temperature and this can be expressed as

$$C_{O_2}^{eq} = B - \exp\left(\frac{\Delta H_s}{RT}\right) \quad (3.15)$$

Where B is a pre-exponential factor and ΔH_s is the enthalpy of the solution. Equation 3.15 is valid only between 86 to 96 wt%.

3.3 Anode electrode model

This section a description of models of reaction kinetics, hydrogen diffusion, electron and proton transport in the anode catalyst layer and GDL is given.

3.3.1 Anode reaction kinetics

In this study all the materials and components of the electrodes are assumed to be identical. This means the properties of the materials used in expressions for the cathode and the anode electrode are the same. In the anode catalyst layer, the hydrogen oxidation reaction (HOR) takes place in the catalyst surface. Hydrogen is oxidised into two electrons and two protons. The hydrogen protons are conducted to the cathode through the electrolyte and the electrons are conducted through the carbon particles to the current collector plate, where they are conducted via an external circuit. Similar to the oxygen reduction reaction in the cathode, the HOR takes place in the catalyst agglomerate. The half reaction taking place in the anode is:

$$\mathrm{H_2} \overset{\mathrm{Pt}}{\rightarrow} 2\mathrm{e^-} + 2\mathrm{H^+} \tag{3.16}$$

Similar to the cathode reaction rate, the rate of the anode reaction is expressed using the exchange current density at the electrode. This can be expressed as:

$$j_{o,a} = i_a^{ref}\, a_a\, L_a \left(\frac{C_{H_2}}{C_{H_2}^{ref}}\right)^{\gamma} \exp\left[-\frac{E_a}{RT}\left(1 - \frac{T}{T_{ref}}\right)\right] \tag{3.17}$$

Where E_a is the activation energy of the HOR in hot phosphoric acid, γ is the reaction order with respect to hydrogen reduction in phosphoric acid. i_a^{ref} is the anode reference exchange current density measured at reference oxygen concentration on the catalyst surface $C_{H_2}^{ref}$. a_a is the available catalyst specific area and L_a is the catalyst loading.

The expression of the anode polarization is:

$$\mathrm{j} = \mathrm{j_{o,a}} \left[\exp\left(\frac{-\alpha_{\mathrm{Rd,a}}\mathrm{nF}}{\mathrm{RT}}\mathrm{V_a}\right) - \exp\left(\frac{-\alpha_{\mathrm{Ox,a}}\mathrm{nF}}{\mathrm{RT}}\mathrm{V_a}\right)\right] \tag{3.18}$$

The variables have the same meaning as those in equation 3.2, with the subscript *a* denoting the anode electrode. Rearranging the equation to give the polarization as:

$$V_a = -\frac{RT}{\alpha nF} \ln\left[\frac{j}{j_{o,a}} + \sqrt{1 + \left(\frac{j}{j_{o,a}}\right)^2}\right] \quad (3.19)$$

The hydrogen oxidation reaction is much faster than the oxygen reduction reaction; this is due to the lower activation energy of the HOR compared to ORR. This, results in an anode polarization being an order of magnitude lower the cathode polarization.

3.3.2 Anode gas transport

In the anode electrode hydrogen is supplied and it is transported to the GDL through convection, in the GDL it diffuses to the catalyst layer. Analogous to the cathode electrode the reactant supply in the anode can be expressed by Faraday's Law:

$$N_{H_2} = \frac{I_{cell}}{nF} \quad (3.20)$$

Where N_{H_2} is the hydrogen molar flux and n is the no of electrons involved in the reaction. The thin film covering the catalyst layer is:

$$\delta_a = \frac{m_{PA,a}/\rho_{PA}}{S_c + S_{Pt,a}} \quad (3.21)$$

The HOR in phosphoric acid has not been studied extensively in literature and hydrogen solubility and diffusivity is not well known. Therefore, the hydrogen diffusion coefficient and solubility will be assumed to be similar to water systems (Liu *et al*., 2006). (Cheddie and Munroe, 2007) came up with an expression for this relationship. The hydrogen solubility is four times the solubility of oxygen and the diffusivity is two times that of oxygen:

$$H_{H_2} = 4\, H_{O_2} \quad (3.22)$$

$$D_{H_2}^{PA} = 2D_{O_2}^{PA} \quad (3.23)$$

As with the diffusion in the cathode catalyst layer, the effects of unbound phosphoric acid to the diffusion of hydrogen in the anode catalyst layer needs to be expressed. Thus yielding to an effective anode diffusion coefficient being:

$$\mathrm{D}_{\mathrm{H}_2}^{\mathrm{eff}} = \mathrm{D}_{\mathrm{H}_2}^{\mathrm{PA}}\ \varepsilon^{\tau} \tag{3.24}$$

The concentration of hydrogen on the catalyst surface is given Fick's Law of diffusion:

$$\frac{\mathrm{N}_{\mathrm{H}_2}}{\mathrm{S}_{\mathrm{Pt,a}}} = \frac{-\mathrm{D}_{\mathrm{H}_2}^{\mathrm{PA}}\left(\mathrm{C}_{\mathrm{H}_2}^{\mathrm{Pt}} - \mathrm{C}_{\mathrm{H}_2}^{\mathrm{eq}}\right)}{\delta_{\mathrm{a}}} \tag{3.25}$$

The $\boldsymbol{C_{H_2}^{Pt}}$ represents the hydrogen concentration on the catalyst surface in PBI membrane and $\boldsymbol{C_{H_2}^{eq}}$ denotes the equilibrium hydrogen concentration in the acid thin film.

3.4 Ohmic losses

In this study the ohmic polarization is assigned exclusively to the resistance of proton transfer in the membrane. The proton conduction in the acid doped PBI membranes is a strong function of the acid doping level (Z) also known as protonation. The doping level is defined as the number of H_3PO_4 molecules absorbed per PBI repeat unit. The structure of PBI membrane allows for maximum doping level of Z=2, after which there would be an excess acid in the membrane (Ma *et al*., 2004). The proton conduction of the membranes increases with the amount of excess acid, until a point where the membrane floods and it conduction is lowered. The doping level depends on the concentration of the acid and can be expressed as (Cheddie and Munroe, 2007):

$$Z = 0.012M^3 - 0.211M^2 + 1.2363M + 0.7199 \tag{3.26}$$

Where *M* is the acid concentration. (Liu *et al*., 2006) studied the ORR at a Pt-surface and found that the oxygen diffusion is a function of doping level and the volume fraction of free unbound H_3PO_4. The volume fraction of free unbound phosphoric acid in the electrolyte can be expressed as:

$$\varepsilon_{PA} = \left(\frac{4.81}{Z-2} + 1\right)^{-1} \tag{3.27}$$

The conductivity of the acid doped PBI membranes is a function of relative humidity, acid doping level and temperature, Ma *et al.* (2004) showed this in their work. However, in this work the conductivity is considered to be a function of temperature and acid doping level because the reactant gases fed to the fuel cell are not humidified. The expression to give the conductivity of the membrane is (Cheddie and Munroe, 2007):

$$\mathrm{k} = \frac{100}{\mathrm{T}} \exp\left[8.0219\text{-}\left(\frac{2605.6\text{-}70.1\,\mathrm{Z}}{\mathrm{T}}\right)\right] \tag{3.28}$$

As mentioned above the conductivity of the membrane also depends on the amount of excess acid in the electrolyte. To account for this an effective conductivity is used. This can be expressed using a Bruggman type relationship based on the volume fraction of free unbound phosphoric acid in the membrane:

$$\mathrm{k}^{\mathrm{eff}} = \mathrm{k}\,\varepsilon_{\mathrm{PA}}^{1.5} \tag{3.29}$$

To obtain the voltage loss caused by resistance to proton conductivity, the resistance on the anode, cathode and by the electrolyte are added using Ohm's Law. The final expression for ohmic polarization is:

$$\eta_{\mathrm{ohmic}} = \mathrm{l\ j}\left(\frac{1}{\mathrm{k}^{\mathrm{eff}}} + \frac{1}{\mathrm{k}_{\mathrm{a}}^{\mathrm{eff}}} + \frac{1}{\mathrm{k}_{\mathrm{c}}^{\mathrm{eff}}}\right) \tag{3.30}$$

3.5 Thermodynamic equilibrium potential

The voltage that arises from a fuel cell when no current is being drawn is known as the thermodynamic equilibrium voltage. From thermodynamics, the amount of energy obtainable from a chemical reaction is equivalent to the Gibbs free energy of reaction. This is expressed as:

$$\Delta\mathrm{G}^{\mathrm{o}} = \Delta\mathrm{H}^{\mathrm{o}}\text{-}\mathrm{T}\Delta\mathrm{S}^{\mathrm{o}} \tag{3.31}$$

ΔH^{o} represents the enthalpy of species and ΔS is the entropy, both are evaluated at standard conditions (101 kPa and 298 K). Conservation of energy directly relates the molar Gibbs free enthalpy of reaction to the theoretical fuel cell voltage E_o :

$$\Delta G^o = -nFE_o \tag{3.32}$$

Where F is the Faradays constant, n is the number of moles of electrons transferred in the reaction. Since ΔG is dependent on reactant pressure and temperature, the obtainable voltage, E^o for a given set of reaction parameters is given as a standard equilibrium voltage corrected by the deviation from those standard conditions. The resulting voltage can be expressed as a function of temperature and pressure using a Nernst type relation when there is no current drawn from the cell. When there is current drawn from the cell the equilibrium voltages are no longer valid:

$$\mathrm{V_o} = \mathrm{V^o} + \frac{\Delta \mathrm{S^o}}{\mathrm{nF}}\left(\mathrm{T}\text{-}\,\mathrm{T_o}\right) + \frac{\mathrm{RT}}{\mathrm{nF}}\ln\frac{\mathrm{P_{H_2}\,P_{O_2}}}{\mathrm{P_{H_2O}}} \tag{3.33}$$

Where $\mathrm{V^o}$ is the standard cell potential expressed as:

$$V^o = \frac{\Delta H^o - T\Delta S^o}{nF} \tag{3.34}$$

P_i repersent partial pressure of hydrogen, oxygen and water. The last term in equation 3.33 represents the effect of the concentration of species, and because the catalyst layers are covered by the electrolyte, the partial pressures of reactant and product can be replaced by their activities/concentration in the electrolyte:

$$\mathrm{V_o} = \mathrm{V^o} + \frac{\Delta \mathrm{S^o}}{\mathrm{nF}}\left(\mathrm{T}\text{-}\,\mathrm{T_o}\right) + \frac{\mathrm{RT}}{\mathrm{nF}}\ln\frac{\mathrm{C_{H_2}\,C_{O_2}}}{\mathrm{a_{H_2O}}} \tag{3.35}$$

The activity of water is given by:

$$\mathrm{a_{H_2O}} = \frac{\mathrm{P_{H_2O}}}{\mathrm{P^{sat}_{H_2O}}} \tag{3.36}$$

Where $P^{sat}_{H_2O}$ is the saturation pressure of water at the operating temperature and P_{H_2O} is the water vapour pressure. The hydrogen and oxygen concentrations in the electrolyte can be obtained from their solubility in phosphoric acid by using Henry's Law at the studied conditions (Sousa *et al.* 2010):

$$C_{H_2} = \frac{P_{H_2}}{H_{H_2}} \quad (3.37)$$

$$C_{O_2} = \frac{P_{O_2}}{H_{O_2}} \quad (3.38)$$

C_i is the dissolved concentration of reactants and H_i is the Henry's constant at the operating temperature.

The voltage produced by the cell can be determined by the thermodynamically predicted voltage (eq. 3.35) minus the activation (eq. 3.6 and 3.19) and ohmic (eq. 3.30) voltage loss:

$$V_{cell} = V_o - V_c - V_a - \eta_{ohmic} \quad (3.39)$$

3.6 Results

3.6.1 Model validation

It is ideal that as a starting point for the investigations of the fuel cell performance a base case is defined. The parameter values chosen for the base case are shown in Table 4.1. The values are chosen from literature to give a performance curve that is typical trend of the polarization curve reasonable for a HTPEM fuel cell. As a base case, a PEMFC was operated at 150 ^{o}C with pure hydrogen and air supplied to the anode and cathode respectively. The anode and cathode gases were supplied at atmospheric pressure at stoichiometry of 1.25 and 2 without humidification respectively.

Before the model can be used to do parametric analysis, simulations of the one dimensional model for a base case parameters was done in order to determine the accuracy and gain confidence on the model. The resulting simulation results were compared with experimental data from Sousa *et al*. (2010). In brief Sousa *et al*., (2010) experimental data was obtained from a PEMFC utilising 50% Pt/C at the cathode and 20% Pt/C at the anode at 150 ^{o}C and at atmospheric pressure. Air was used at the cathode and hydrogen at the anode. Anodes were prepared using 0.2 mg_{Pt} cm^{-2} 20% Pt/C (ETEK) with PBI loading of 0.28 and 0.7mg cm^{-2} and fixed doping level of 8 PRU. MEAs were prepared by hot pressing the GDL supported catalysts onto the PBI membrane at 150 ^{o}C and 40 kg cm^{-2} for 10 min The membranes were prepared from PBI powder dissolved in N,N0-dimethylacetamide (DMAc) by casting onto optical glass and kept in an oven at a temperature of 90–110 ^{o}C over night to produce a 40 µm thick membrane.

Figure 3.1 shows the comparison of the model results with the experimental results from Sousa *et al*., (2010). The results of the modelling predictions are labelled “model initial” where model parameters are taken directly from open literature. Although the model predictions follow the “trademark” trend of a typical polarization curve, it did not agree well with the experimental results (there voltage was under predicted). This clearly shows the importance of validation of model results before it can be used to analyse any system. Some parameters had to be optimised in order to get good agreement between the two curves. The deviation of model results from the experimental is visible in the two studied voltage loss regions.

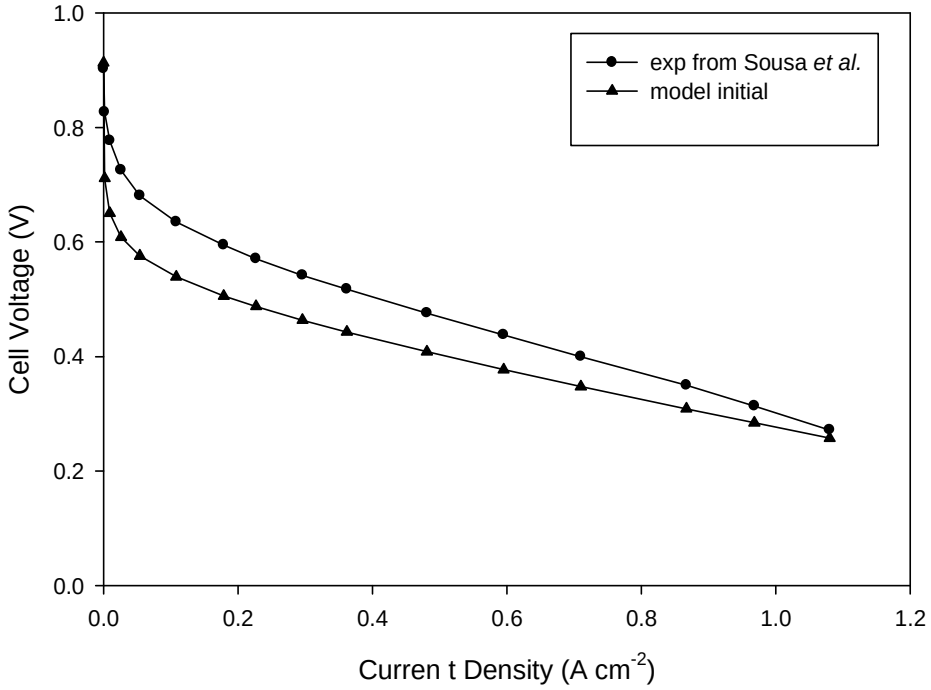

Figure 3. 1: Comparison between model predictions and experimental data at 150 ^{o}C

The first deviation is observed in the activation voltage loss region of the polarisation curve; therefore the parameters (reference exchange current density and activation energy) in this region need to be optimised to get good agreement with between the two curves. It is well known that the limiting reaction is the cathode oxidation reduction reaction as the anode hydrogen reaction proceeds fast over a Pt-catalyst (Iranzo *et al*., 2010). For this reason the cathode activation parameters were chosen to be optimised. The activation overpotential was observed to be sensitive to two parameters; the activation energy and the reference exchange current density, and for this reason the two are chosen to be optimised. The second deviation of model from experimental is observed in the slope of the ohmic overpotential region. Similarly to

the activation overpotential region, parameters that affect the ohmic overpotential were chosen to be optimised. The two parameters that were observed to have effect on the slope are the acid doping level and the transfer coefficients. Figure 3.2 shows the model results and experimental results after the model was optimised and a good prediction of the experimental results can be observed. This model can now be used to investigate the single cell behaviour.

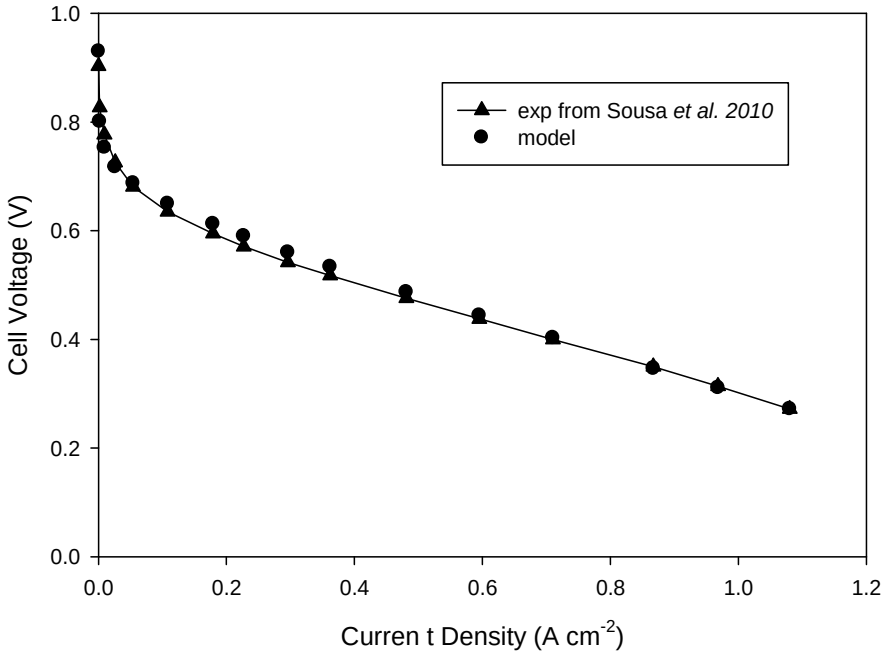

Figure 3.2: Comparison between model predictions and experimental data at 150 ^{o}C

3.6.2 Temperature effects

Figure 3.3 shows the simulation results at three different operating temperatures (135 ^{o}C, 150 ^{o}C and 175 ^{o}C). Oxygen was used at the cathode at a stoichiometry of 2 and hydrogen at the anode at stoichiometry of 1.25. The performance predicted by the model showed that increasing the operating temperature results in increased performance. The increased performance is a result of several changes in the cell electrochemistry influenced by temperature. Firstly the reaction kinetics are enhanced due to improved reactant solubility and diffusivity. Klinedinst *et al.,* (1974) studied the effects of temperature on oxygen solubility and diffusivity and found that they increase with temperature, whilst keeping the H_3PO_4 concentration constant, thus resulting in better performance of the electrode.

The increase in the diffusivity and solubility of reactants directly results in increased concentration of the reactant on the catalyst surface, therefore speeding up the rate of the

reaction (Jiao and Li, 2010, Chen and Lai, 2010). This can be seen in the increased exchange current density calculated by equation 3.17 when increasing operating temperature. Secondly the increased temperature results in increased membrane conductivity, which promotes faster proton transfer. Similar observations have been reported by (Bouchet and Siebert, 1999), who studied the proton conduction of PBI membranes and showed that the temperature dependency of conductivity obey Arrhenius Law. There were no mass transport losses observed for all operating temperatures due to high stochiometries and because there is no formation of liquid water (single phase flow assumption), similar observations have been reported (Jiao and Li, 2010, Ubong *et al*., 2009).

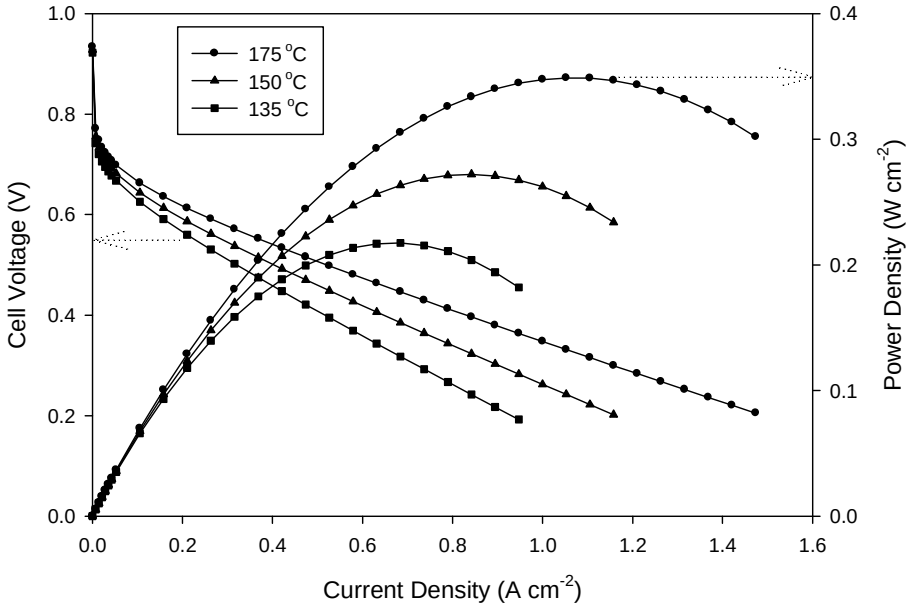

Figure 3.3: Simulated temperature dependency of polarisation curve for operation with pure hydrogen at the anode and air at the cathode.

3.6.3 Acid doping level

The performance curves at different acid doping levels (4, 6 and 8) of the membrane are shown in Figure 3.4. The comparison of the acid doping level is made with a fuel cell operating with oxygen and hydrogen without humidification at the cathode and anode respectively. The operating temperature is 160 ^{o}C at 1 bar and the stoichiometry of feed gasses is 2 and 1.25 for cathode and anode respectively. It was observed that the cell performance increased with increased acid doping level (ADL), similar observations have been reported by (Mamlouk and Scott, 2010).

The increase performance is due to increased reactant activity as a result of excess acid in the electrolyte. The excess acid improves the membrane conductivity and the solubility of reactants (Lobato *et al*., 2007). Liu *et al.,* (2006) explains that the diffusion of oxygen in phosphoric acid doped PBI is dependent on the amount of amphorous “free bound” acid. By increasing the doping level, the amphorous acid in the electrolyte is also increased thus increasing the reactant diffusion rate to the catalyst sites. There is a limit on the amount of the doping level, too much acid result in poor mechanical properties and poor performance (Liu *et al*., 2004, Ma *et al*., 2004). The membrane conductivities calculated using equation 3.16 at 160 ^{o}C are 0.033 S/cm, 0.045 S/cm and 0.063 S/cm corresponding to 4, 6 and 8 acid doping levels respectively, which is in the same order of magnitude as conductivities reported by Ma *et al*., (2004). The values give an indication that the increment in the conductivity when the doping level is increased from 4 to 6 (0.012 S/cm) is lower than 6 to 8 (0.018 S/cm), which agrees with the cell performance. Overall the results indicate that increasing phosphoric acid doping level of PBI membranes has significant improvements on the cell performance.

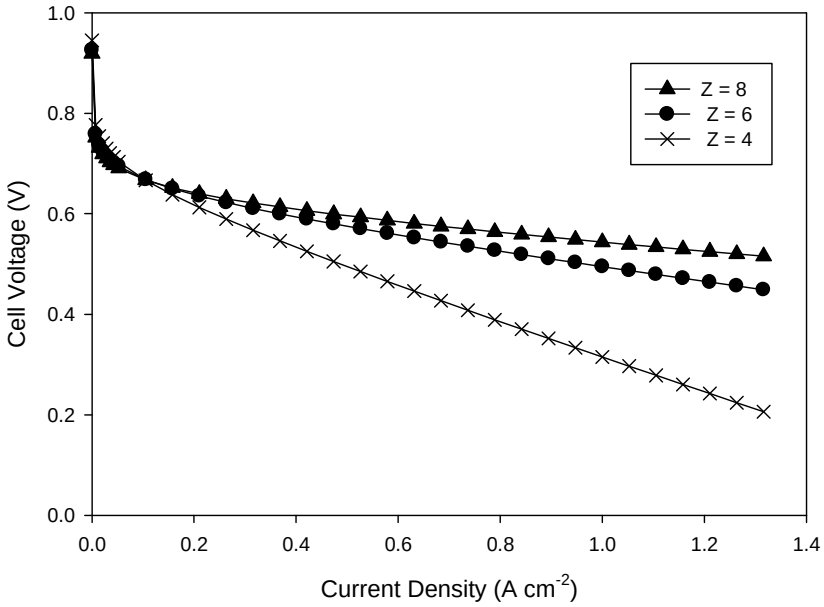

Figure 3.4: Effects of phosphoric acid doping level on the cell performance

3.6.4 Catalyst loading

One of the commercial barriers of wide spread PEM fuel cell is the cost of the system, which can be associated with the use of noble metal catalyst. It is therefore desirable to reduce this cost without reducing the overall efficiency for fuel cells to be competitive with other power generation technologies. This can be achieved in two ways, by increasing the utilisation efficiency of the

catalyst (improving deposition methods) or by using alternative catalysts (made from alloys or intermetalics that uses less or no platinum) (Zeis *et al*., 2007). In this work the effect of lower platinum loading was studied for the anode and cathode electrodes.

The cell performance predictions showing the effects of cathode and anode platinum loading is shown in Figures 3.5 and 3.6. The polarisation curves show three different platinum loadings for anode and cathode 0.2, 0.1 and 0.025 mg /cm^2. In order to investigate the effect of cathode catalyst loading, the anode catalyst loading was kept constants whilst the cathode loading was being varied and verse-versa. It was observed that when both the anode and cathode catalyst loadings were decreased, the cell performance also decreased. This can be explained by the increase in activation polarization caused by decrease in rate of reaction or catalytic activity (Cho *et al*., 2007). For the cathode, decreasing the catalyst loading from 0.2 to 0.025 mg/cm^2 resulted in a drop in voltage of 2.5 mV at a current density of 1 A/cm^2, which is the same order of magnitude as values reported by (Gasteiger *et al*., 2004 and Cho *et al*., 2007). There was little visible voltage loss when the platinum loading was decreased from 0.2 to 0.1 mg/cm^2, similar observations when the anode catalyst loading was varied were visible.

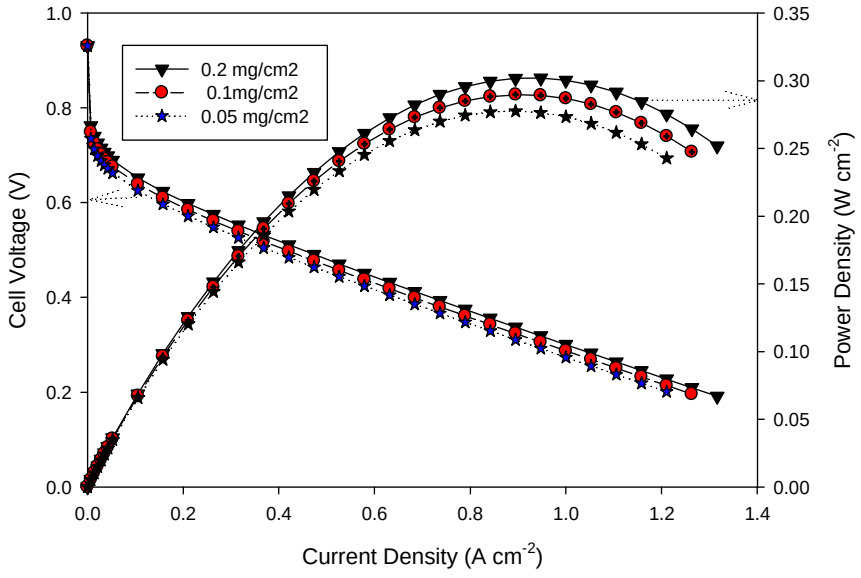

Figure 3.5: Polarization curves for the different anode platinum loading

3.6.5 Reformate fuel

High temperature PEM fuel cells have received attention particularly because of improved carbon monoxide (CO) tolerance at elevated temperatures (120-180 ^{o}C) as it allows for use of reformed fuel with a higher traces of CO without loss of cell voltage and rapid degradation. The use of reformed fuel also gives an advantage of using different fuel sources such as biomass, petroleum gas, renewables etc. In this section, the use fuel gas mixture containing of (i) H_2 and CO and (ii) a typical mixture of reformed natural gas are investigated. The introduction of CO in the anode gas changes the electrode kinetics, in particular, the exchange current density.

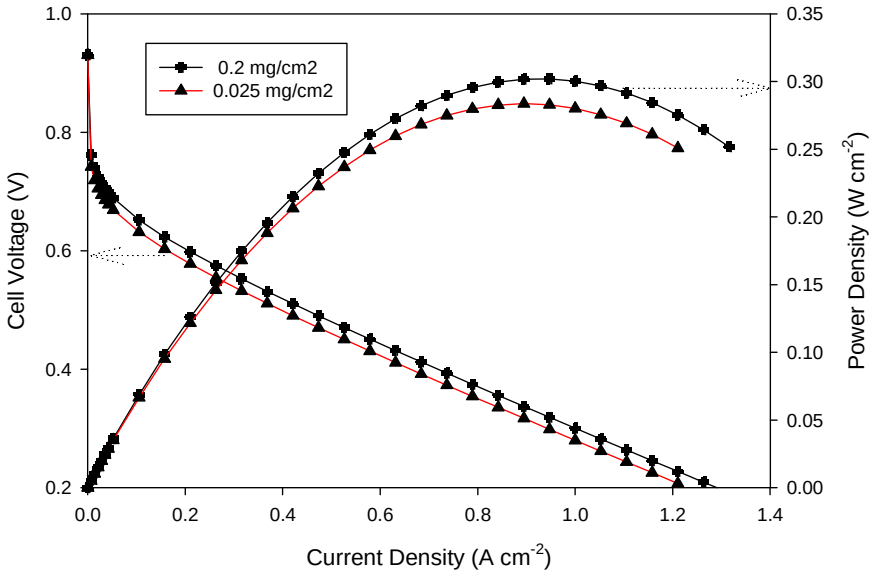

Figure 3. 6: Polarization curves for the different cathode platinum loading

Vogel *et al*. (1974) studied the effect of CO poisoning on the hydrogen electrode and suggested the following equation to account for the exchange current density:

$$j_o^{CO} = j_{o,a}\,(1 - \theta_{CO})^{2} \tag{3.40}$$

Where j_o^{CO} is the exchange current density after CO poisoning, $j_{o,a}$ is the current density without CO poisoning calculated using equation 3.17 and θ_{CO} is the surface coverance of the reaction site by CO. Dhar *et al*. (1986) proposed the following equation to calculate θ_{CO} as a function of temperature

$$\theta_{CO} = 19.9\exp(-7.69E-3\,T) - 0.085\ln\left[\frac{CO}{H_2}\right] \tag{3.41}$$

The simulated results showing the influence of CO in the anode gas feed has on the fuel cell performance at different operating temperatures is shown in Figure 3.7. The results compare the polarisation curve when the anode feed is pure hydrogen and when 2% CO is added to the feed gas. Firstly the performance when hydrogen is used and when carbon monoxide is added to the reactant gas is compared at a fixed temperature of 160 ^{o}C. It can be seen that the cell performance drops, this becomes more pronounced when the temperature is decreased to 130 ^{o}C. When the temperature is 160 ^{o}C the cell voltage decreases from 0.49 V for pure hydrogen to 0.46 V (6 %) for feed with 2% CO content at a current density of 0.53 A/cm^2. This is further reduced to 0.4 V (13 % loss) when the operating temperature is reduced from 160 to 130 ^{o}C with the same CO content. The decreased performance is due to CO adsorption on the available sites on the catalyst surface, thus making a portion of catalyst site that would be otherwise available for hydrogen oxidation not to be available (Dhar *et al.,* 1986). This results to increased anode polarization caused by lower catalytic activity in the anode. These results show general agreement with what has been reported in literature by (Das *et al.,* 2009). The high reduction in voltage at low temperatures as compared to high temperature is because of high energy of adsorption of CO on the platinum surface (Modestov *et al*., 2010). High temperature reduces CO adsorption whilst it does not affect the hydrogen adsorption on the catalyst surface.

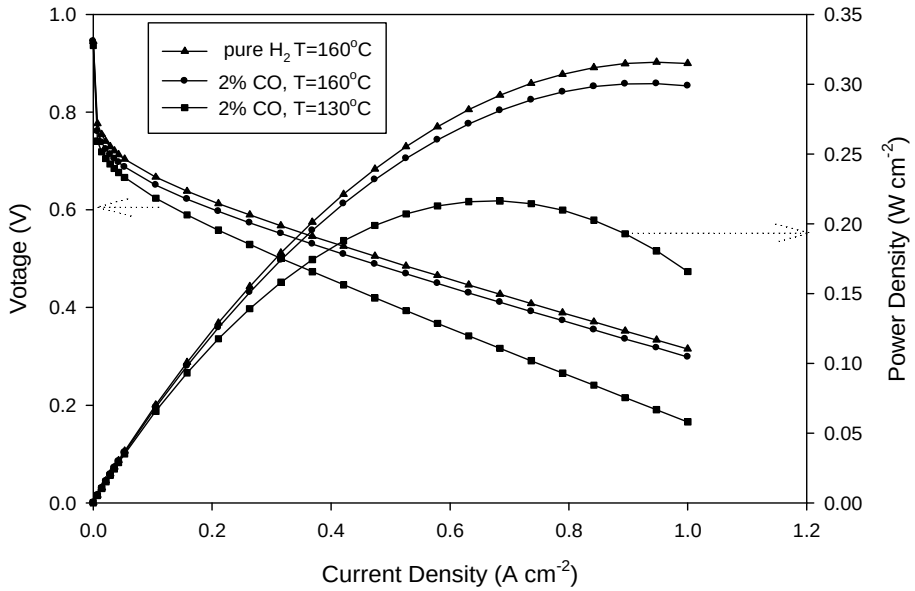

Figure 3. 7: Predicted effects of CO poisoning on the cell performance

Figure 3.8 shows the simulation results comparing the use of pure hydrogen and a reformate gas composed of (2% CO, 19% CO_2, 3% CH_4 and 76% H_2). There is a huge loss in cell voltage

when the cell was simulated for reformate use, which can be explained by the combined effect of CO poisoning and the drop of H_2 partial pressure as its mass fraction is reduced from 1 to 0.6. The drop in H_2 partial pressure results reduced concentration of H_2 in the catalyst surface; hence there is less hydrogen that is available for reaction.

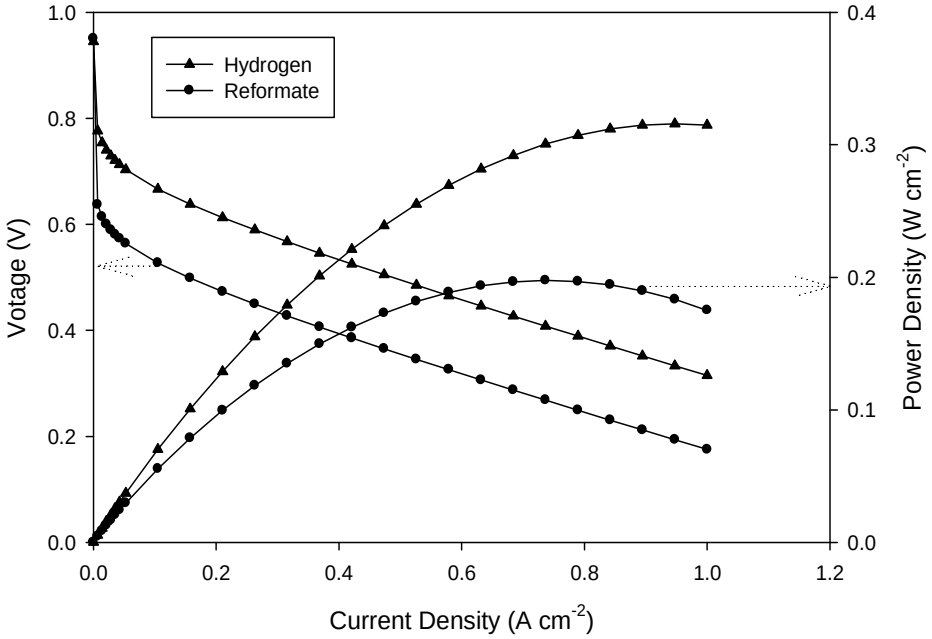

Figure 3.8: Predicted effects of reformate gas poisoning on the cell performance

CHAPTER FOUR
MULTIPLE CELL STACK MODELLING

4 Introduction

As mentioned in chapter 2, one of the most attractable use of high temperature PEM fuel cell is the quality of the heat produced that could have beneficial use in combined heat and power system. Most of the work done in FC modelling is devoted to a single cell stack analysis, particularly because the behaviour of a multiple cell stack may be obtained by simply multiplying by the no of cells in the stack. However, before the stack is incorporated within a CHP system, it is necessary to understand its energetic behaviour. This section is therefore devoted to analysis of energetic behaviour and their corresponding efficiencies at different operating modes of the HT-PEM fuel cell stack. This is done by making evaluation of the electrical and thermal energetic flows of a 1 kW_{el} stack. To do this, an energy model of a 1 kW_{el} stack is developed. The purpose of the energy model is to analyse energy balances around the fuel cell stack, thereby giving some idea about possible heat management of the stack. This is done by estimating the energy supplied/consumed, produced and recoverable from the stack.

4.1 Energy Model

The amount of energy that is contained in a fuel (hydrogen) is defined by either the lower heating value LHV or the higher heating value HHV. Both values are defined as the ratio between the energy released during fuel burning and the fuel mass; the difference is in the measuring procedure (Jovan *et al*., 2010).

4.1.1 Electricity production

The electrical power generated by single cell is estimated by:

$$P_{cell} = E_{cell}\, I_{cell} \tag{4.1}$$

Where E_{cell} is the average cell voltage calculated by eq. (3.39) and I_{cell} is the average current drawn from the single cell. From this we can get the electrical efficiency of a single cell using

$$\eta_{cell} = \frac{P_{cell}}{\dot{m}_{H_2} HV} \tag{4.2}$$

where $\dot{m}_{H_2}$ is the hydrogen mass flow-rate into a single cell and HV is the hydrogen heating value. Since the product of the reaction is in gaseous phase, the LHV is used. The theoretical hydrogen flow rate can be calculated from Faraday's Law:

$$\dot{m}_{H_2} = \frac{MM_{H_2} I_{cell}}{nF} \tag{4.3}$$

Where MM_{H_2}represents the molar mass of hydrogen. Since the fuel cell stack consists of single cells connected in series, the efficiency properties of the stack are the same as those of a single cell (Hou *et al*., 2007). Therefore, it follows that the power and efficiency of a stack is:

$$P_{stack} = N_{cell}\, E_{stack}\, I_{stack} \tag{4.4}$$

$$\eta_{electrical} = \frac{P_{stack}}{\dot{m}_{H_2} HV} \tag{4.5}$$

Where N_{cell} is the number of cells in the stack, I_{stack} and E_{stack} are the stack current and voltage respectively.

4.1.2 Thermal Production

The thermal power produced by the stack is the difference between the energy supplied by the stack and the electrical power produced:

$$Q_{thermal} = \dot{m}_{H_2} HV - P_{stack} \tag{4.6}$$

And the thermal efficiency is estimated similarly to the electrical efficiency:

$$\eta_{thermal} = \frac{Q_{thermal}}{\dot{m}_{H_2} HV} \tag{4.7}$$

By adding equation (4.6) and (4.7) the overall (CHP or cogeneration) efficiency of the stack is obtained:

$$\eta_{cogen} = \frac{P_{stack} + P_{thermal}}{\dot{m}_{H_2} HV} \tag{4.8}$$

Figure (4.1) shows the stack user interface developed

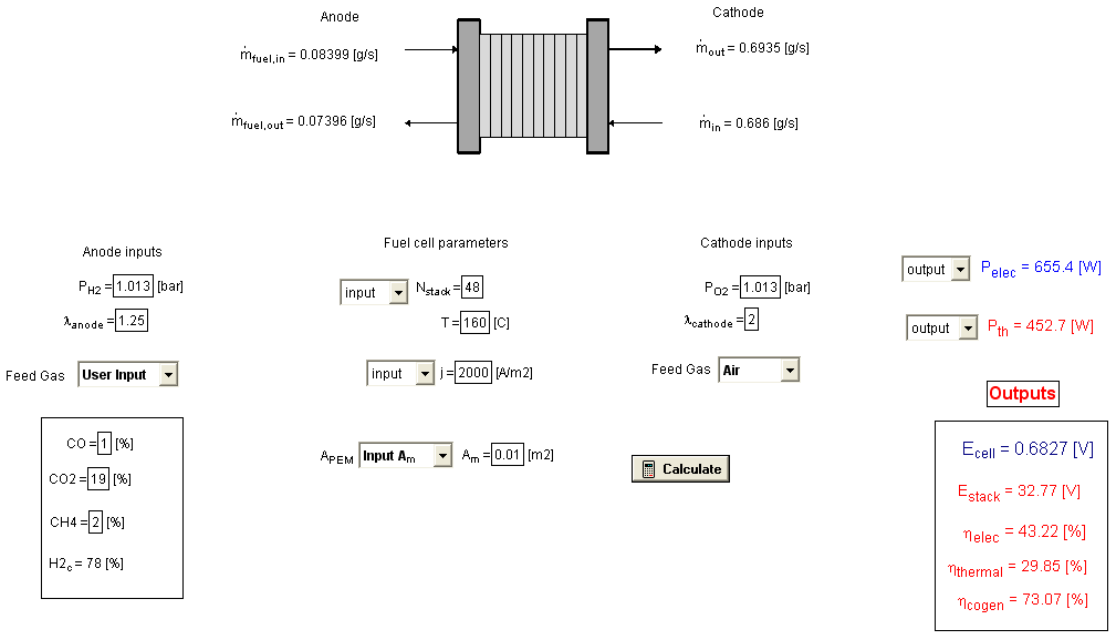

Figure 4.1: 48 cell stack user-interface

4.2 Experimental

Test Station

In order to validate the energy model in section 4.1.2 performance measurements have been performed in a 48 cell stack. This section describes the test station and experimental work performed to validate the model. The experiments were performed on a HT PEMFC stack available at *HySA* Systems laboratory at the University of the Western Cape. A schematic drawing and a photo of the test station can be seen in Figures 4.2 and 4.3 respectively. The stack is made of Celtec –P-2100 MEAs from BASF with thickness of the MEA was 884 µm and the active area of electrodes was 100 cm^2. The stack is designed to produce 1 kW_e. In the testing station, all parameters that have influence on performance of the stack can be controlled using an on-board computer. The reactants are supplied from storage cylinders using mass flow controllers. The flow rate of the reactants to the stack is controlled by the amount of current that is drawn from the stack and also by the stoichiometry. For each measured point the current is set at a fixed stoichiometry and the system calculates the required amount of reactant for that current to be produced. However in order to make sure that sufficient amount of gases are available in the stack a minimum flowrate equivalent to the production of 20 A was set. This

means that for current values below 20 A, the required amount of gases will be equal to that of 20 A. The temperature of the reactant and product gases is measured by type T thermocouples. Thermal oil was used in the high temperature system to heat up the stack to operation temperature at the start up and maintain proper temperature during up the stack to operation

The stack was tested using pure hydrogen as a fuel that was supplied to the anode and air as oxidant that was supplied to the cathode. Both the fuel and oxidant were not humidified and were supplied to respective electrode at ambient pressure. The air stoichiometry was set at 2 and the hydrogen stoichiometry at 1.25. The stack was operated at a temperature of 140 °C. The power and polarization curves were recorded for current load requirements. The current drawn from the stack was chanced in steps of 5 A from 10 A to 35 A. A stabilization time of five minutes at which the system was assumed to reach steady state was applied for each current

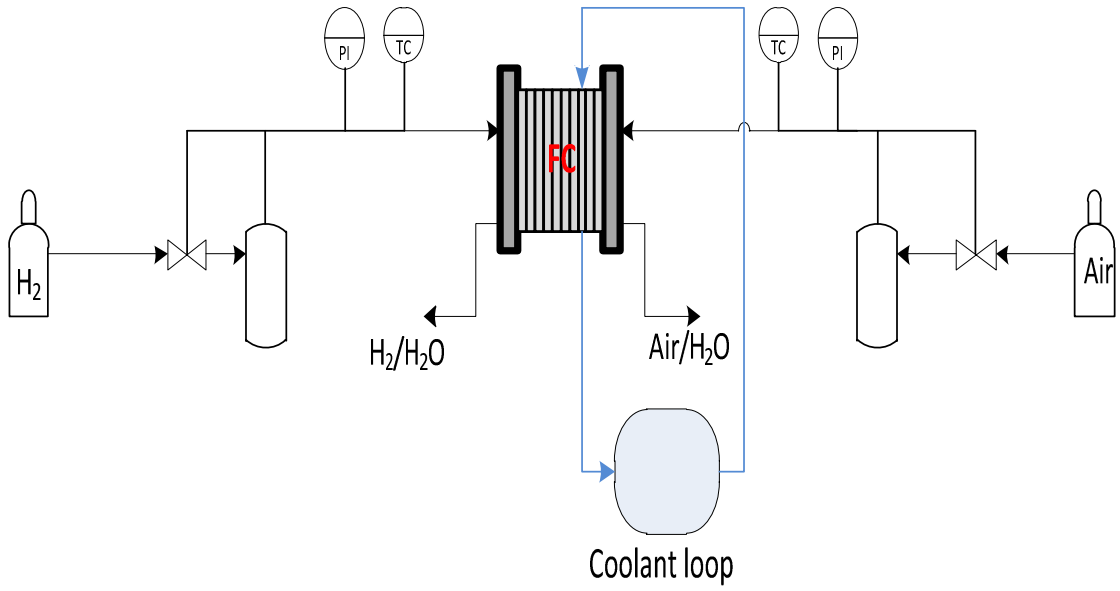

Figure 4.2: Schematic of the test station

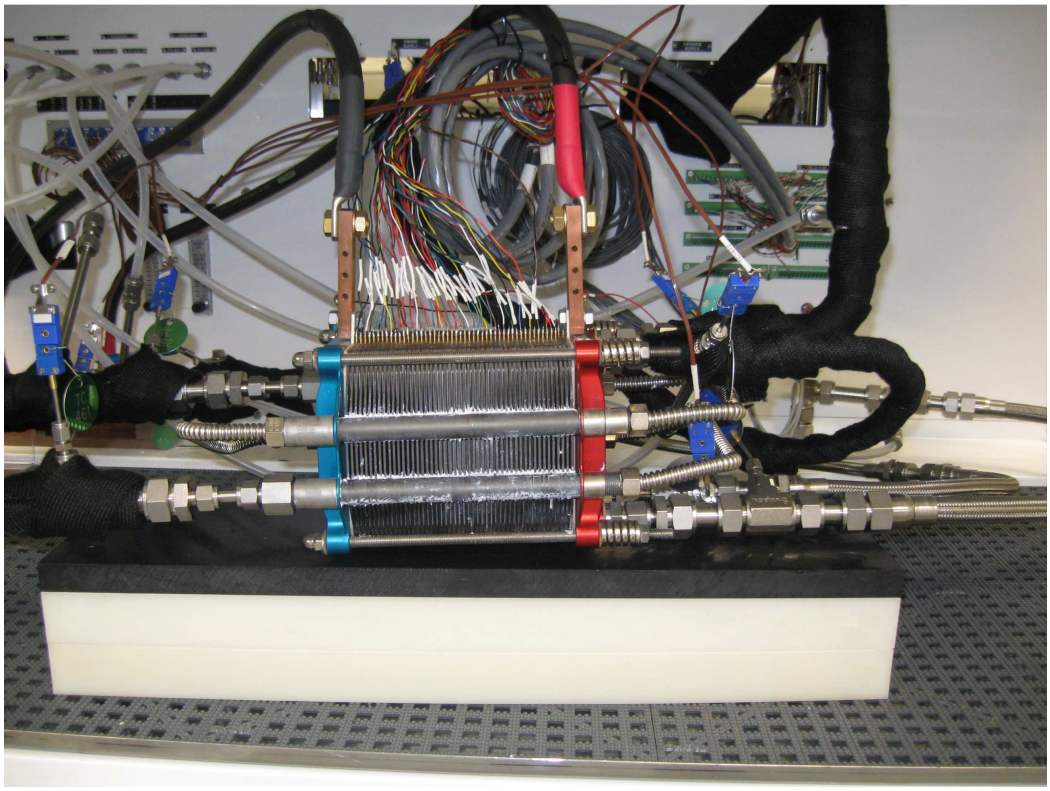

Figure 4.3: Pictorial view of the 48 cell stack test station

4.3 Results

In this section the results of numerical analysis of the stack are presented. Before any measurements for experimental validation were taken, the stack's stability was evaluated by measuring the cell voltage distribution at different loads. It can be seen from Figure 4.4 that there is no major variation between the individual cell voltages of the stack indicating steady state operating conditions. Since the core of the stack model is the electrochemical model developed in Chapter 3, it was necessary to modify the model in order to fit the experimental data from the test station. In doing this, a method similar to the one employed in validation of the single cell performance was used. The results of this are shown in Figures 4.5 and 4.6, where the average stack voltage and the power produced by the stack and by the model at different current densities are compared.

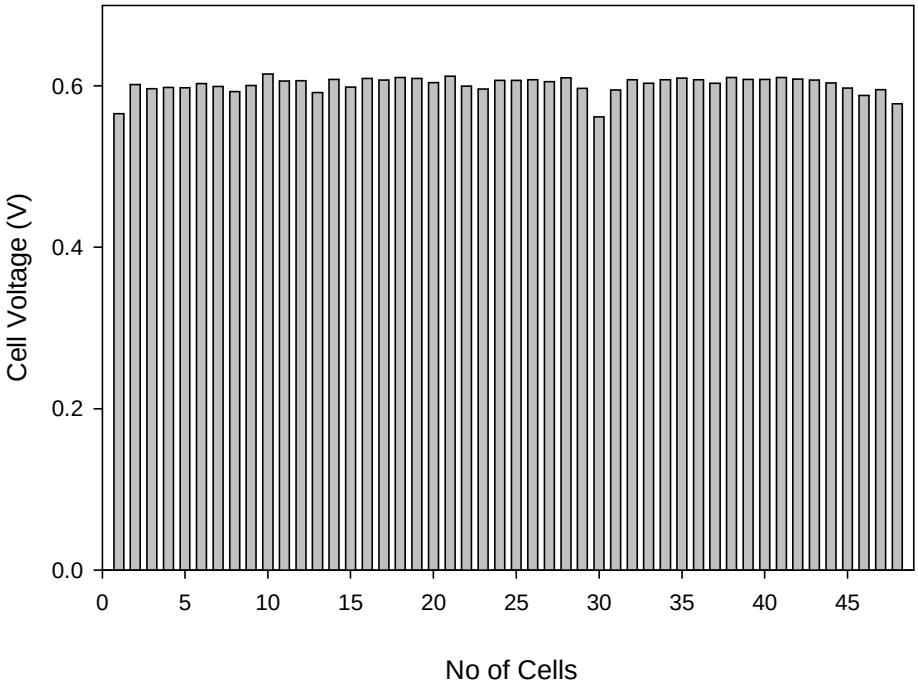

Figure 4.4: Cell voltage distribution measured at 20 A

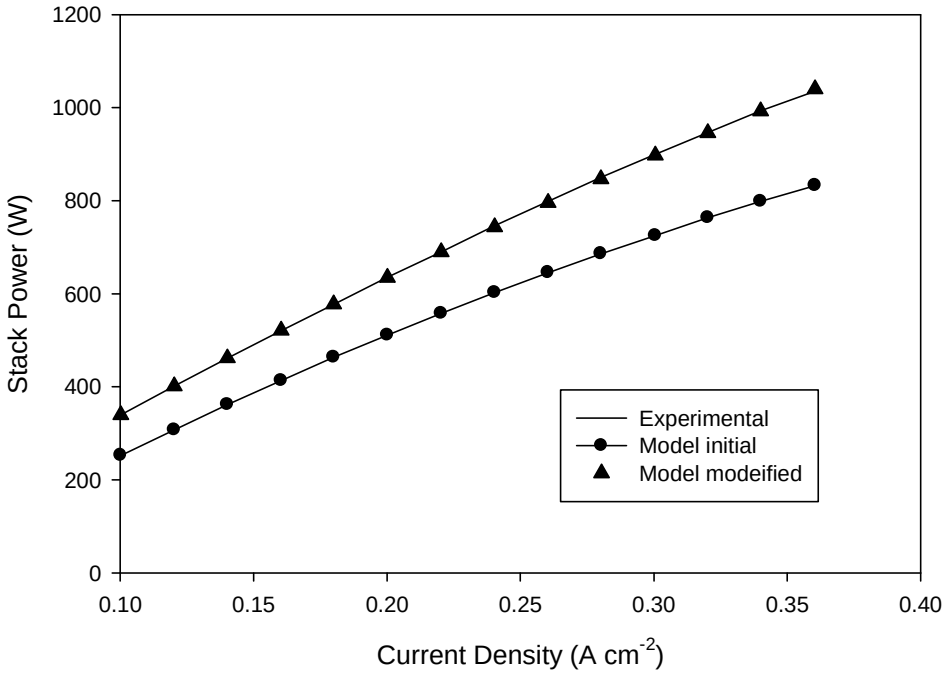

Figure 4.5: Experimental vs. simulated stack power

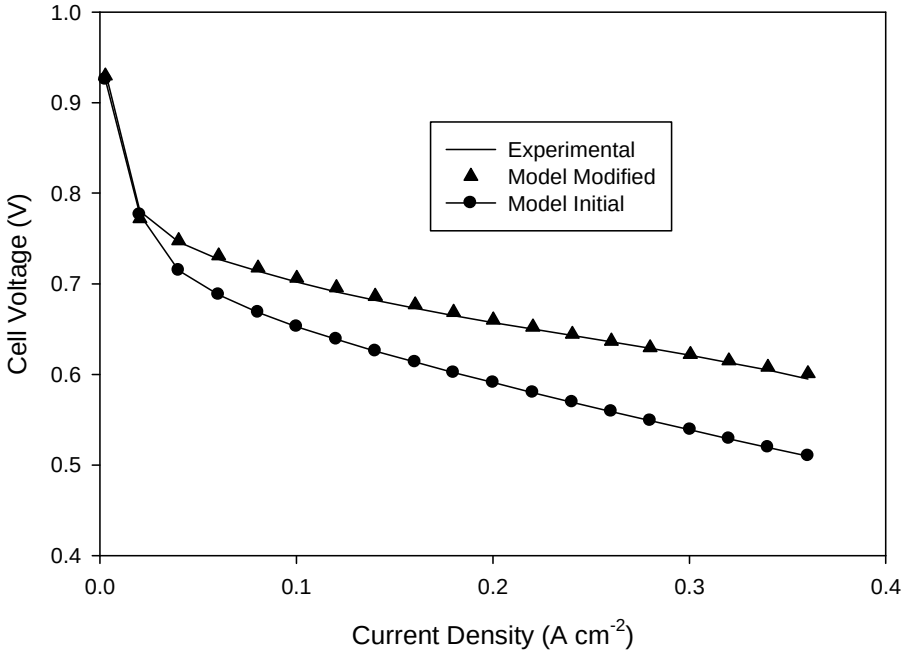

Figure 4.6: Average stack Voltage vs. simulated voltage

A multiple parameter sensitivity analysis using the built-in EES uncertainty propagation tool was used to determine the stack performance for the selected parameter range. The results show how the outputs of the model vary with variations in the input values. When selected system variables are varied, their effect on the stack efficiencies is calculated, using the law of uncertainty propagation. Uncertainty Propagation determines the uncertainty of a selected calculated variable as a function of the uncertainties of one or more measured variables upon which it depends. By assuming the individual measurements are uncorrelated and random, the uncertainty in the calculated parameter can be expressed as:

$$U_Y = \sqrt{\sum_i \left(\frac{\partial Y}{\partial X_i}\right)^2 U_{X_i}^2} \tag{4.9}$$

Where Y is a function of (X_1, X_2, X_3, …..,X_n,)

The results of the uncertainty propagation of the 1 kW_{el} stack are shown in Table 4.1 where the sensitivity of each system efficiency as a function of variables is presented. For the uncertainty estimations variable parameters were set with a fixed relative uncertainty of 0.15% (higher values caused simulation inconsistencies). The result shows that the cogeneration, electrical and thermal efficiencies is affected by an uncertainty value of $\pm$ 4.888%, $\pm$ 6.535%, $\pm$ 10.42%

for outputs value of 84.66%, 39.97%, 44.69% efficiency, respectively. The uncertainty are moderately high, signalling that some of the input parameters can cause a highly considerable effect on the model performance when varied, while others have little or no effect. For the three output stack efficiencies, it is observed that the major sources of uncertainty are the current density, hydrogen utilization and the operating temperature. Whilst for the cogeneration efficiency, there is larger uncertainty that is caused by area of the cell. It was not worthwhile to investigate this, because the area of the cell should remain fixed as it is a basis for the stack design.

Table 4. 1: Uncertainity analysis of the stack

Parameters	*% Uncertainty Overall Efficiency*	*% Uncertainty electrical Efficiency*	*% Uncertainty thermal Efficiency*
A_m	22.14 %	0.00 %	4.87 %
α_a	0.00 %	3.48 %	1.37 %
α_c	0.00 %	2.02 %	0.79 %
j	22.14 %	2.35 %	10.05 %
λ_{H_2}	22.14 %	84.19 %	63.40 %
λ_{O_2}	0.00 %	0.00 %	0.00 %
N	3.72 %	0.00 %	0.82 %
T_{stack}	29.34 %	0.00 %	18.58 %
T_{surr}	0.51 %	7.96 %	0.11 %

Selected output parameters	*Value $\pm$ Uncertainty*
$\eta_{overall}$	84.66 $\pm$ 4.888 %
$\eta_{electrical}$	39.97 $\pm$ 6.535 %
$\eta_{thermal}$	44.69 $\pm$ 10.42 %

4.3.1 Parametric Analysis

The purpose of the parametric analysis is to investigate the parameters that were major cause of uncertainties in the uncertainty propagation done in the previous section. The influence of four operating variables, namely, the stack operating temperature (T_{stack}), hydrogen utilization (λ_{H_2}) stoichiometry and the carbon monoxide (CO) content in the anode gas feed and the current density (j) on the efficiency of the fuel cell stack are studied for the required stack electrical output. For all the studied conditions, the stack design parameters such as cell active area, no of cells in the stack were kept constant in order to provide a design basis for the system. Furthermore, other operating variables such as the feed gas pressures and the cathode gas feed were also kept constant to remain within realistic operating conditions. Table 4.2 gives the description of fixed parameters along with their values.

Table 4. 2: Description and values of parameters held constant for the parametric study

Fixed Parameter	Value
Cell active area, A_{cell}	0.01 cm^2
Number of cell, N_{stack}	48
Anode gas pressure, P_{anode}	1 atm
Cathode gas pressure, $P_{cathode}$	1 atm

The effect of stack operating temperature on the performance of the stack is shown in Figures 4.7 and 4.8. Figure 4.7 shows effects on the stack electrical and thermal power output, it is observed that when temperature is increased from 130 ^oC to 160 ^oC, the electrical power increased from 989 W to 1063 W whilst the thermal output of the stack decreased from 1346 W to 1181 W. The increase in electrical power is a result of increase in stack voltage caused by better electrode kinetics and increase in reversible cell potential. For the same amount of energy that is feed to the stack, when the temperature is increased, the electrical power increases. This increase result in less energy being available for thermal conversion, hence there is a decrease in the stacks thermal power output. Figure 4.8 shows the effect of the temperature on the thermal, electrical and overall efficiency on the stack. A similar trend is observed for the electrical and thermal efficiency as that of respective power outputs. It is found that when temperature is increased from 130 ^oC to 160 ^oC, the thermal and cogeneration efficiency decreases from by 6% and 4% respectively whilst the electrical efficiency increases by 3%.

It can be seen from Figure 4.9 that the ratio between the electrical power output and thermal increases as the current density increases. When the current density is 0.20 A/cm^2 this ratio is 0.7, this indicates that 70% of the energy input to the stack is converted to electrical energy with the remainder to thermal energy. This ratio becomes unity at an operating current density of 0.30 A/cm^2 and at this load the electrical and thermal power outputs are equal, this is the optimal operating current density of the stack. When the operating current is increased the ratio increases to 1.11 for an operating voltage of 0.35 A/cm^2 indicating that at this load 11% more thermal energy is produced. The dependence of thermal, electrical, and cogeneration efficiencies on current density is shown in Figure 4.10. Although the effect of current density on the electrical efficiency is not as pronounced as in the overall and thermal efficiency, there is

some noticeable decrease as the current density rises, due to the higher ohmic losses and decrease in

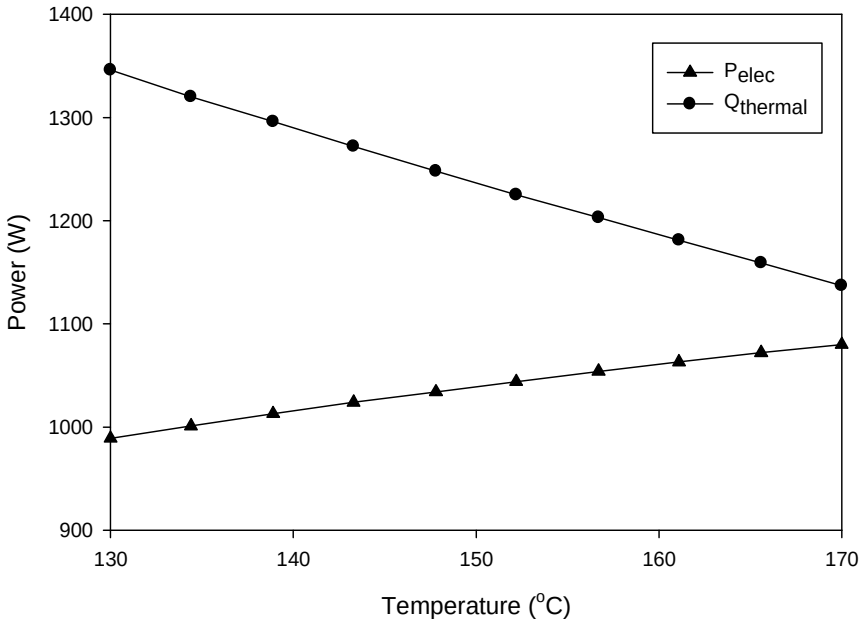

Figure 4.7: Temperature of the stack vs. stack power outputs efficiencies

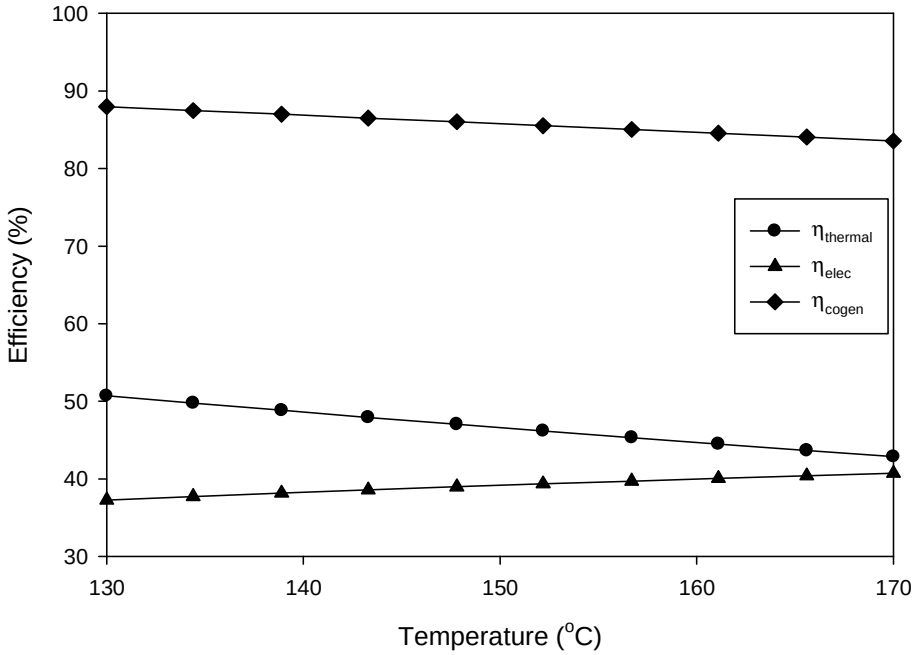

Figure 4.8: Temperature of the stack vs. stack

stack voltage. The electrical efficiency reaches its minimum value 39.97% at 0.35 A/cm^2 which is some 3.11% lower than the value at 0.20 A/cm^2. There is significant rise in the thermal efficiency

observed when the current density is increased because of the increase in heat being produced by the stack. At 0.35 A/m^2 operating condition the thermal efficiency is at its maximum value equal to 44.7%. It is observed that the overall efficiency of the stack increases from 73% to 84% while electrical power and the thermal power output increases from 653 W to 931 W and around 456 W to 936 kW, respectively when current density is increased from 0.20 A/cm^2 to 0.30 A/cm^2. Other observations at different current density are that the voltage of the stack decreased with increased current density. These results indicate that for a given operating conditions, thermal energy can be harnessed from the stack without significant lost in the stack electrical output.

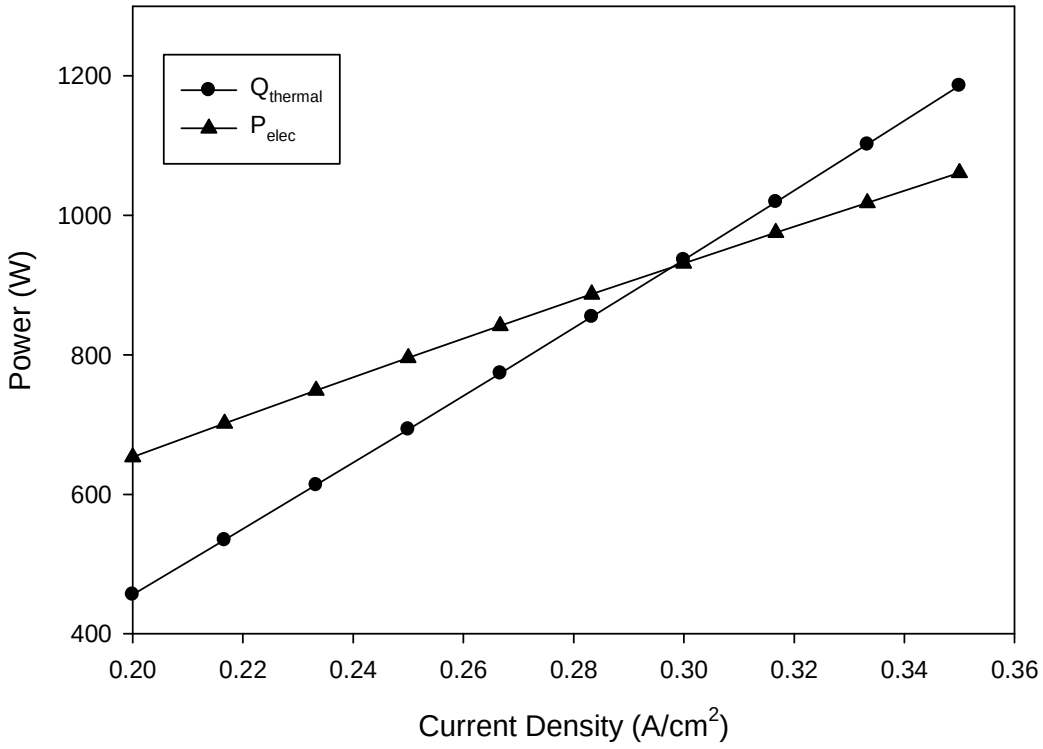

Figure 4.9: Current density of the stack vs. stack electrical and power output

The hydrogen utilization is the amount of hydrogen in the reactant feed that is converted in the anode electrochemical reaction. Figure 4.11 shows the stack performance for anode utilization of up to 2. An increase in the hydrogen utilization has positive effects on both the cogeneration and thermal efficiency, having an increase from 80.8% and 30.9% to 90.4% and 65.4% respectively. From the definition of the thermal efficiency (Equation 4.7), when there is more flow of the fuel into the fuel cell stack, an increase in the thermal output is to be expected. This can be seen when the hydrogen utilization is increased (more flow of fuel in the anode), where the thermal power produced increases from 799 W when simulated for a dead-end mode (H_2

stoichiometry of 1) to 1270 W at 1.22 hydrogen stoichiometry. It is observed that the electrical power output is slightly affected by the change in hydrogen utilization. This explains why the electrical efficiency drops with increased hydrogen utilization.

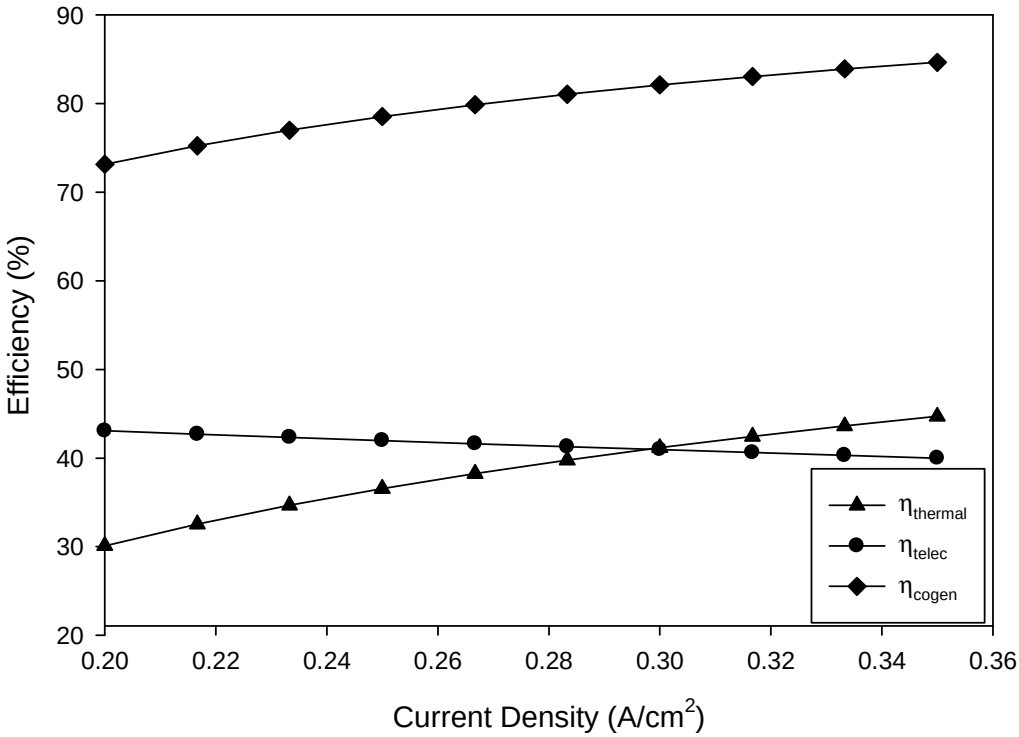

Figure 4.10: Current density of the stack vs. stack efficiencies power outputs

This is particularly due to the stack voltage not changing with the hydrogen utilization; it can be concluded that at different hydrogen utilization and fixed current density, that there is always sufficient hydrogen available for chemical reaction. The effects of hydrogen utilization was also simulated at different reformate composition. This was done to see how the carbon monoxide poisoning may affect the stack performance when the hydrogen conversion was varied. There was no significant performance drop at when the hydrogen partial pressure was decreased from 0.8 to 0.77. There was a small decrease in the electrical efficiency from 35.7 to 35.4 and an increase in thermal efficiency from 48.6 to 49 % at a hydrogen utilization of 1.22.

The main function of the PEMFC stack is to generate electrical power; therefore the electrical power produced is evaluated at different operating conditions. The stack performance at different current density, temperature and hydrogen stoichiometry is shown in Figure 4.12 (a) and (b). As can be seen in if Figure 4.12 (a) the stack electrical power increases as both the

current density and hydrogen stoichiometry increases. At hydrogen stoichiometry that is less than 1.3 and low current density the power produced is low.

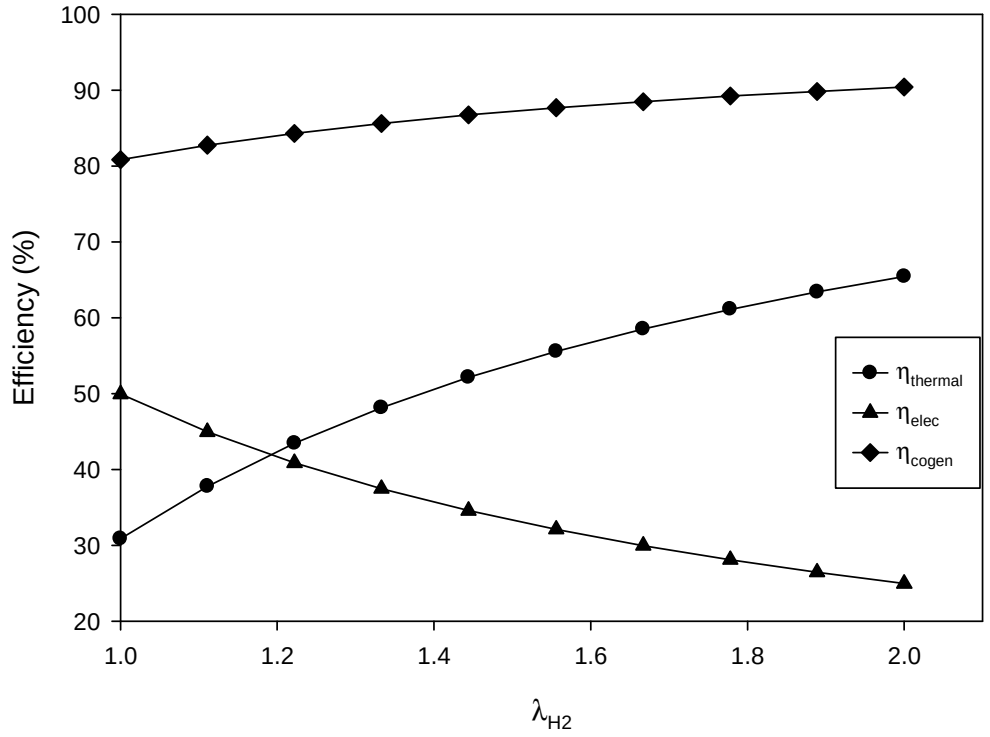

Figure 4.11: hydrogen utilisation vs. stack efficiencies

It can thus be concluded that when the stack is operated at “normal stoichiometry” of 1.25 high current must be drawn from the stack for better performance in terms is electricity produced. Similarly, when the same stoichiometry is used high temperature are favourable for better performance as can be seen in Figure 4.12 (b).

Figure 4. 13 (a) and (b) shows 3D graph depicting the stacks electrical efficiency at different hydrogen stoichiometry, current density and temperature. It can be seen that the electrical efficiency drops as both the current density and temperature increases.

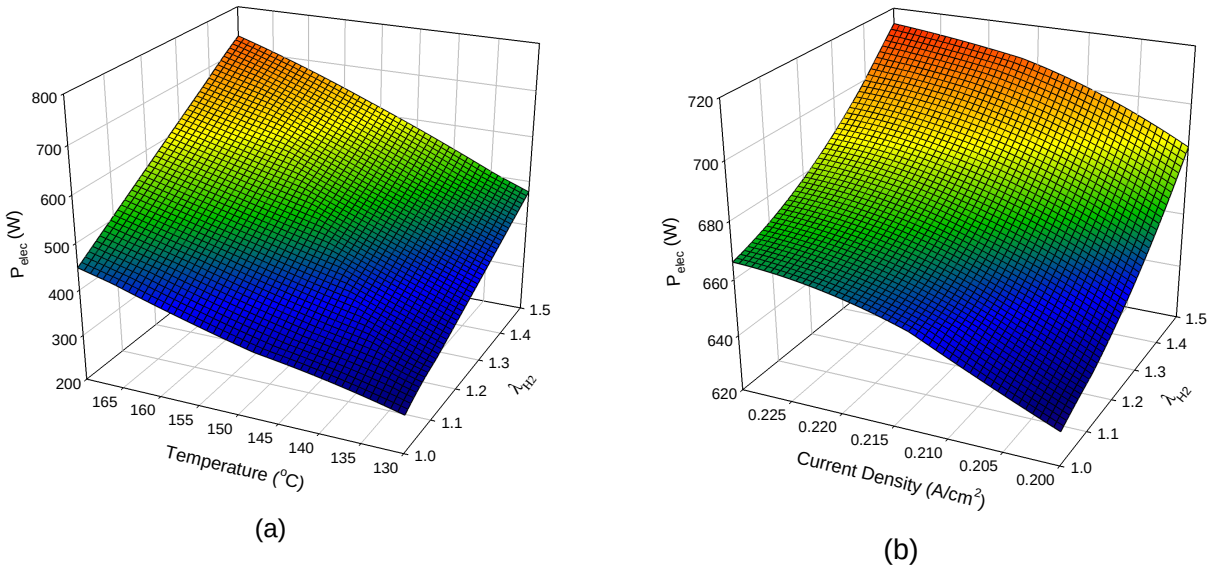

(a) (b)

Figure 4.12: Current density, hydrogen stoichiometry, and operating temperature effects on electrical power output

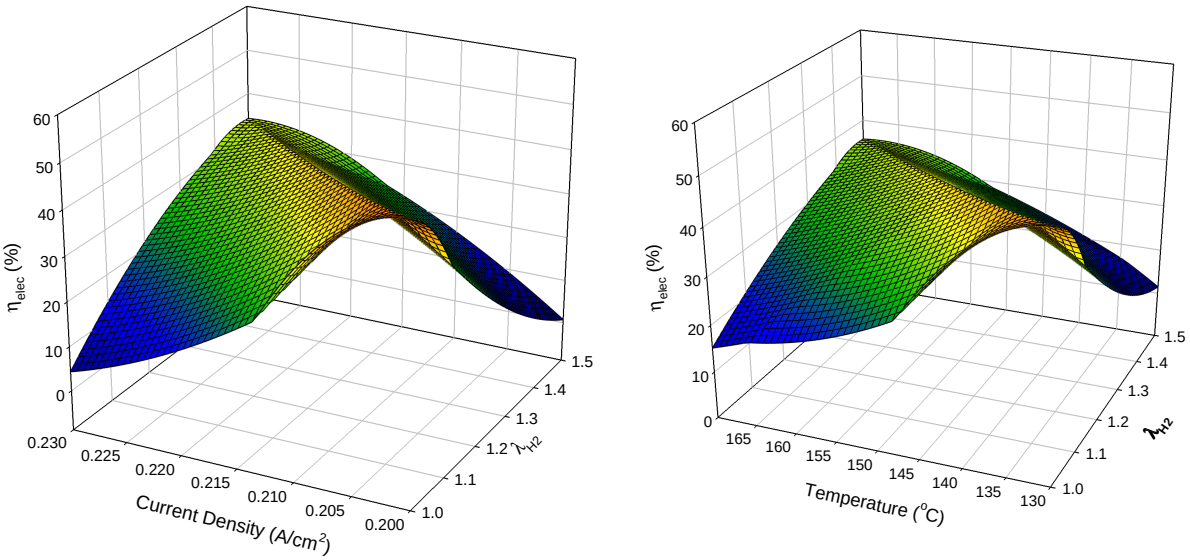

(a) (b)

Figure 4.13: Current density, hydrogen stoichiometry, and operating temperature effects on electrical efficiency

CHAPTER FIVE
1 kW_{el} µ-CHP MODELLING

5 Introduction

In order to evaluate the micro-CHP (µ-CHP) system performance, a system similar to the one proposed by Kim (2008) has been used. However, because this work focuses on the thermodynamic and kinetic modelling, the geometrical model of the system components has not been considered. Another noticeable difference from the model proposed by (Kim 2008) is two stage fuel processor and the exclusion of the work recovery and air supply subsystem. PEMFC systems for stationary applications generally have their on-board fuel conversion systems. These may consist of several subsystems; a fuel processor, fuel stack, work and recovery air-supply system and power electronic system. The purpose of the fuel processor is to generate rich gas (syngas/reformate) for the fuel cell stack. The fuel processor modelled in this work consist of a reformer step to reform methane, two part water gas shift for CO removal, steam generator, a combustor to supply heat to the reformer and heat exchangers for thermal integration.

The fuel feed to the system is fed by a compressor to the methane pre-heater, where it is heated up to 250 ^{o}C by the combustor flue gas. This stream is then separated by a by-pass valve/splitter and one stream goes to a mixer to be mixed with steam and the other is sent to the combustor. Water at room temperature is pumped to a steam generator where it is heated (also by the combustor flue gas) to produce steam for the SMR reactor. The use of the flue gas to preheat the methane feed and to generate steam is exemplary of how heat integration to recover the heat available in the anode off gas is used in the system as compared to when the system does not produce its on hydrogen for the fuel cell stack. The mixture of methane and steam is supplied to the SMR reactor. In the SMR reactor, the conversion of methane to reformate/syngas gas through catalytic reforming is achieved. Because the reaction steam methane reforming reaction is endothermic, heat needs to be supplied to the SMR reactor. The heat required in the SMR is supplied by the flue gas from the combustor. Downstream the SMR reactor are two water gas shift (WGS) reactors, whose purpose are to reduce the carbon monoxide (CO) produced by the reforming reaction. The syngas is first fed to the high water temperature WGS reactor operating at temperatures between 500 ^{o}C and 350 ^{o}C where about 60 percent conversion of CO in the syngas is achieved. After the high temperature WGS reactor

is a low temperature WGS operating at around 250 ^{o}C where the rest of the CO left in the syngas is converted.

In between the SMR, HTWGS and LTWGS heat exchangers compact type heat exchangers are used to regulate the temperature of the syngas for the inlet operating conditions of the reactor. Air supplied to the burner is first preheated using the between the reactors using these heat exchangers. Since no humidification of the reactant gasses supplied in the fuel cell stack is needed, a condenser is used to remove the remaining water from the syngas. In the fuel cell stack, the syngas from the fuel processor and air is supplied to the anode and cathode respectively. The unused hydrogen and the syngas from the anode are fed to the combustor where it is burned with the methane from feed and air. The cathode off gas is sent to a cogeneration heat exchanger to produce hot water for thermal load demand.

The fuel cell stack model developed in chapter 4 is coupled with a fuel processor model to form a μ-CHP system. The system is designed to produce a maximum of electrical power of 1 kW_e and the thermal power was fixed to be 1.5 kW_{th} all times. The energy output would typically provide electricity and thermal power for a house-hold. The system's user-interface is shown in Figure 5.1 where the system inputs and outputs are shown. The system inputs in the fuel processor include amount of excess air feed to the combustor, the reactor (SMR, HT-WGS and LT-WGS) operating temperatures and pressure, the SMR steam-to-carbon ratio. From the fuel stack the operating current density, temperature, hydrogen and oxygen stoichiometry and the no of cells in the stack are the inputs. When all these inputs are set, the system calculates all the flowrates into and out of the system. The performance outputs of the system are the voltage, current electrical and thermal power and their corresponding efficiencies.

5.1 Micro-CHP System Model

The models of the fuel processor components consist of equations that describe mass and energy flows around the system. The equations are based on the reaction kinetics inside each reactor and on the laws of conservation of mass and energy for each component in each reactor under steady state conditions. The reaction kinetics modelling method is chosen over the equilibrium method because it provides more realistic results and maybe easily modified when new experimental data is available. The conservation of mass and energy for each component can be written as

$$\sum_{in} \dot{m}_{mix} = \sum_{out} \dot{m}_{out} \quad (5.1)$$

$$\sum_q \dot{Q}_{reaction} + \sum_{in} \dot{m}_{mix}\ \dot{h}_{mix} = \sum_{out} \dot{m}_{mix}\ \dot{h}_{mix} + \dot{W} \quad (5.2)$$

Where in and out refer to the inlet and outlet flow streams, respectively, and q to the number of heat interactions $\dot{Q}_{reaction}$ of the component with other components or system. $\dot{W}$ represents the work done by the component, $\dot{m}_{mix}$ is the inlet or outlet gas mass flow rate, and $\dot{h}_{mix}$ is the corresponding specific enthalpy of the gas. The gas molar flow rate, $\dot{m}_{mix}$ is defined as the sum of the mass flow rates of components and the corresponding specific enthalpy $\dot{h}_{mix}$ is given by the following relation

$$\dot{h}_{mix}\,(T) = \sum_{i=1}^{n} y_i h_i\ (T) \quad (5.3)$$

y_i represents the mass fraction of the component i and h_i is its corresponding partial enthalpy. The partial enthalpies of each component were obtained from EES thermodynamic functions based on JANAF thermo-chemical tables.

5.1.1 Steam Methane Reformer

The reactions that are chosen to describe the steam reforming of methane are the endothermic demethanation reaction and the exothermic water gas shift reaction and the overall reaction. The kinetics chosen for the SMR modelling were developed by (Xu and Froment, 1989) over a $Ni/MgAl_2O_4$ catalyst. These reactions used to the model the reactor are shown below

$$CH_4 + H_2O \rightarrow CO + 3H_2 \qquad \Delta h^o = 206.1\ kJ\ mol^{-1} \quad (5.4)$$

$$CO + H_2O \rightarrow CO_2 + H_2 \qquad \Delta h^o = -41.2\ kJ\ mol^{-1} \quad (5.5)$$

$$CH_4 + 2H_2O \rightarrow CO_2 + 4H_2 \qquad \Delta h^o = 164.9\ kJ\ mol^{-1} \quad (5.6)$$

The reaction rates r_i are expressed as follows:

$$r_1 = \frac{\frac{k_1}{P_{H_2}^{2.5}}\left[P_{CH_4} P_{H_2O} - \frac{P_{H_2}^3 P_{CO}}{K_{eq_1}}\right]}{DEN^2} \quad (5.7)$$

$$r_2 = \frac{\frac{k_2}{P_{H_2}}\left[P_{CO} P_{H_2O} - \frac{P_{H_2} P_{CO_2}}{K_{eq_2}}\right]}{DEN^2} \quad (5.8)$$

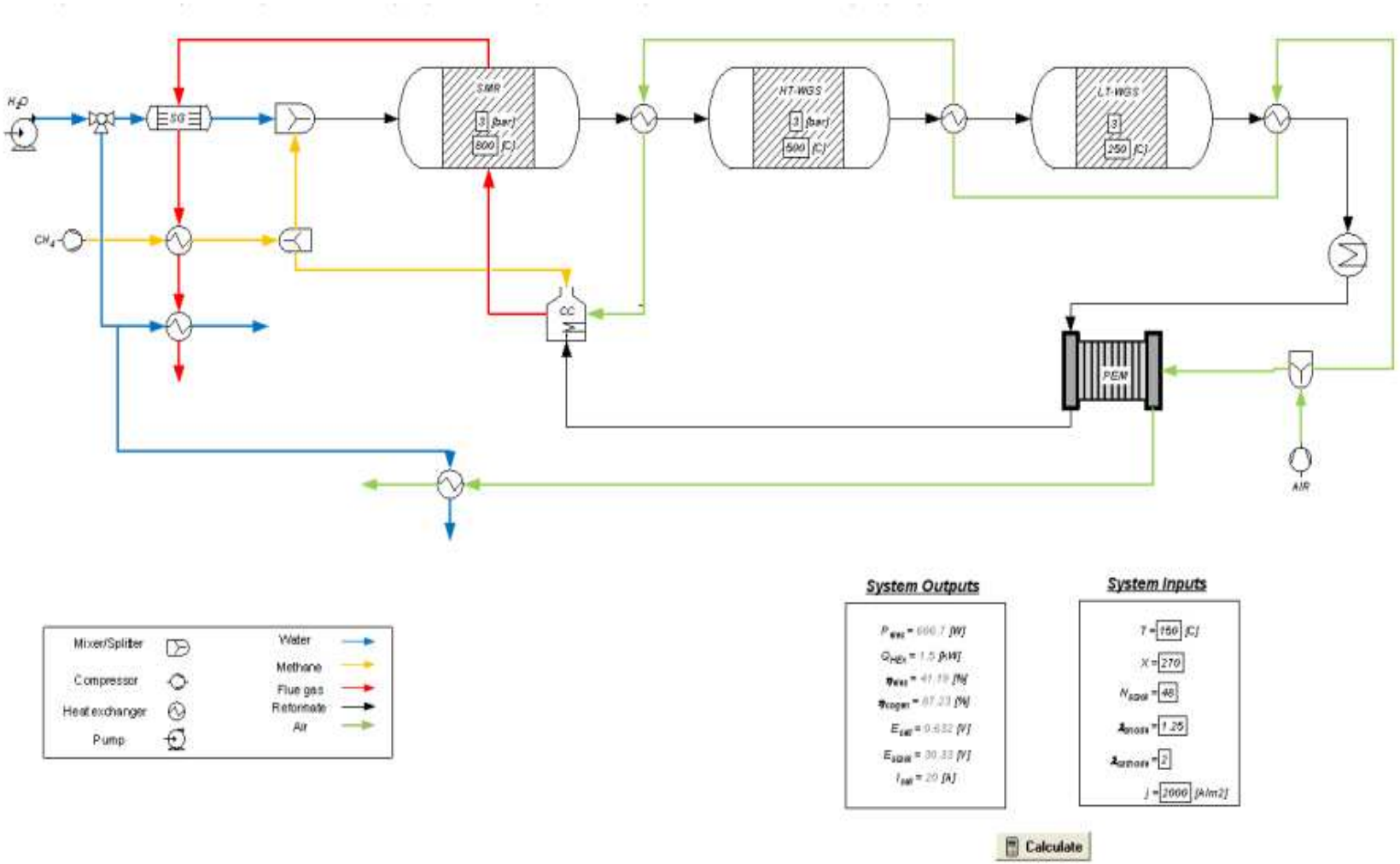

Figure 5.1*: Proposed CHP system user-interface*

$$r_3 = \frac{\frac{k_3}{P_{H_2}^{3.5}}\left[P_{CH_4} P_{H_2O}^2 - \frac{P_{H_2}^4 P_{CO_2}}{K_{eq_3}}\right]}{DEN^2} \tag{5.9}$$

where

$$DEN = 1 + K_{CO} P_{CO} + K_{H_2} P_{H_2} + K_{CH_4} P_{CH_4} + K_{H_2O} \frac{P_{H_2O}}{P_{H_2}} \tag{5.10}$$

k_i represent the rate constants of each reaction i , P_j is the partial pressures of each species j , the K_{eq_i} the equilibrium constants of each reaction i , and the K_j the adsorption constants of each species. The rate constants and adsorption constants are determined by the Arrhenius and Van't Hoff relations, respectively.

$$k_i = A_i \exp\left(\frac{-E_i}{RT}\right) \tag{5.11}$$

$$K_i = B_i \exp\left(\frac{-\Delta H_i}{RT}\right) \tag{5.12}$$

The pre-exponential factors, the reaction enthalpies and activation energies are given in appendix. The equilibrium constants of the reactions can be determined by the following expressions

$$K_{eq_1} = \exp\left(\frac{-26830}{T} + 30.114\right) \tag{5.13}$$

$$K_{eq_2} = \exp\left(\frac{4400}{T} - 4.036\right) \tag{5.14}$$

5.1.2 High- and Low-Temperature Shift Reactors

The amount of CO exiting the SMR is significantly lower compared to the other species, however for use in a PEMFC it has to be decreased to less than one percent because at higher concentration it acts as poison to the fuel cell electrode catalyst. To reduce the CO concentration coming out of the SMR, a two part water-gas shift reactors (High and Low temperature) are used to convert CO to CO_2 .The chemical reaction in both the high and low water gas shift reactors are the same.

$$CO + H_2O \rightarrow CO_2 + H_2 \qquad \Delta h^o = -41.2\ kJ\ mol^{-1} \tag{5.15}$$

The rate of the reaction inside the high water gas shift reactor using Fe_2O_2 – Cr_2O_3 catalyst is given by

$$r_{co} = K_{Hs} \exp\left[\frac{E}{R}\left(\frac{1}{T_{Hs}} - \frac{1}{T}\right)\right] \sqrt{P}\,(x_{CO})\left(1 - \frac{K}{K_{eq}}\right) \tag{5.16}$$

Where T_{Hs} and K_{Hs} are the temperature and standard catalyst activity, E is the activation energy. K_{eq} is the equilibrium constant. K is the mole fraction ratio and is given by

$$K = \frac{x_{H_2}\, x_{CO_2}}{x_{H_2O} x_{CO}} \tag{5.17}$$

The rate of the reaction inside the low water gas shift reactor using CuZnO - Al_2O_3 is given by

$$r_{co} = K_{Ls}\ P_{CO}\, P_{H_2O}\left(1 - \frac{K}{K_{eq}}\right) \tag{5.18}$$

Where K_{Ls} is the rate constant, P_{CO} and P_{H_2O} respectively represents the partial pressure of carbon monoxide and water.

$$K_{Ls} = A_{Ls} \exp\left(\frac{-E_{Ls}}{RT}\right) \tag{5.19}$$

The pre-exponential factor and the activation energy given in 5.19 are given in appendix.

5.1.3 Mixer

The mass and energy balance equations for the mixer are given by equation 5.20 and 5.21. The outlet mass flow rate and temperature are calculated based on the inlet flow conditions. An assumption of no accumulation of mass and no energy losses through the mixer walls is made.

$$\sum_{in} \dot{m}_i = \sum_{out} \dot{m}_i \tag{5.20}$$

$$\sum_{in} \dot{m}_i\, h_i\,(T_{in}) = \sum_{out} \dot{m}_i\, h_i\,(T_{out}) \tag{5.21}$$

The index $\boldsymbol{i}$ represents different components of the gas in the mixer (CH_4, H_2, O_2, N_2, etc), the $\boldsymbol{\dot{m}_i}$ is mass flow rate of component $\boldsymbol{i}$, which is constant through the mixer and $\boldsymbol{h_i}$ represents enthalpy.

5.1.4 Heat exchangers

The main objective of modelling the heat exchangers in this work is to obtain the outlet temperatures of either the cooling or the heat fluid and to obtain the heat duties of the heat exchangers. There are two types of heat exchangers that were modelled in this work, a shell-tube type heat exchangers and compact heat exchangers. The shell-tube type heat exchanger is used to model the steam generator and the compact heat exchanger type model is applied to the methane pre-heater and the heat exchangers between the reactors for thermal management. The thermal analysis of the heat exchangers is based on the number of transfer units (NTU) method based on the concept of heat exchanger effectiveness. The effectiveness, $\boldsymbol{\varepsilon}$, of a heat exchanger is the ratio of the actual heat transfer rate to the thermodynamically limited maximum possible heat transfer rate if an infinite heat transfer surface area were available (Welty et al., 2008). The actual heat transfer is obtained either by the energy given off by the hot fluid or the energy received by the cold fluid. The ratio of heat transfer is obtained using equation 5.23 when the hot fluid is the minimum fluid and by equation 5.24when the cold fluid is the minimum fluid.

$$\varepsilon = \frac{Q}{Q_{max}} \tag{5.22}$$

$$\frac{Q}{Q_{max}} = \frac{\dot{m}^h_{mix}\left[cp^h_{mix}\left(T_{h,i}\right) - cp^h_{mix}\left(T_{h,o}\right)\right]}{Q_{max}} \tag{5.23}$$

$$\frac{Q}{Q_{max}} = \frac{\dot{m}^c_{mix}\left[cp^c_{mix}\left(T_{c,i}\right) - cp^c_{mix}\left(T_{c,o}\right)\right]}{Q_{max}} \tag{5.24}$$

where Q_{max} the maximum possible heat transfer and Q is the actual heat transfer. The indices i and o represent inlet and outlet respectively, and h and c representing hot and cold fluid. cp_{mix} is the arithmetic mean heat capacity of the fluids and $\dot{m}_{mix}$ is the gas mass flow rate.

The system efficiencies that are used in analysis of the CHP system are; the thermal efficiency is defined as the ratio of the heat recoverable from the thermal management subsystem and the amount chemical available in the input gas (Methane) entering the system

$$\eta_{thermal} = \frac{P_{elec} + Q_{TM}}{\dot{m}_{CH_4,in} \ LHV_{CH_4}} \quad (5.25)$$

The system electrical efficiency is defined as the ratio of the electrical power output of the system divided the chemical energy of the hydrogen produced in the fuel processing unit

$$\eta_{elec} = \frac{P_{elec}}{\dot{m}_{CH_4,in} \ LHV_{CH_4}} \quad (5.26)$$

The overall system efficiency is defined as the sum of the thermal and electrical efficiencies

$$\eta_{overall} = \eta_{elec} + \eta_{thermal} \quad (5.27)$$

5.2 Simulation results

The results of the uncertainty propagation of the system are shown in Table 5.1 where the sensitivity of each system efficiency as a function of variables is presented. For the uncertainty estimations variable parameters were set with a fixed relative uncertainty of 0.15% (higher values caused simulation inconsistencies). The result shows that the cogeneration, electrical and thermal efficiencies is affected by an uncertainty value of 3.067 %, 2.139 %, 1.619 % for outputs value of 87.3 %, 41.29 %, 46.02 % efficiency, respectively. The uncertainties are signal that some of the input parameters can cause a highly considerable effect on the model performance when varied, while others have little or no effect.

5.2.1 Parametric Analysis

The purpose of the parametric analysis is to investigate the parameters that were major cause of uncertainties in the uncertainty propagation done in the previous section. The influence of four operating variables, namely, the stack operating temperature (T_{stack}), hydrogen utilization (λ_{H_2}) and temperature of the combustion gases (T_{comb}), the current density (j) on the efficiency of the fuel cell stack are studied for the required system electrical output. Similarly to the stack analysis the system design parameters were kept constant in order to provide a design basis for the system. Furthermore, other operating variables were also kept constant to remain within realistic operating conditions.

The fuel processor's efficiency is evaluated firstly before the systems performance is evaluated. Since the purpose of the fuel processor is to produce hydrogen rich gas, it follows that the performance of the fuel processor is measured by conversion of methane to hydrogen rich gas. The fractions of the reacting species in the fuel processor as they go through different stages of the fuel processing subsystems are shown in Figure 5.2. About 97 percent of the methane fed to the steam reformer is converted to reformate gas. In the high temperature WGS reactor the 88 percent of the carbon monoxide produced in the reformer is converted with the low temperature WGS reactor contributing about 10 percent of the total CO conversion. The low temperature WGS reactor reduces the carbon monoxide content in the reformate gas to amount that is tolerable in the PEMFC and has a minor contribution to further production of hydrogen. The increase of component fractions in the PEMFC stack feed is as a result of decrease in the number of components due to water removed in the water-knock out stage

Table 5.1: Uncertainty analysis of the CHP system

Parameters	*% Uncertainty Cogen Efficiency*	*% Uncertainty electrical Efficiency*	*% Uncertainty thermal Efficiency*
T_{comb}	12.3	0.00	43.9
j	11.45	1.26	24.2
λ_{H_2}	66.9	93.3	7.49
λ_{O_2}	0.00	0.00	0.00
N	6.76	0.00	24.24
T_{stack}	2.54	5.22	0.00
T_{SMR}	0.03	0.12	0.01
T_{HTWGS}	0.00	0.00	0.00
T_{LTWGS}	0.03	0.11	0.02
P_{SMR}	0.00	0.00	0.00
P_{HTWGS}	0.00	0.00	0.00
P_{LTWGS}	0.00	0.00	0.00
SC_{ratio}	0.00	0.00	0.00

Selected output parameters	*Value $\pm$ Uncertainty*
η_{cogen}	87.3 ± 3.067
$\eta_{electrical}$	41.29 ± 2.139
$\eta_{thermal}$	46.02 ± 1.619

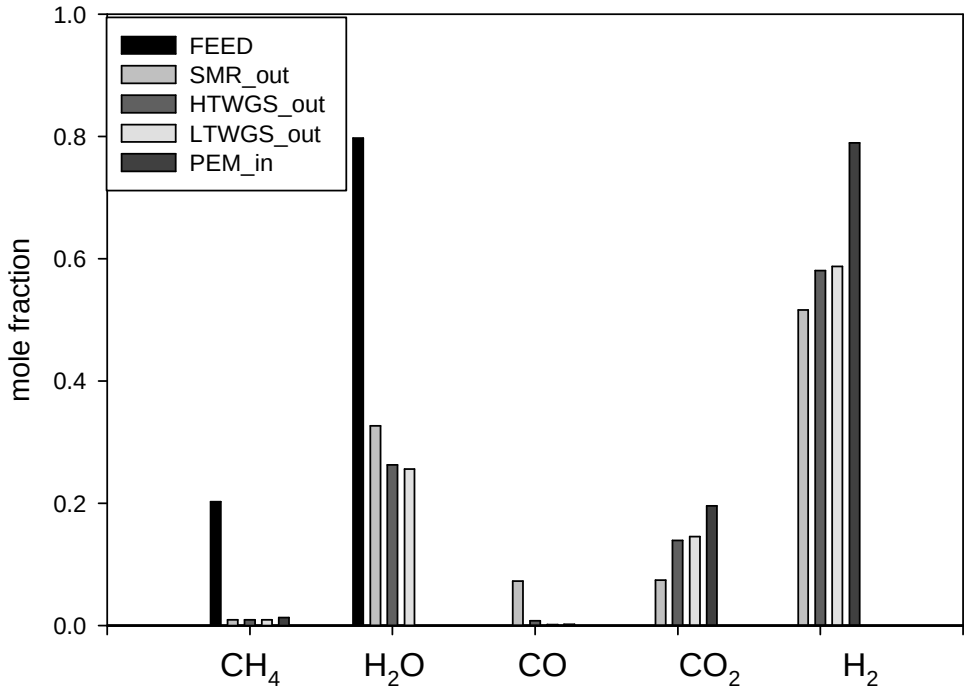

Figure 5.2: Composition of the synthesis gas at different stages of the fuel processor

The performance of the system at part load requirements was simulated by varying the current density. Because an operational fuel cell system is subject to load variations due to demands of energy at specific times, it is worthwhile to investigate how the load variations affect the electrical and thermal power with their corresponding efficiencies. The results for three different load requirements are shown in table 5.2 for 0.25 A/cm^2, 0.23 A/m^2 and 0.20 A/m^2. It can be seen from Figure 5.3 at part-load operations the thermal and overall efficiency decreases. The electrical efficiency does not seem to be affected by varying the current density; this was expected as was shown in the 48 cell stack analysis. Similarly to the stack simulations results, the overall system efficiency follows an analogous path with the thermal efficiency decreasing from 87.3% to 82.5% when the current density is increased from 0.20 A/m^2 to 0.25 A/m^2.

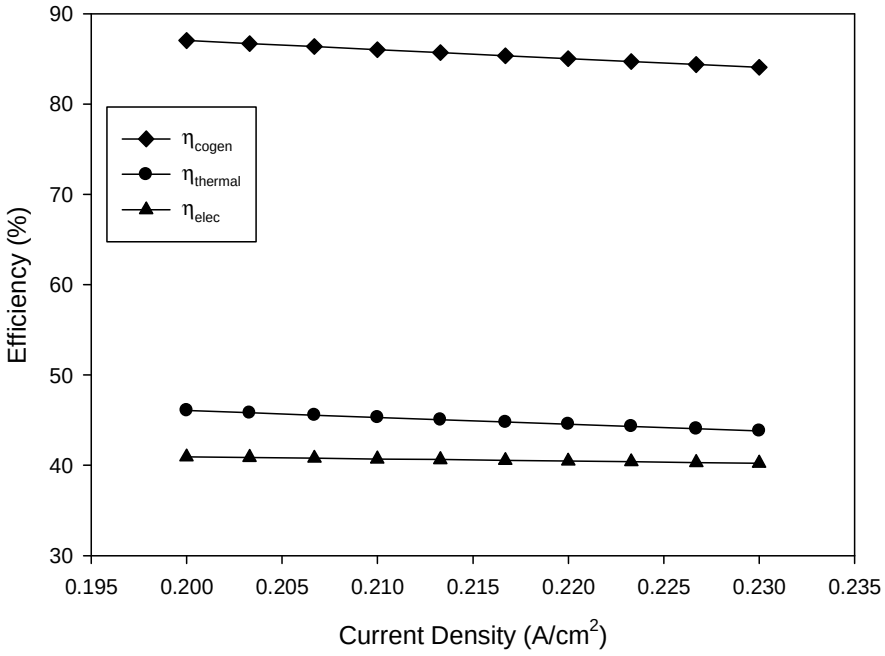

Figure 5.3: System efficiencies at different current density

Table 5.2: Model outputs at different load requirements

Load	0.25 A/cm^2	0.23 A/cm^2	0.20 A/cm^2
Electrical Power of Stack (kW)	767	713	631
Current of the stack (A)	25	23	20
Average Cell voltage (V)	0.64	0.65	0.66
Voltage of the stack (V)	30.68	31.03	31.56
Flowrate of CH_4 (kg/s)	7.08E-05	6.8E-05	6.52E-05
Cogeneration efficiency (%)	82.48	84.33	87.3
Electrical efficiency (%)	40.13	40.58	41.29
Thermal efficiency (%)	42.35	43.74	46.02

Figure 5.4 shows the behaviour of the system when the hydrogen utilisation is varied. The values are varied linearly from 1 to 1.5. The hydrogen utilisation 1 corresponds to 100 percent conversion and 1.5 to 66 percent conversion. The hydrogen utilisation was observed to have a negative impact on the system cogeneration performance when increased. The highest efficiency is obtained when a stoichiometry of 1 is used. However, values below 1.25 are not feasible when a reformate fuel is used and because there is a required amount of the anode off gas for the combustor (Barbir, 2005). Figure 5.5 shows the systems cogeneration efficiency against the hydrogen stoichiometry and current density. The system efficiency is highest when

the fuel cell stack is operated at low current density and low stoichiometry. The decay in the system cogeneration efficiency is a result of the drop in the electrical efficiency caused by less hydrogen being converted to electricity as explained in chapter 4.

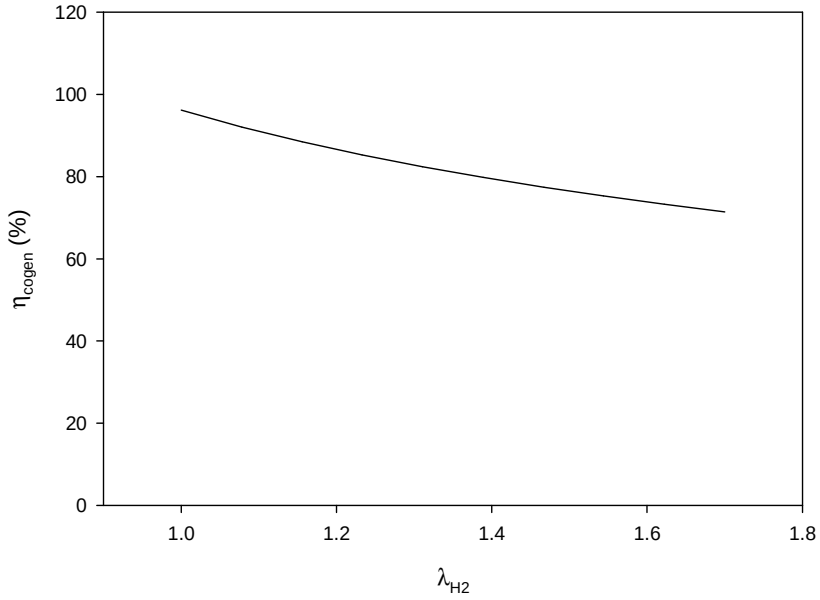

Figure 5.4: System cogeneration efficiency at different anode stoichiometry

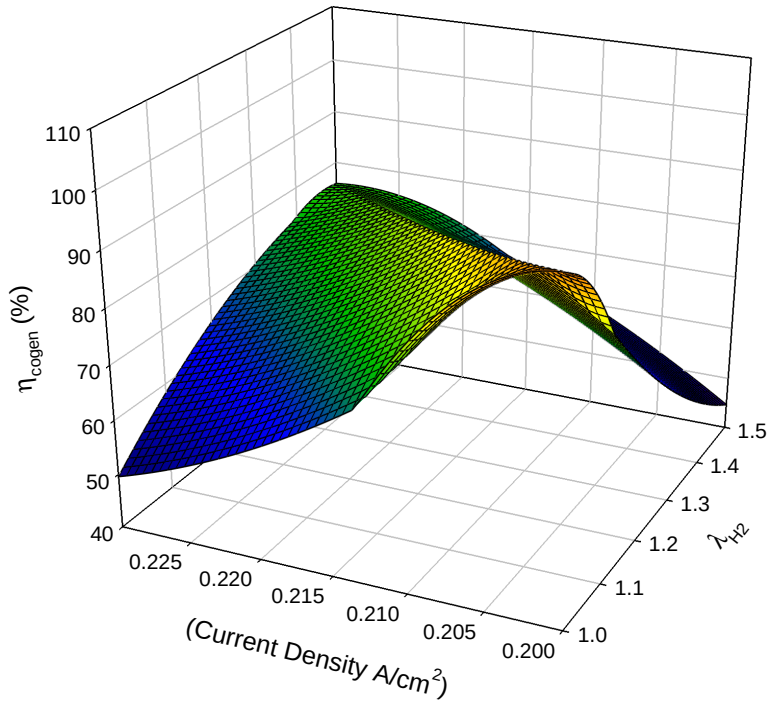

Figure 5.1: System cogeneration efficiency at different current density and anode stoichiometry

From the uncertainty propagation simulation (Table 5.1) the fuel cell operating temperature has an effect on cogeneration and electrical efficiencies. The latter has been investigated in the stack analysis and is expected not to change for the CHP system simulations as the balance of plant components were not modelled, which may lead to decrease in electrical power produced. The effect of stack operating temperature on the performance of the system cogeneration efficiency is shown in Figure 5.6; it is observed that when temperature is increased from 140 ^{o}C to 160 ^{o}C, the efficiency increases linearly. This was expected since there is an increase in the electrical efficiency as explained in section 4.2. From Figure 5.7 it can be seen that the maximum cogeneration efficiency is favoured at high temperatures and low current densities.

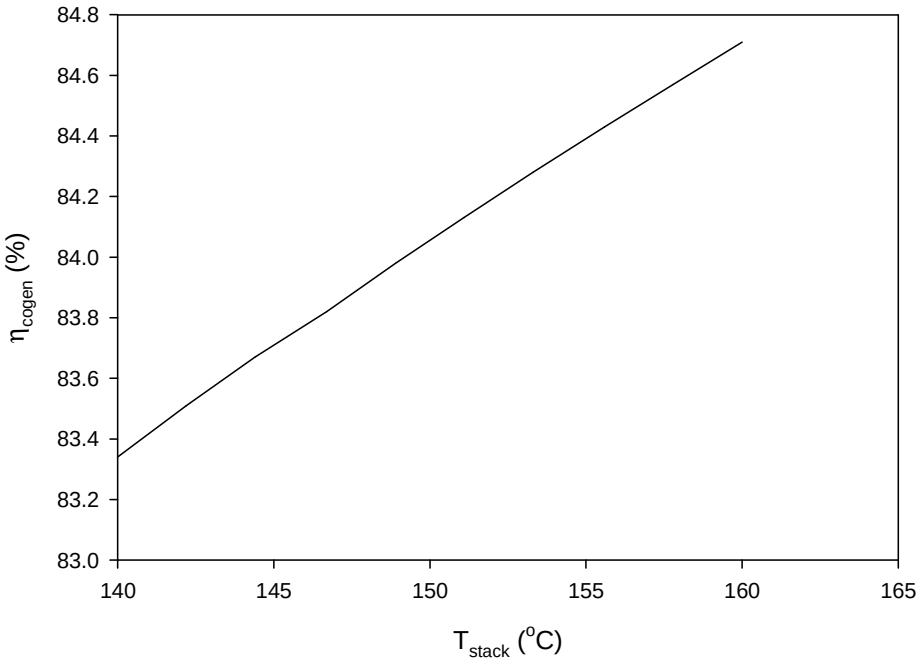

Figure 5.2: System cogeneration efficiency at different fuel cell stack temperature

The S/C ratio plays an important role in influencing the systems efficiencies because it influences the amount of hydrogen produced in the fuel processor and the energy required by the SMR. To investigate this effect, simulations were made to determine the systems performance at different S/C ratio, with the cogeneration and thermal efficiency being the objective functions. The S/C ratio was varied linearly from 2.5 to 4. Values below 2.5 have been excluded because they may result in carbon deposition and coke formation on the fuel cell anode (Arsalis *et al*., 2011). Although higher S/C ratios result in more hydrogen production (has positive effect on the performance of the fuel cell stack) values more than four are not included because they are not favourable for process economics as alluded to by (Kolb, 2008).

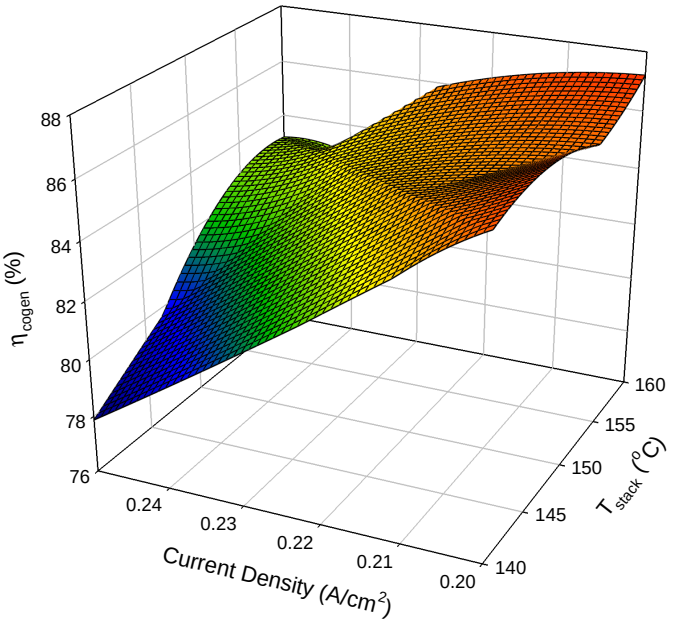

Figure 5.3: System cogeneration efficiency at different fuel cell stack temperature and current density

It was observed from Figures 5.8 and 5.9 that both the cogeneration and thermal efficiencies increased as the steam to carbon ratio increased, similar observations were made by Arsalis *et al*., 2011. Figure 5.10 shows that maximum cogeneration efficiency is reached at low hydrogen stoichiometry and high S/C ratios at low current densities. This figure shows contradicting results from figure 5.8 because of the varied hydrogen stoichiometry. For this system it can be concluded that the optimum steam to carbon ratio is 3 when operating at a hydrogen stoichiometry of 1.25 and a current density of 0.20 A/cm^2.

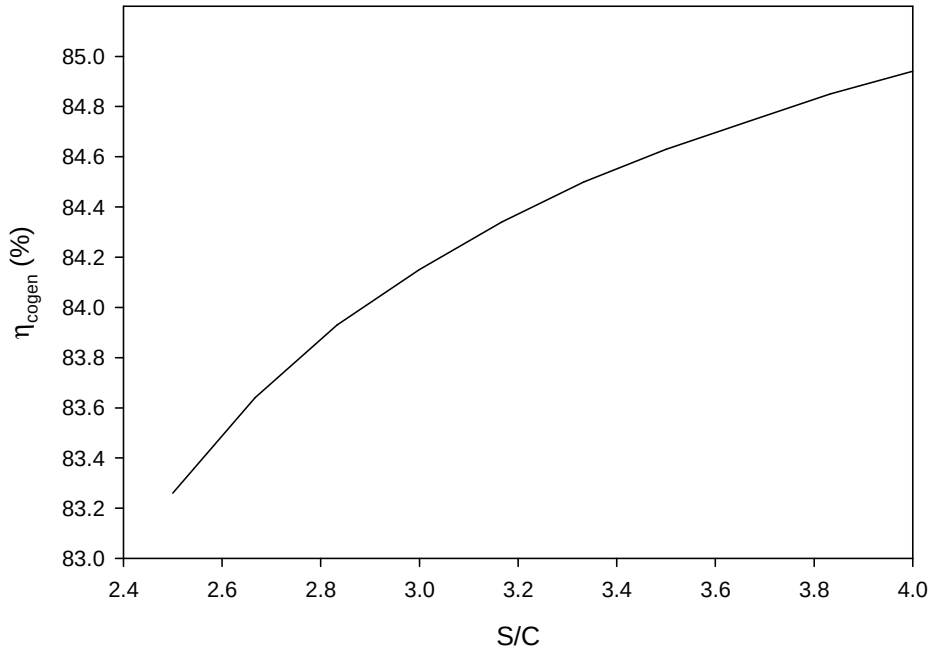

Figure 5.4: System cogeneration efficiency at different steam to carbon ratio

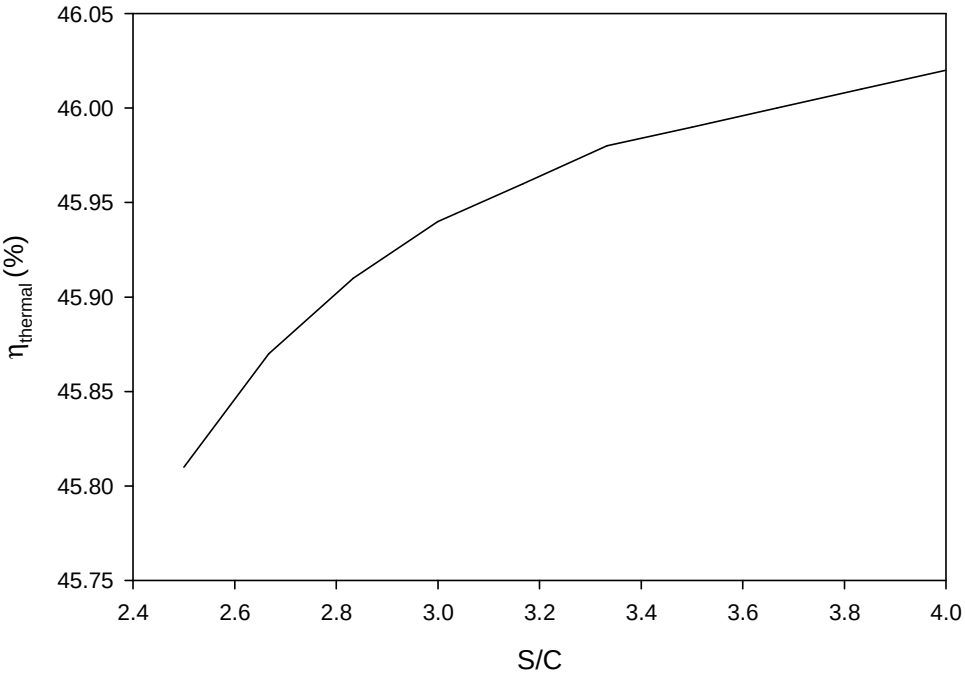

Figure 5.5: System thermal efficiency at different steam to carbon ratio

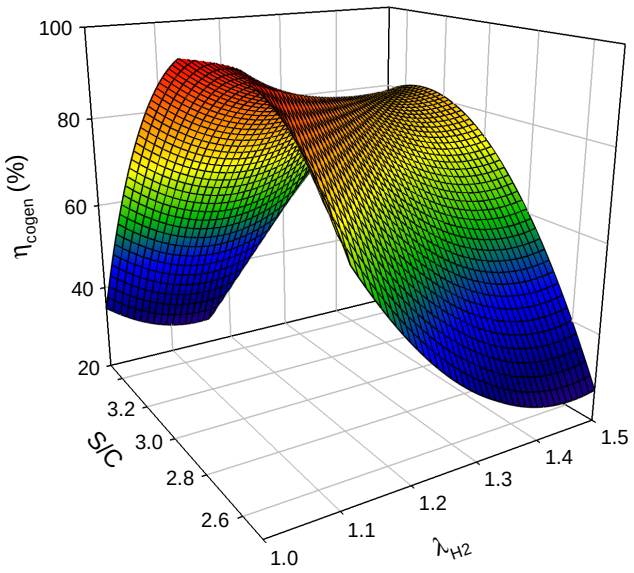

Figure 5.6: System cogeneration efficiency at different steam to carbon ratio and hydrogen stoichiometry

The temperature of the combustion gases plays a role in the system's efficiencies because it supplies the energy needed in the steam methane reformer and also the hot water produced in the cogeneration heat exchanger. Simulation to determine the influence the combustion gas temperature has on the system cogeneration and thermal efficiencies were made. The simulation results shows that $\boldsymbol{T_{comb}}$ has a positive effect on the cogeneration efficiency as can be seen in Figure 5.11. The cogeneration efficiency increased from 78.7 to 92.5 % when $\boldsymbol{T_{comb}}$ increase from 816 to 979 ^{o}C. Contrary to the cogeneration efficiency, $\boldsymbol{T_{comb}}$ has a negative on the systems thermal efficiency as shown in Figure 5.12. When combustion gas temperature was varied the thermal efficiency decreased from 44 to 41 %. This is not a significant decrease but it shows that there is some thermal energy that is not recovered from the flue gas exiting the methane pre-heater. So to increase the system thermal efficiency this energy needs to be utilised somewhere in the system. It is suggested that the energy may be used for heating up the fuel cell stack at start-up of the system.

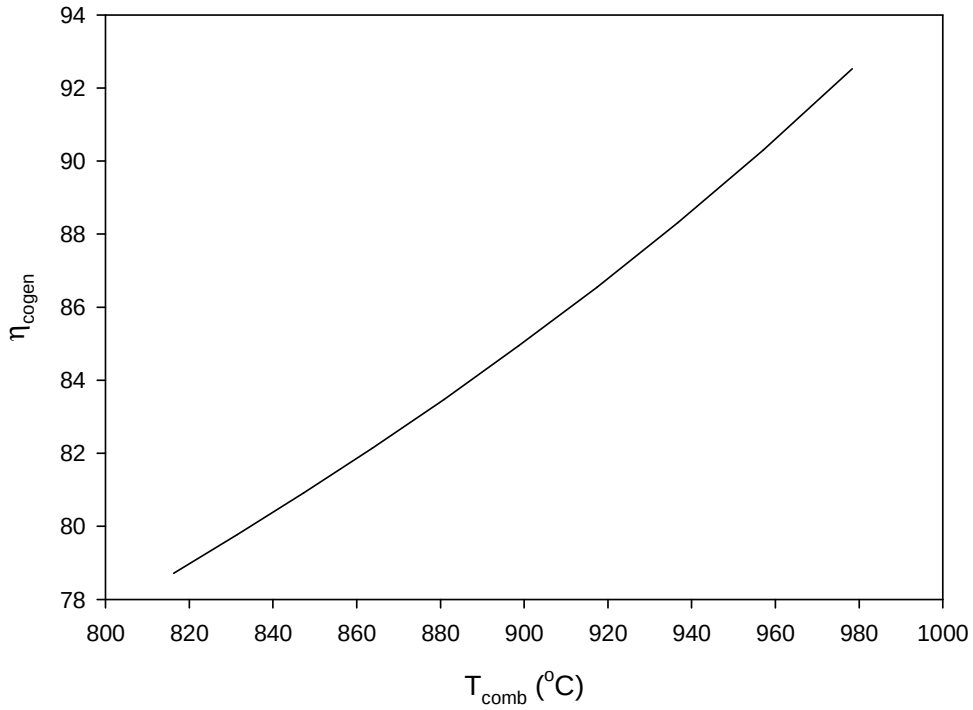

Figure 5.7: System cogeneration efficiency at different combustion gas temperature

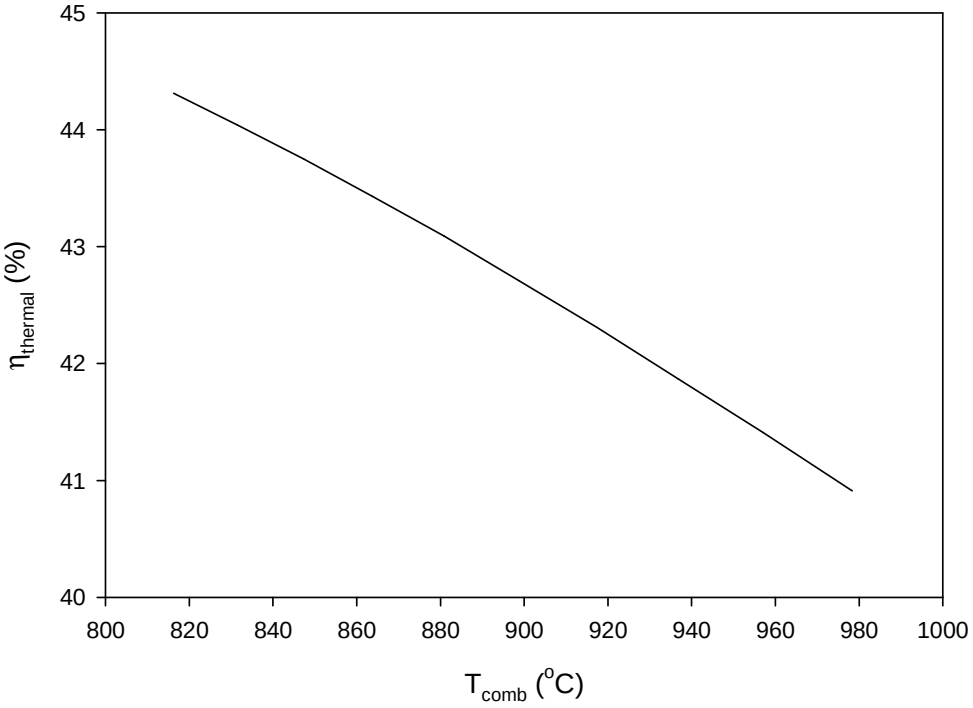

Figure 5.8: System thermal efficiency at different combustion gas temperature

CHAPTER SIX
CONCLUSIONS AND RECOMMENDATIONS

6.1 Summary

The focus of this research was to develop modelling tools for micro combined heat and power systems based on proton exchange membrane fuel cells. In doing this, models for predicting the steady-state operation of the core technology, the High Temperature PEMFC, was done. The predictive capabilities of this model were tested against well-known data from literature. After satisfactory optimization of this model, it was used to investigate catalyst loading, amount of CO in fuel, current density, temperature and acid doping level. The results showed that increasing the operating temperature, and current density results in increased performance. The performance also increased when the acid doping level increased. However it was shown that this has limit as the increase in performance when the acid doping level was increased from 4 to 6 (0.012 S/cm) is lower than for 6 to 8 (0.018 S/cm).

The single cell model was further developed for a 1 kW_e high temperature PEMFC stack. The stacks model was validated using experimental data from a test station that was used to investigate the performance PEMFC stack. A sensitivity analysis of the models outputs was done using the EES built-in uncertainty propagation. The analysis showed the cogeneration, electrical and thermal efficiencies is affected by an uncertainty value of 4.8%, 6.5%, 10.4% for outputs value of 84.7%, 38%, 44.7% efficiency, respectively. The major sources of the uncertainty were the hydrogen stoichiometry, current density and operating temperature.

A micro-CHP model to predict steady-state behaviour was developed by coupling the stack model with a fuel processor model. The system sensitivity analysis using the uncertainty propagation was also done. The highest combined cogeneration system efficiency is calculated with a value of 87.3% with the corresponding electrical and thermal efficiencies of 41.3% and 46.% respectively. The fuel processing subsystem provides an adequate rate of CH_4 conversion and acceptable CO-removal, making it appropriate for integration with an HT PEMFC stack. In the steam methane reformer 97% of CH4 conversion is achieved and the water gas shift reactors achieve about 98% removal of CO.

6.2 Future work

- The exclusion of the work recovery and air supply subsystem in the micro-CHP system limited the model in predicted parastatic losses caused by the subcomponents and hence they should be included in order to get realistic system performance of an operational system.

- In order to for the fuel cell based CHP systems to be compared to traditional CHP systems their price and economic evaluation should be made. To do this the model should be extended to include the geometry of the subcomponents in order to cost them

- The model should be developed further to include transient behaviour

- The CHP model should be validated using experimental data

REFERENCES

Andreasen, S. J. 2009. Design and Control of High Temperature PEM Fuel Cell System. PhD, Aalborg University.

Andújar, J. M. & Segura, F. 2009. Fuel cells: History and updating. A walk along two centuries. *Renewable and Sustainable Energy Reviews,* 13: 2309-2322.

Arsalis, A., Nielsen, M. P. & Kær, S. K. 2011. Modeling and parametric study of a 1kWe HT-PEMFC-based residential micro-CHP system. *International Journal of Hydrogen Energy,* 36: 5010-5020.

Barbir, F. 2005. PEM Fuel Cells: Theory and Practise, California, Elsevier Academic Press.

Bergmann, A., Gerteisen, D. & Kurz, T. 2010. Modelling of CO Poisoning and its Dynamics in HTPEM Fuel Cells. *FUEL CELLS,* 10: 278–287.

Blanchette Jr, S. 2008. A hydrogen economy and its impact on the world as we know it. *Energy Policy,* 36: 522-530.

Bouchet, R. & Siebert, E. 1999. Proton conduction in acid doped polybenzimidazole. *Solid State Ionics,* 118: 287-299.

Cheddie, D. & Munroe, N. 2005. Review and comparison of approaches to proton exchange membrane fuel cell modelling. *Journal of Power Sources,* 147: 72–84.

Cheddie, D. & Munroe, N. 2006. Mathematical model of a PEMFC using a PBI membrane. *Energy Conservation and Management,* 47: 1490-1504.

Cheddie, D. F. & Munroe, N. D. H. 2007. A two-phase model of an intermediate temperature PEM fuel cell. *International Journal of Hydrogen Energy,* 32: 832-841.

Chen, C.Y. & Lai, W.H. 2010. Effects of temperature and humidity on the cell performance and resistance of a phosphoric acid doped polybenzimidazole fuel cell. *Journal of Power Sources,* 195: 7152-7159.

Cho, Y.H., Park, H.S., Cho, Y.H., Jung, D.S., Park, H.Y. & Sung, Y.E. 2007. Effect of platinum amount in carbon supported platinum catalyst on performance of polymer electrolyte membrane fuel cell. *Journal of Power Sources,* 172: 89-93.

Cowey, K., Green, K. J., Mepsted, G. O. & Reeve, R. 2004. Portable and military fuel cells. *Current Opinion in Solid State and Materials Science,* 8**:** 367–371.

Crawley, G. 2006. Alkaline Fuel Cells (AFC). Fuel Cell Today.

Das, S. K. & Bansode, A. S. 2009. Heat and Mass Transport in Proton Exchange Membrane Fuel Cells - A review. *Heat Tranfer Engineering,* 30: 691-719.

Das, S. K., Reis, A. & Berry, K. J. 2009. Experimental evaluation of CO poisoning on the performance of a high temperature proton exchange membrane fuel cell. *Journal of Power Sources,* 193: 691-698.

Dhar, H. P., Christner, L. G., Kush, A. K. & Maru, H. C. 1986. Performance Study of a Fuel Cell Pt-on-C Anode in Presence of CO and CO_2 and Calculation of Adsorption Parameters for CO Poisoning *Journal of the Electrochemical Society,* 133: 1574-1582.

EG&G TECHNICAL SERVICES, I. 2004. Fuel Cell Handbook. *In:* ENERGY, U. S. D. O. (ed.) 7 ed.

FUEL CELL TODAY. *Stationary* [Online]. Available: http://www.fuelcelltoday.com/about-fuel-cells/applications/stationary [Accessed 15 September 2011].

Gasteiger, H. A., Panels, J. E. & Yan, S. G. 2004. Dependence of PEM fuel cell performance on catalyst loading. *Journal of Power Sources,* 127: 162–171.

Haraldsson, K. & Wipke, K. 2004. Evaluating PEM fuel cell system models. *Journal of Power Sources,* 126: 88–97.

Haubold, H. G., Vad, T., Jungbluth, H. & Hiller, P. 2001. Nano structure of NAFION: a SAXS study. *Electrochimica Acta,* 46**:** 1559-1563.

Hermann A., Chaudhuri T. & Spagnol P. 2005. Bipolar plates for PEM fuel cells: A review*. International Journal of Hydrogen Energy*, 30(12): 1297-1302.

Hinnells, M. 2008. Combined heat and power in industry and buildings. *Energy Policy* 36**,** 4522–4526.

Hongbo, R. & Weijun, G. 2010. Economic and environmental evaluation of micro CHP systems with different operating modes for residential buildings in Japan. *Energy and Buildings***,** 1-9.

Hou, Y., Zhuang, M. & Wan, G. 2007. The analysis for the efficiency properties of the fuel cell engine*. Renewable Energy*, 32(7):1175-1186.

Institution of Engineering and Technology 2007. Combined Heat and Power.

Iranzo, A., Munoz, M., Rosa, F. & Pino, J. 2010. Numerical model for the performance prediction of a PEM fuel cell. Model results and experimental validation. *International Journal of Hydrogen Energy***,** 1-18.

Jiao, K. & Li, X. 2010. A Three-Dimensional Non-isothermal Model of High Temperature Proton Exchange Membrane Fuel Cells with Phosphoric Acid Doped Polybenzimidazole Membranes. *FUEL CELLS,* 10: 351–362.

Jovan, V., Perne, M. & Petrovčič, J. 2010. An assessment of the energetic flows in a commercial PEM fuel-cell system. *Energy Conversion and Management,* 51**:** 2467-2472.

Kamarudina, S. K., Achmada, F. & Dauda, W. R. W. 2009. Overview on the application of direct methanol fuel cell (DMFC) for portable electronic devices. *International Journal of Hydrogen Energy,* 34: 6902 – 6916.

Kim, H., Shin, S., Park, Y.G., Songa, J. & Kimb, H. 2006. Determination of DMFC deterioration during long-term operation. *Journal of Power Sources,* 160: 440–445.

Kim, J., Lee, S. M., Srinivasan, S. & Chamberlin, C. E. 1995. Modelling of proton exchange membrane fuel cell performance with an empirical equation. *Journal of the Electrochemical Society,* 142: 2670-2674.

Kim, K. 2008. Dynamic Proton Exchange Membrane Fuel Cell System Synthesis/Design and Operation/Control Optimization under Uncertainty, in Mechanical Engineering. PhD. Virginia Polytechnic Institute and State University: Blacksburg.

Klinedinst, K., Bett, J. A. S., Macdonald, J. & Stonehart, P. 1974. Oxygen solubility and duffusivity in hot cencentrated H_3PO_4. *Electroanalytical chemistry and Interfacial Electrochemistry,* 57: 281-289.

Kolb, G., *Fuel Processing for Fuel Cells*. 2008, Weinheim: Wiley

Korsgaard, A. R., Refshauge, R., Nielsen, M. P., M. Banga & Kær, S. K. 2006. Experimental characterization and modeling of commercial polybenzimidazole-based MEA performance. *Journal of Power Sources,* 162: 239-245.

Krewer, U., Song, Y., Sundmacher, K., Johnb, V., Lubkeb, R., Matthiesb, G. & Tobiskab, L. 2004. Direct methanol fuel cell (DMFC): analysis of residence time behaviour of anodic flow bed. *Chemical Engineering Science,* 59: 119 – 130.

Larminie, J. & Dicks, A. 2003. *Fuel cell systems explained*, John Wiley & Sons Ltd.

Li, Q. Hjuler, H. A. & Bjerrum, N. J. 2001. Phosphoric acid doped polybenzimidazole membranes: physiochemical characterization and fuel cell applications. *Journal of Applied Electrochemistry*, 31: 773–779,

Li, Q., Jensena, J. O., Savinell, R. F. & Bjerruma, N. J. 2009. High temperature proton exchange membranes based on polybenzimidazoles for fuel cells. *Progress in Polymer Science,* 34**:** 449–477.

Li, X. 2006. *Principles of fuel cells,* New York, Taylor & Francis Group.

Litster, S. & Mclean, G. 2004. PEM fuel cell electrodes. *Journal of Power Sources,* 130**:** 61–76.

Liu, Z., S.Wainright, J. & Savinell, R. F. 2004. High-temperature polymer electrolytes for PEM fuel cells: study of the oxygen reduction reaction (ORR) at a Pt–polymer electrolyte interface. *Chemical Engineering Science,* 59: 4833-4838.

Liu, Z., Wainright, J. S., Litt, M. H. & Savinell, R. F. 2006. Study of the oxygen reduction reaction (ORR) at Pt interfaced with phosphoric acid doped polybenzimidazole at elevated temperature and low relative humidity. *Electrochimica Acta,* 51: 3914-3923.

Lobato, J., Cañizares, P., Rodrigo, M. A., Linares, J. J. & Aguilar, J. A. 2007. Improved polybenzimidazole films for H3PO4-doped PBI-based high temperature PEMFC. *Journal of Membrane Science,* 306: 47-55.

Ma, Y. L., Wainright, J. S., Litt, M. H. & Savinell, R. F. 2004. Conductivity of PBI Membrane for High-Temperature Polymer Electrolyte Fuel Cell. *Journal of the Electrochemical Society,* 151: A8-A16.

Mamlouk, M. & Scott, K. 2010. The effect of electrode parameters on performance of a phosphoric acid-doped PBI membrane fuel cell. *International Journal of Hydrogen Energy,* 35: 784-793.

Marbán, G. & Valdés-Solís, T. 2007. Towards the hydrogen economy? *International Journal of Hydrogen Energy,* 32: 1625-1637.

Mathias, M. Roth, J. Flemimg, J. & Lehnert, W. (2003) Diffusion media materials and characterization, Chapter 46, Handbook of Fuel Cells - Fundamentals, Technology and Applications, edited by Wolf Vielstich, Hubert A. Gasteiger, Arnold Lamm. Volume 3: Fuel Cell Technology and Applications, John Wiley & Sons, Ltd.

Mathiesen, B. V., Lund, H. & Karlsson, K. 2011. 100% Renewable energy systems, climate mitigation and economic growth. *Applied Energy,* 88: 488-501.

Macdonald, D.I. Boyack, J.R. 1969. Density, electrical conductivity, and vapor pressure of concentrated phosphoric acid. *Journal of Chemical and Engineering Data*, *14* (3):380–384

Mclean, G. F., Niet, T., Prince-Richard, S. & Djilali, N. 2002. An assessment of alkaline fuel cell technology. *International Journal of Hydrogen Energy,* 27: 507-526.

Mehlomakulu, B. *Hydrogen and fuel-cell technology issues for South Africa: The emerging debate* [Online]. Available: http://web.idrc.ca/en/ev-132192-201-1-DO_TOPIC.html [Accessed 26-07 2010].

Mérida, W., Harrington, D. A., Le Canut, J. M. & Mclean, G. 2006. Characterisation of proton exchange membrane fuel cell (PEMFC) failures via electrochemical impedance spectroscopy. *Journal of Power Sources,* 161: 264-274.

Modestov, A. D., Tarasevich, M. R., Filimonov, V. Y. & Davydova, E. S. 2010. CO tolerance and CO oxidation at Pt and Pt–Ru anode catalysts in fuel cell with polybenzimidazole–H_3PO_4 membrane. *Electrochimica Acta,* 55: 6073–6080.

Peng, J. & Lee, S. J. 2006. Numerical simulation of proton exchange membrane fuel cells at high operating temperature. *Journal of Power Sources,* 162: 1182–1191.

Reum, M. 2008. Sub-Millimeter Resolved Measurement of Current Density and Membrane Resistance in Polymer Electrolyte Fuel Cells (PEFC). PhD, Swiss Federal Institute of Technology.

Schulze, M., Knöri, T., Schneider, A. & Gülzowa, E. 2004. Degradation of sealings for PEFC test cells during fuel cell operation. *Journal of Power Sources,* 127: 222–229.

Scott, K., Pilditch, S. & Mamlouk, M. 2007. Modelling and experimental validation of a high temperature polymer electrolyte fuel cell. *Journal of Applied Electrochemistry,* 37: 1245-1259.

Scott, K. & Mamlouk, M. 2009. A cell voltage equation for an intermediate temperature proton exchange membrane fuel cell. *International Journal of Hydrogen Energy*, **34**(22): 9195-9202.

Songprakorp, R. 2008. *Investigation of Transient Phenomena of Proton Exchange Membrane Fuel Cells.* PhD, University of Victoria.

Sousa, T., Mamlouk, M. & Scott, K. 2010. An isothermal model of alaboratory intermediate temperature fuel cell using PBI doped phosphoric acid membranes. *Chemical EngineeringScience,* 65: 2513-2530.

Staffell, I. 2009. *FUEL CELLS FOR DOMESTIC HEAT AND POWER: ARE THEY WORTH IT?* PhD, University of Birmingham.

Ubong, E. U., Shi, Z. & Wang, X. 2009. Three-Dimensional Modeling and Experimental Study of a High Temperature PBI-Based PEM Fuel Cell. *Journal of the Electrochemical Society,* 156: B1276-B1282.

Verhaerta, I., Paepea, M. D. & Mulderc, G. 2009. Thermodynamic model for an alkaline fuel cell. *Journal of Power Sources,* 193: 233–240.

Vogel, W. Lundquist, J. Ross, P. Stonehart, P. 1974. Reaction Pathwayspathways and Poisonspoisons—II. The rate controlling step for electrochemical oxidation of hydrogen on Pt in acid and poisoning of reaction by CO*. Electrochimica. Acta*, 20:79–93.

Welty, J., Wicks, C. E., Wilson, R. E. & Rorrer, G. L. 2008. *Fundamentals of Momentum, Heat, and Mass Transfer* Wiley.

Xu, J. & Froment, G. F. 1989. Methane Steam Reforming, Methanation and Water-Gas Shift: 1. Intrinsic Kinetics. *AIChe Journal,* 35: 88-96.

Zeis, R., Mathur, A., Fritz, G., Lee, J. & Erlebacher, J. 2007. Platinum-plated nanoporous gold: An efficient, low Pt loading electrocatalyst for PEM fuel cells. *Journal of Power Sources,* 165: 65-72.

Zhang, J., Xie, Z., Zhang, J., Tang, Y., Song, C., Navessin, T., Shi, Z., Song, D., Wang, H., WilkinsoN, D. P., Liu, Z. & Holdcroft, S. 2006. High temperature PEM fuel cells. *Journal of Power Sources,* 160**:** 872–891.

APPENDIX

Table A- 1: List of the pre-exponential factors and activation energies for the SMR reaction kinetics

	Pre-exponential factors
$A(k_1)$	**4.255E15 [kmol bar$^{0.5}$ / (kg$_{cat}$ h)]**
$A(k_2)$	**1.955E6 [kmol / (kg$_{cat}$ bar h)]**
$A(k_3)$	**1.020E15 [kmol bar$^{0.5}$ / (kg$_{cat}$ h)]**
$A(K_{co})$	**8.23E-5 (bar^{-1})**
$A(K_{H2})$	**6.12E-9 (bar^{-1})**
$A(K_{CH4})$	**6.65E-4 (bar^{-1})**
$A(K_{H2O})$	**1.77E-05**

Table A- 2: List of the reaction enthalpies for the SMR reaction kinetics

Activation energy/ Reaction enthalpy (kJ/kg)	
E_1	**240.1**
E_2	**67.13**
E_3	**243.9**
ΔH_{CO}	**-70.65**
ΔH_{H2}	**-82.9**
ΔH_{CH4}	**-32.28**
ΔH_{H2O}	**88.68**

Table A- 3: Parameter values in the kinetic equation for the HT-WGS

Parameter	Value
KHs	**42.699 [mol$_{CO2}$/(s atm$^{0.5}$ m^3)]**
THs	**706.15 K**
E	**48150 J/mol**

Table A- 4: activation energies and pre-exponential factors for the LT-WGS

Parameter	Pre-exponential factor / Activation energy
E_{Ls}	**12.88 - 1885.5 / T (kJ/kg)**
A_{Ls}	**-5.97E-04 (mol/kg s)**

Table A- 5: Membrane Electrode Assembly Parameters

Description	Value	Reference
$i_{o,c}^{ref}$	2.6 x10^{-5} A/m^2	Sousa et al 2010
E_a	16.9 kJ/mol	Scott and Mamlouk 2009
$i_{o,a}^{ref}$	1.44 x10^{3} A/m^2	Sousa et al 2010
E_c	66 kJ/mol	This work
γ_a	1	
γ_a	1	
α_c	0.7	This work
α_c	0.7	This work
L_a	2000 mg/m^2	This work
L_c	2000 mg/m^2	This work
$C_{H_2}^{ref}$	0.211 mol/m^3	Sousa et al 2010
$C_{O_2}^{ref}$	0.107 mol/m^3	Sousa et al 2010
X	4	This work
l	60 x10^{-6} m	This work
A_a	0.03545 m2/mg	Sousa et al 2010
A_c	0.03155 m2/mg	Sousa et al 2010